Predicting Riparian Wetland Community Transitions using Hydraulic Metric Thresholds Derived from Dynamic 2D Modeling

By

Erin C. Reinkemeyer
B.S., University of Missouri, Columbia, 2016

Submitted to the graduate degree program in Civil, Environmental and Architectural Engineering and the Graduate Faculty of the University of Kansas in partial fulfillment of the requirements
for the degree of Master of Science in Environmental and Water Resources Engineering

---

Chair: Dr. Amy Hansen

Dr. Joshua K. Roundy

Dr. C. Bryan Young

Date Defended: 21 December 2021

The thesis committee for Erin Reinkemeyer certifies that this is the approved version of the following thesis:

Predicting Riparian Wetland Community Transitions using Hydraulic Metric Thresholds Derived from Dynamic 2D Modeling

Chair: Dr. Amy Hansen

Date Approved: 21 December 2021

Abstract

Agricultural expansion and flood mitigation activities have had unintentional, negative impacts on threatened, critical, and at-risk riparian wetland ecosystems in the Midwestern United States. Resulting changes in land use, stream channelization and levee construction have amplified bank erosion and channel degradation and have reduced floodplain connectivity. Projected increases in both drought and flood severity for the region further complicate hydrologic and hydraulic interactions between river channels and wetlands and create challenges for predicting ecosystem response. Hydraulic changes occurred gradually and abruptly in the form of changing water tables, log jams, and avulsions. In order for wetland managers to appropriately protect critical wetlands or adapt management to forecasted changes, a deeper understanding of the effect of altered hydraulics on wetland communities is needed. Important work has been completed pertaining to the relation of hydraulic traits and individual aquatic plant species and plant traits; however, large scale dynamic hydraulic changes and effects on wetland ecosystems are still poorly understood. Prior limitations to studying this problem included insufficient modeling tools for processing two dimensional systems and complexity of the system across multiple wetland species. Recent advances in modeling technology enabled study of two-dimensional (2D) hydraulics across entire floodplains and varying ecosystems.

This project investigated the effect of flood inundation dynamics on wetland ecosystems. The analysis simulated two-dimensional channel and floodplain hydraulics for a sub-basin of the Grand River in the central United States (U.S.). U.S. Geological Survey (USGS) flow records for Locust Creek at Linneus, Missouri (MO); Grand River near Fountain Grove; and Grand River near Sumner, in addition to U.S. Army Corps of Engineers (USACE) Hydrologic Engineering Center (HEC) Hydrologic Modeling Software (HMS) generated flows were used to simulate a continuous

period of record for Pershing State Park over a 10-year time period. Records of log jam formation and removal obtained from the Missouri Department of Natural Resources (MoDNR) were used to estimate changes to channel capacity and split flows. Hydraulic parameters from the HEC River Analysis System (RAS) 2D unsteady flow model were extracted annually and used to determine changes in wetland communities. Changes in the hydraulic parameters including inundation duration and depth were compared and tested as predictive variables for changes in wetland community boundaries. This project used overall wetland community metrics instead of indicator species for evaluation. Predicted transitions in wetland communities based on the hydraulic model simulations were compared to 2011 MoDNR and 2019 USACE ecosystem observational surveys to determine if hydraulic habitat suitability metrics predicted spatial changes in wetland communities. The analysis identified that inundation duration and inundation depth habitat metrics were overall predictive of wetland community transitions for bottomland hardwood forests and wet prairie. Inundation duration less than the specified threshold was a better metric than inundation depth for predicting both bottomland hardwood forest and wet prairie community gains or spatial expansion. Conversely, inundation depth exceeding the specified threshold was a better metric than inundation duration for predicting bottomland hardwood forest loss. Finally, wet prairie inundation depth thresholds could be used to predict both community gains and community losses depending on the selection of the habitat threshold magnitude. Overall, this thesis demonstrated that there was no singular hydraulic habitat metric that captured both community gains and losses. This improved understanding of the influence of large-scale hydraulics on wetland trajectories will help resource managers adapt to the changing hydraulic conditions and inform decisions of how to allocate monitoring, sampling, and rehabilitation resources to manage wetlands more efficiently and effectively.

Acknowledgments

Thank you to everyone who helped get this thesis over the finish line including Joey Craft for constantly running and rerunning simulations, Dr. Hansen for putting up with my VERY last-minute reviews, Tom Woodward and Pershing State Park for providing and verifying data, and the U.S. Army Corps of Engineers and the FOIA request process for providing the initial models and datasets. Without these people and agencies, this research never would have happened.

Table of Contents

List of Figures

List of Tables

List of Appendices

Acronyms

2D……Two Dimensional

ArcGIS……..Aeronautical Reconnaissance Coverage Geographic Information System

BC……Boundary Condition

BH……Bottomland Hardwood

CDT……..Central Daylight Time

cm……centimeters

cms……cubic meters per second

CST……...Central Standard Time

EC……Existing Condition

EG……Energy Grade Line

HEC……..Hydrologic Engineering Center

HEC DSSVue or DSSVue……Hydrologic Engineering Center Data Storage System Visual Utility Engine

HEC-HMS or HMS……..Hydrologic Engineering Center Hydrologic Modeling System

HEC-RAS or RAS……Hydrologic Engineering Center River Analysis System

HWM……High Water Marks

km……kilometer

LGR……..Lower Grand River

LiDAR……..Light Detection and Ranging

LWD ……Large Woody Debris

m……...meter

MDC…….Missouri Department of Conservation

MO……Missouri

MoDNR……Missouri Department of Natural Resources

mps……meters per second

NAD83…….North American Datum of 1983

NAVD88……..North American Vertical Datum of 1988

NLCD……...National Land Cover Database

NRCS……Natural Resources Conservation Service

NSE……..Nash-Sutcliffe Efficiency

NWI……..National Wetland Inventory

SIR……Special Investigation Report

SSURGO …….Soil Survey Geographic

TIFF……. Tagged Image File Format

U.S. ……..United States

USDA……...United States Department of Agriculture

USGS……United States Geologic Survey

USACE…….United States Army Corps of Engineers

USFWS…….United States Fish and Wildlife Service

UTC……..Coordinated Universal Time

UTM…….Universal Transverse Metacator

VRS……..Virtual Reference Stations

WP……Wet Prairie

Chapter 1: Introduction

Wetland loss and degradation are widespread throughout the Midwest and United States. Over the course of 200 years, between 1780 and 1980, it was estimated that 87% of wetlands were removed in Missouri (MO); 80% of wetlands were destroyed in Iowa, Missouri, and Illinois; and on average 0.24 square kilometers (km^2) of wetland were destroyed every hour in the contiguous United States (Dahl, 1990). Although wetland area stabilized, wetland type and quality continue to change (Dahl, 2011). While absolute wetland losses are well documented, the trajectory of degradation of remaining wetland ecosystems is less understood. Wetland degradation results in the loss of important wetland functions such as water purification, soil erosion prevention, flood reduction, and carbon sequestration (Meli et al., 2014; Nahlik & Fennessy, 2016).

Studies indicate that riparian wetlands are most at risk for change in spatial extent (Berhane et al., 2020) largely due to their position at the aquatic-terrestrial interface. Riparian zones are the areas defined as segments in the floodplain, typically near the stream, that are influenced by waterway hydraulics and contain both aquatic and terrestrial components (Naiman & Decamps, 1997; Verry et al., 2004). Riparian wetlands provide vital habitat, biodiversity, and pollution filtration processes within the floodplain (Naiman & Decamps, 1997; Richardson et al., 2007; Webster et al., 2018). Riparian wetland degradation is primarily driven by hydrologic changes due to agricultural expansion, intentional stream channelization, and climate change all of which reduce the quality of the wetland and riparian environmental functions.

Agricultural Expansion. Agricultural expansion and intensification altered floodplain hydraulics and consequently, riparian wetland function. Conversion of natural habitat to agricultural fields increases runoff and flood peaks (Poff et al., 1997) contributing to increased erosion and sediment loads in nearby streams (Alberto et al., 2016). Changes in land use within

the watershed, such as deforestation or agricultural production, alter hydrologic processes including evapotranspiration and infiltration (Clark, 1987). Agricultural production can further reduce infiltration capacity by compacting soils (O'Connell et al., 2007). The altered land cover and hydrology can then increase peak runoff volume and flow, thus increasing flood risk (Bradshaw et al., 2007; Laurance, 2007; O'Connell et al., 2007). Additionally, irrigation and tile drains reduce groundwater tables, decrease groundwater discharge, and deteriorate water quality (Brierley & Stankoviansky, 2002). Increased streamflow can increase bank erosion (Gellis et al., 2016) and cause floodplain inundation, exposing floodplain communities to sedimentation and pollutants (C. Hupp et al., 2013). Increased bank erosion can increase the amount of large woody debris (LWD) entering the stream channel. Additional LWD can increase maximum floodplain inundation extent and inundation depths (Keys et al., 2018). Alternatively, increased streamflow can increase channel cross sectional area via erosion and reduce channel-floodplain connectivity (Beck et al., 2019; Knox, 2006; Poff et al., 2006).

Intentional Stream Channelization. Flood mitigation activities such as stream channelization and levee construction have unintentional negative impacts on riparian wetlands. Human activities such as channelization and levee construction modify flow and sediment regimes (Schumm, 1969; Simon, 1994). Channelization includes removing natural river bends which shortens the overall stream length and induces channel incision, bank erosion, and lower ground water levels resulting in loss of stream habitat (Funk & Ruhr, 1971). Stream channelization increases channel slope which can further increase channel erosion and degradation (Shankman & Samson, 1991; Simon, 1989). Levee construction inhibits floodplain and channel connectivity by concentrating flow in the channel (Funk & Ruhr, 1971), separating streams from the floodplain, and reducing community biodiversity (Galat et al., 1998; Verhoeven et al., 2008). Additionally,

the widespread channelization and levee construction may paradoxically contribute to increased frequency or severity of flooding by impacting peak hydrograph timing (U.S. Army Corps of Engineers, 1932). These negative impacts include bank erosion, channel degradation, and reduced floodplain connectivity and, consequently, threaten critical and at-risk ecosystems.

Climate Change. Additionally, climate models predict that extreme event intensity will increase along with time between events, further complicating hydrologic and hydraulic interactions between river channels and wetlands and create additional challenges for predicting ecosystem response. Both observed and projected climate trends indicate increased precipitation and runoff in the Midwest (Bates et al., 2008; Environmental Protection Agency, 2016; Pryor et al., 2013; Qiao et al., 2014). Other studies have identified increasing low flows in the Upper Midwest (Douglas et al., 2000) and identified increases in periods of wet or dry weather resulting in larger floods and more extensive droughts (Angel et al., 2018; NOAA, 2013). Additionally, climate simulations predict increasing temperatures in the Midwest throughout all seasons, contributing to a longer growing season (Angel et al., 2018; Byun & Hamlet, 2018; Pryor et al., 2013). These climate changes impact water availability and the channel-floodplain relationship, requiring additional modeling tools for predicting wetland community response to hydraulic traits influenced by climate change. All of these factors have the ability to impact wetland community transitions, and the specific relationship between changing hydrology and community degradation is unknown.

Impacts of Hydrologic Changes on Wetlands. Wetland community development and diversity are strongly influenced by hydrologic and hydraulic changes resulting from agricultural expansions, stream channelization, and climate change. Several hydrologic factors influence wetland community development and diversity including flood frequency, flood magnitude, flood

duration, time of occurrence, and sediment deposition (Galat et al., 1998; Jacobson & Faust, 2014; Teskey et al., 1977). The varying water surface elevations and timing result in different placement or settlement locations of seeds (Fraaije et al., 2015; Soons et al., 2017). Large flood magnitudes and long durations can prevent sprouting and kill seedlings and saplings via oxygen deprivation (Briscoe, 1961; Guo et al., 1998; Hall & Smith, 1955; Hook, 1984; Hosner, 1958, 1960). Floodplain ecosystem diversity is also influenced by upstream drainage area size and condition (Jacobson & Faust, 2014; Montgomery, 1999; Montgomery & Buffington, 1997), lateral topography, sedimentation, groundwater variation, and soil composition (Fraaije et al., 2015; C. R. Hupp & Osterkamp, 1985; Noe et al., 2013; Osterkamp & Hupp, 1984; Pizzuto et al., 2016; Silvertown et al., 1999; Ström et al., 2011).

Bottomland Hardwood Forest. Bottomland hardwood forest (BH) is one such riparian wetland community within the study area that is influenced by floodplain hydraulics. Bottomland hardwood forests are usually located within floodplains on slightly higher elevations and terraces between wet prairies and riverfront forests (Hodges, 1997; C. R. Hupp & Osterkamp, 1985; U.S. Army Corps of Engineers, 2020). Additionally, bottomland hardwood forests act as a food source for several animals including migratory waterfowl (Heitmeyer et al., 2011; Twedt & Mini, 2019; Yin et al., 1997). Bottomland hardwood forests in Missouri have changed from historic conditions by increasing in density, largely due to fewer seasonal fires and recruitment failure (Hanberry et al., 2014; Kabrick et al., 2012). Additionally, land use conversion, altered hydrology, flood control projects, sedimentation, and invasive species contributed to wetter conditions within the Grand River Basin (Heitmeyer et al., 2011; Tomer & Schilling, 2009) and overall degradation of historic bottomland hardwood extents (Heitmeyer et al., 2011; U.S. Fish and Wildlife Service, 2011). Trends in wetter conditions resulted in a transition to more water tolerant species (Heitmeyer et

al., 2011; Nelson, 2010). Historically, bottomland hardwood forests were tolerant of both wet and dry conditions and benefited from seasonal drought. Mature forest can withstand flooding lasting approximately 12% to 20% of the growing season which extends from spring to fall (Burke et al., 2003; Kabrick et al., 2012; Nelson, 2010). When flooded, the water depths at which the trees can survive depends on the height of the vegetation. If partially inundated rather than completely inundated, survival rates improve (Hosner, 1960; Kabrick et al., 2012). Additionally, studies indicate inundation duration is more detrimental to bottomland hardwood survival than inundation depths (Hodges, 1997), especially as it relates to seedling recruitment. Increases in inundation duration cause increases in seedling mortality (Jacques et al., 2021; Kabrick et al., 2012; Krzywicka et al., 2017).

Wet Prairie. Wet prairies (WP) are a second type of riparian wetland community within the study area that are impacted by floodplain hydraulics. Wet prairies are typically comprised of wetland grasslands that are tolerant of both dry and wet conditions (Nelson, 2010; Slaughter & Kost, 2010). Historically, wet prairies tend to have standing water over winter and spring months, but dry out as summer progresses, indicating dry conditions may be beneficial for wet prairie survival (Nelson, 2010; U.S. Army Corps of Engineers, 2020). Additionally, the occurrence of fires prevented forest expansion and enhanced species diversity (Slaughter & Kost, 2010). The survival of wet prairie species during flooding conditions is largely dependent on the height of the vegetation. If the plants are taller than observed flood depths, then the plants are more likely to survive (Nelson, 2010; Weaver, 1960). As a result, the timing of flood events and associated vegetation height contributes to wet prairie survival. However, wet prairie communities are also reported as more sensitive during summer floods (Gattringer et al., 2017; van Eck et al., 2006), contrary to the larger vegetation height. By July, wet prairie vegetation within Missouri is usually

0.6 to 0.9 meters tall and can thus withstand flood events producing depths less than the vegetation height (Nelson, 2010; Weaver, 1960). While tolerant of wet conditions, continuous inundation has negative impacts on wet prairie growth by impacting nutrient and light availability (S. Kercher et al., 2007). Past studies indicate wet prairie can withstand inundation durations ranging between three weeks and six months (Banach et al., 2009; S. Kercher et al., 2007; Kushlan, 1990; Olmstead & Loope, 1984; U.S. Fish and Wildlife Service, n.d.), but are more negatively impacted by continuous inundation durations ranging between three and four weeks (Banach et al., 2009; S. Kercher et al., 2007; U.S. Army Corps of Engineers, 2020). Additionally, flooding and associated sedimentation can contribute to habitat zonation in floodplains (van Eck et al., 2006), causing transitions to forested communities (Johnston, 2003) or invasive species such as reed canary grass (S. Kercher et al., 2007; S. M. Kercher & Zedler, 2004; U.S. Army Corps of Engineers, 2020).

Past Research. Previous studies demonstrated that individual aquatic plant species (cottonwoods, marsh grasses, alfalfa - *medicago sativa*) and plant characteristics (leaf area index, shoot elongation, root growth, root density, biomass, stem diameter) respond to local hydraulic traits such as velocity, depth, duration, and sediment transport (Garssen et al., 2015; Lukács et al., 2019; Mahoney & Rood, 1998; Nepf, 2011; Piliouras et al., 2017; Yang et al., 2016). For example, extensive research exploring the effects of water transport on seed dispersion exists in several forms including physical (Merritt & Wohl, 2002) and probabilistic (Groves et al., 2009; Tealdi et al., 2010) models. Additionally, the impact of plant form on hydraulic characteristics such as flow resistance (Aberle & Järvelä, 2013; Baptist et al., 2007; Dijkstra & Uittenbogaard, 2010; Järvelä, 2004; Luhar & Nepf, 2013; Nepf, 2012) and sediment transport (Kothyari et al., 2009; Liu et al., 2018; Yager & Schmeeckle, 2013; Zong & Nepf, 2011) were examined. Limited research considered the effect of large scale, dynamic hydraulic changes, categorized quantitatively, on

wetland ecosystems. The past research often investigated what was typically observational in nature and did not apply investigations to hydraulic modeling software. Prior studies related to channel reach or floodplain-scale riparian community transitions included qualitative and statistical analyses (Camporeale et al., 2013; Camporeale & Ridolfi, 2006; Collins et al., 2012; Hooke et al., 2005; McKenney et al., 1995). A few studies experimentally examined the influence of floods on entire riparian plant communities using physical experiments with natural vegetation plots (Garssen et al., 2017; Ström et al., 2011). These studies transplanted plots of riparian vegetation with multiple species to different locations in the floodplain examined impacts of flooding characteristics on biodiversity. However, these studies interpolated results between plot locations to develop relationships for the entire floodplain and lacked site specific results throughout the entire reach or floodplain. There have been few computer simulated analyses of floodplain hydraulics and vegetation changes, which has been attributed to previously insufficient modeling tools for representing complex system hydrology and multiple wetland species in large two-dimensional (2D) models (Camporeale et al., 2013). There remains a gap in scientific understanding of the interactions between riparian wetland communities and hydrologic processes which is necessary to address to effectively manage these dynamic environments.

Thesis Objective. This research investigated the effects of flood inundation dynamics on wetland ecosystem spatial transitions in a watershed located in the agriculturally intensive Midwestern United States subjected to the three stressors of agricultural expansion, stream channelization, and climate change. Using a two-dimensional hydraulic model to simulate flow over a 10-year period, the analysis tested whether common hydraulic parameters, including inundation duration, depth, and dry day duration, could be used to predict shifts in riparian wetland ecosystem boundaries. The goal of this effort was to identify easily monitored hydraulic metrics

that could be used to forecast wetland risk and, overall, to improve understanding of large-scale hydraulics on wetland trajectories.

Chapter 2: Methods

The following sections discuss the processes used to analyze Locust Creek floodplain hydraulics from a continuous period of record between 2008 and 2018.

Study Area

The research was applied to ecosystems within Pershing State Park, located in the Locust Creek Basin. The Locust Creek Basin was largely an unregulated basin located in north-central Missouri and southern Iowa draining approximately 1,666 km^2 north of Sumner, Missouri (Figure 1). Elevations in the Locust Creek Basin and southern modeling domain range from a minimum elevation of 194 meters in the North American Vertical Datum 1988 (NAVD88) at the Locust Creek confluence with the Grand River to a maximum elevation of 340 meters (m) NAVD88 in the northern most region of the watershed located in southern Iowa (Figure 2a). Topographical data was sourced from the Hydrologic Engineering Center (HEC) Hydrologic Modeling System (HMS) hydrologic model of the basin as documented in Appendix A.1.2 of the 2020 Grand River Feasibility Study (U.S. Army Corps of Engineers, 2020). Locust Creek Basin slopes generally ranged between 0 to 3% in the floodplain with larger slopes of 10 to 30% located along the transition to bluffs and hills with a maximum slope of 76.5% (Figure 2b). Land use in Locust Creek Basin was primarily agricultural with approximately 20% and 47% of the drainage area classified as cultivated crops and pasture/hay, respectively (Multi-Resolution Land Characteristics Consortium, 2019). Table 1 displays the percentages of the 2019 National Land Cover Database (NLCD) land cover classification contributing to the total Locust Creek Basin and hydraulic model domain. Figure 2c displays the Locust Creek Basin and modeling domain 2019 NLCD landcover. Soils in the lower Locust Creek Basin primarily consisted of alluvium in the floodplain and a combination of loess and glacial till in the surrounding bluffs and hills. The alluvium material was

primarily poorly drained (Meinert et al., 2011). Additionally, according to the SSURGO soil database, soils were primarily silty clay loam and silt loam in the southern regions of the basin (NRCS USDA, 2020). In the central portion of Locust Creek Basin, soils ranged from silt loam to clay loam whereas in the northern portion of the basin soils were largely comprised of loam (NRCS USDA, 2020) (Figure 2d).

Table 1:
Locust Creek Basin Land Cover Composition

NLCD Land Cover	Area (km^2)	Percentage of Total Area
Pasture / Hay	821	47%
Cultivated Crops	346	20%
Deciduous Forest	325	19%
Woody Wetlands	66.3	4%
Mixed Forest	64.3	4%
Developed, Open Space	45.7	3%
Emergent Herbaceous Wetlands	21.1	1%
Developed, Low Intensity	19.1	1%
Open Water	16.3	1%
Grassland / Herbaceous	8.46	0%
Shrub / Scrub	6.25	0%
Evergreen Forest	3.65	0%
Developed, Medium Intensity	2.81	0%
Barren Land	1.75	0%
Developed, High Intensity	0.54	0%

Since European settlement, Locust Creek Basin experienced significant alteration resulting from human activity. Upper portions of the basin exhibited significant changes in landcover. Historic and native prairie extending along southern Iowa and northern Missouri were almost completely transitioned to crop production since 1850 (Claassen et al., 2011). More recently, between 2008 and 2016, portions of the Grand River and Locust Creek Basins in Iowa displayed cropland expansion of 6% to 8% with respect to total area (Lark et al., 2020). Additionally, agricultural expansion contributed to loss of freshwater emergent marshes between 2004 and 2009 in several states including Iowa and Missouri (Dahl, 2011). In addition to changing landcover,

Locust Creek was channelized north of Highway 36 in the early 1900's (Searcy, 1955). Additionally, extensive levee construction along the channel occurred during the 1940's and 1950's (U.S. Army Corps of Engineers, 2020). Land conversion to agriculture and stream channelization likely contributed to increased runoff and altered floodplain connectivity, changing water availability to floodplain wetlands.

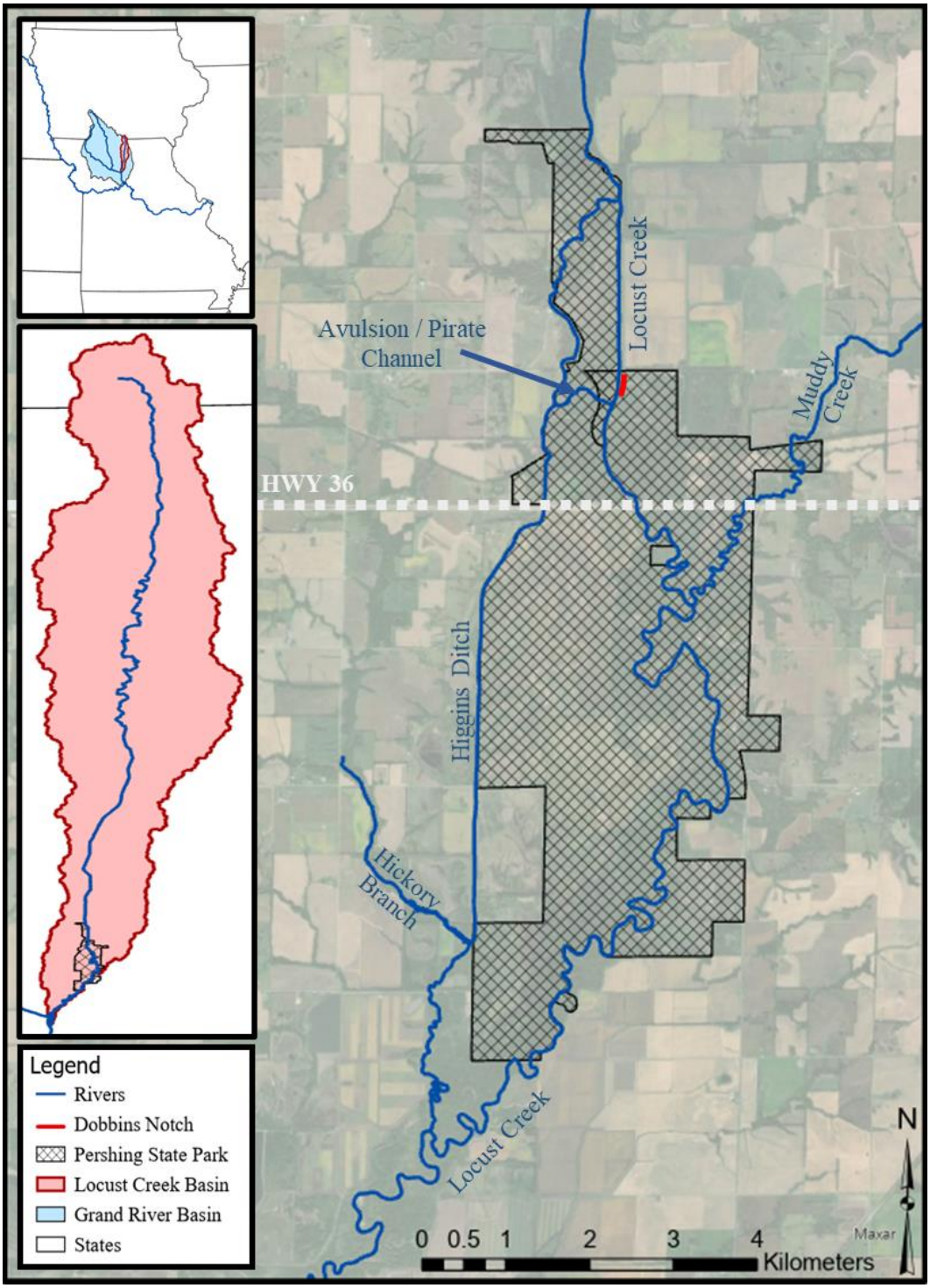

Figure 1:
Locust Creek and Pershing State Park Location Map

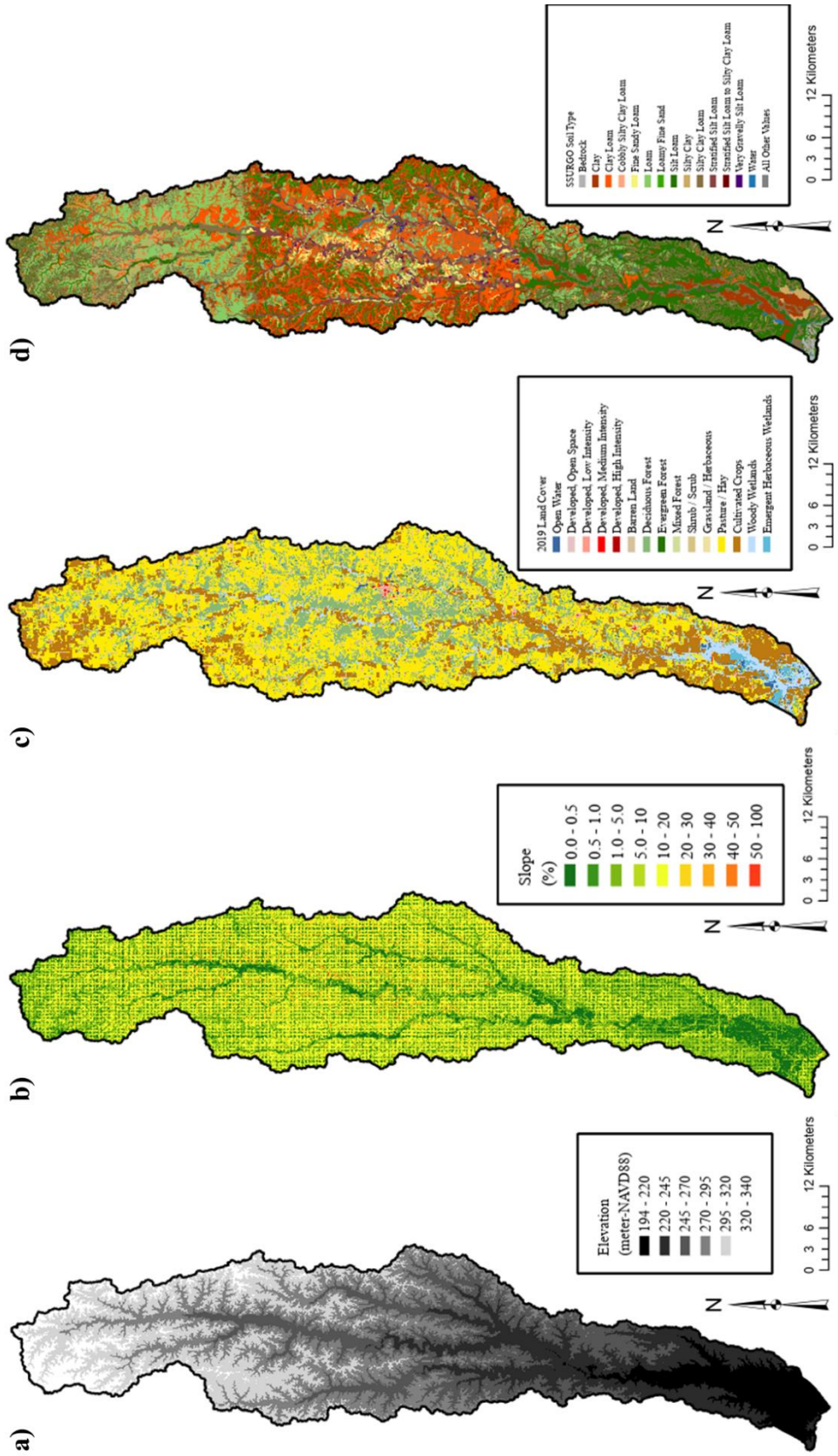

Figure 2:
Locust Creek Basin and Hydraulic Modeling Domain Characteristics.
a) Map of the Locust Creek Basin and model domain elevations. b) Map of Locust Creek Basin and model domain slopes. c) Map of Locust Creek Basin and model domain 2020 NLCD land cover. d) Map of Locust Creek Basin and model domain SSURGO soils.

Pershing State Park. The habitat analysis documented within this thesis was confined within Pershing State Park, which is owned and operated by the Missouri Department of Natural Resources (MoDNR) in Linn County, MO. Pershing State Park covered approximately 20 square kilometers near Highway 36 (Figure 1). The park included several major streams including Locust Creek, Muddy Creek, Higgins Ditch, and Hickory Branch. Figure 1 displays the major rivers and tributaries located within Pershing State Park. Pershing State Park had significant environmental relevance in that the watershed contained the last remnants of wet prairie in Missouri, primarily located along Locust Creek, a Grand River tributary (Figure 3). This wetland community was impacted by sediment deposition, erosion, log jams, and frequent inundation (U.S. Army Corps of Engineers, 2020). Additionally, Pershing State Park experienced more frequent, large scale flooding within the past 20 years (Pekel et al., 2016), contributing to ecosystem degradation in streams, tallgrass prairie, wetlands, and bottomland hardwood forests along the Grand River and within Pershing State Park (Heimann & Survey, 2017; U.S. Army Corps of Engineers, 2020). Figure 3 displays the spatial distribution of wet prairie and bottomland hardwood forests within Pershing State Park in 2011 and again in 2019, illustrating the changes over the decade. 2011 ecosystem locations were published in February 2011 for the Missouri Department of Conservation (MDC) and U.S. Fish and Wildlife Service (USFWS) but were likely identified in the previous year (Heitmeyer et al., 2011). 2019 ecosystem locations were developed in 2019, verified by Pershing State Park staff, and published in 2020 by the U.S. Army Corps of Engineers (USACE) (U.S. Army Corps of Engineers, 2020).

Wetland ecosystems within Pershing State Park were impacted by altered hydraulics resulting from sedimentation, log jams, and levee notches that occurred within the modeling timeframe and, thus, needed to be reflected within the hydraulic model. Sedimentation and log

jams within the Pershing State Park Locust Creek channel near Highway 36 caused the Locust Creek channel to become perched. The perched channel combined with continued log jams and sedimentation resulted in the formation of avulsions from the Locust Creek channel to a drainage ditch, referred to as Higgins Ditch. Higgins Ditch was located west of the Locust Creek channel and was an agricultural drainageway traveling through the west side of Pershing State Park. The avulsion formation process started before 2008; however, the hydraulic model does not simulate avulsion progression and adaptation but rather a stationary channel state representative of 2017 conditions. With the redirected Locust Creek flow, Higgins Ditch incised and widened, and as of 2018, carried most of the Locust Creek flows throughout the entire modeling period. The ground surface elevations used in the model captured the avulsions and channel conditions as of 2017. In an effort to restore historic flows to the original Locust Creek channel south of Highway 36 and prevent larger volumes of water from entering Higgins Ditch, MoDNR notched a levee on the left bank of Locust Creek in 2010 (Figure 1). The levee notch was referred to as Dobbins Notch. Although Dobbins Notch was originally effective at diverting Locust Creek flows to the Muddy Creek Highway 36 bridge opening, the notched area quickly filled with sediment and prevented further flow diversions. Sampling at Highway 36 bridge openings between 2015 and 2017 determined that, after the notch was added, 0 - 8%, 0 - 19%, and 74 - >99% of Locust Creek flows were distributed between Locust Creek, Dobbins Notch and Muddy Creek, and Higgins Ditch, respectively (Heimann & Survey, 2017). Since the levee notch resulted in altered floodplain hydraulics and flow distribution, the notched levee was accounted for in the hydraulic model.

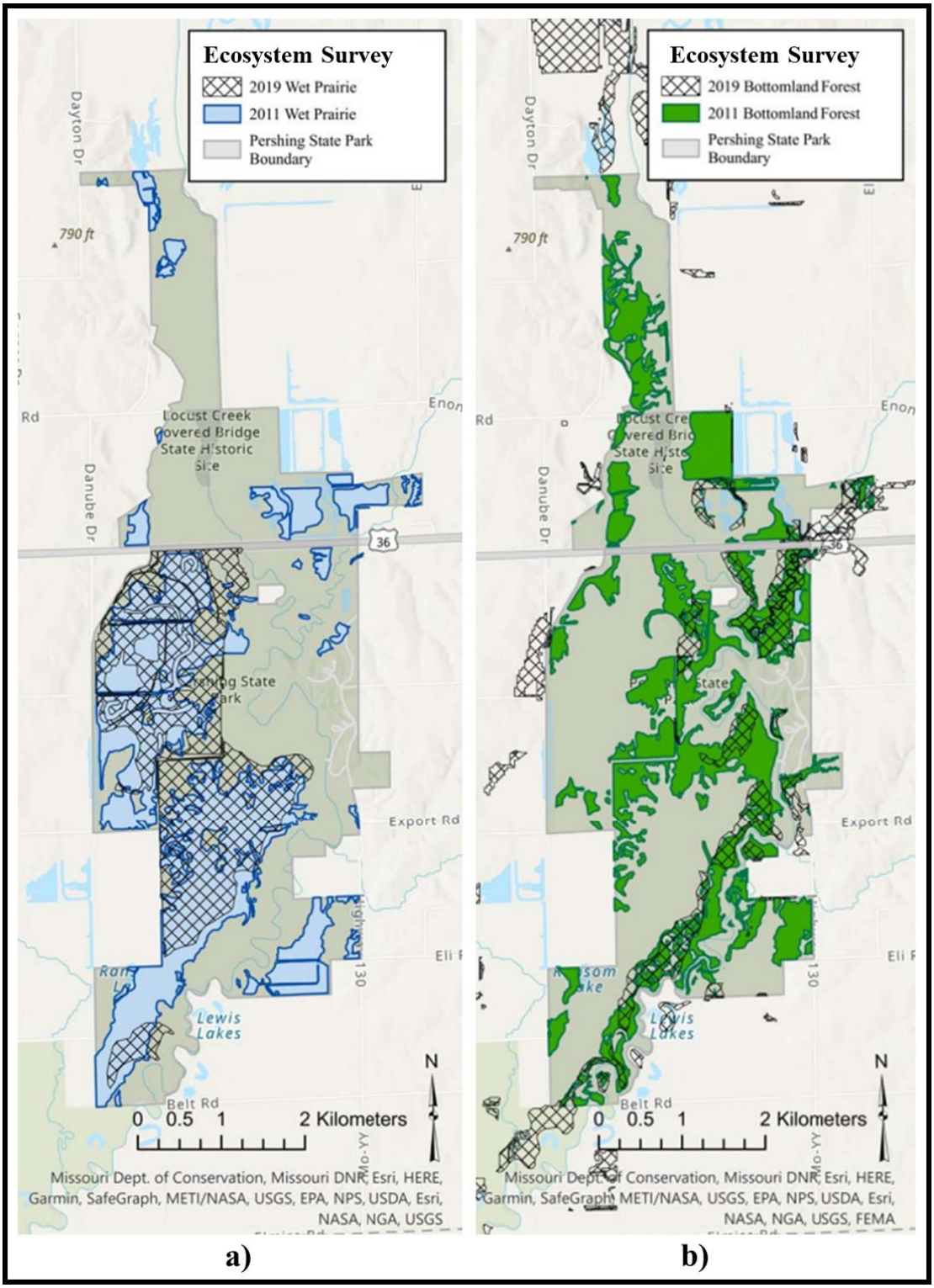

Figure 3:
Ecosystem Spatial Changes within Pershing State Park between 2011 and 2019.
a) Map of spatial extents for wet prairie communities. b) Map of spatial extents for bottomland hardwood forests.

Large Woody Debris (LWD)

Large woody debris (LWD) is common within Pershing State Park and had to be incorporated into the analysis. LWD is often considered beneficial for providing aquatic habitat and function (Hafs et al., 2014; Keys et al., 2018; Roni et al., 2014). However, LWD significantly impacts channel and floodplain hydraulics by increasing floodplain connectivity (Brummer et al., 2006; Covino, 2017; Keys et al., 2018), increasing stage (Brummer et al., 2006; Keys et al., 2018; Phillips, 2012), decreasing velocity (Davidson & Eaton, 2013; Keys et al., 2018; Shields Jr et al., 2003), and influencing sediment transport and channel geomorphology (Davidson & Eaton, 2013; Montgomery et al., 2003; Pagliara & Carnacina, 2011; Parker et al., 2017). Several of these components, including increased stage, may contribute to avulsion formation (Brummer et al., 2006; Phillips, 2012; Sear et al., 2010; Wohl, 2011), similar to the avulsion between Locust Creek and Higgins Ditch. As a result, LWD or log jams are often removed from river channels to reduce flood impacts to surrounding land and infrastructure (Pagliara & Carnacina, 2011; Wohl & Beckman, 2014), as was the case in the Locust Creek Basin.

Since 1993, log jam formation and removal were regular occurrences in Pershing State Park. Records of log jam removal between 2008 and 2018 were available from MoDNR, U.S. Geological Survey (USGS) Special Investigation Report (SIR) 2017-5120 (Heimann & Survey, 2017), Google Earth, and project staff (Woodward, 2020). Figure 4 displays the location of each documented log jam, the year of removal, and associated log jam length. Locust Creek log jam surveys in 2015 indicated that most of the LWD were 0.3 to 0.6 meters in diameter, 1.5 to 4.9 meters in length (less than one-half of the channel width), and displayed signs of advanced decay. The overall length relative to the channel width indicated that the LWD was easily transportable, and the advanced decay condition indicated that the LWD originated from outside of Pershing

State Park. Approximately 20% of the surveyed LWD had root wads indicating bank erosion as a source (Heimann & Survey, 2017).

Pershing State Park
Log Jams
2007-2018

Log Jam ID	Year Log Jam Removed	Log Jam Length, m
1	2008	792
2	2008	610
3	2009	91
4	2009	823
5	2011	91
6	2011	91
7	2012	46
8	2013	762
9	2015	152
10	2015	61
11	2015	61
12	2016[1]	762

[1] Log jam removal process initated in 2016 but was not completed until 2017. Month of completion in 2017 is unknown so full log jam was only applied to 2016.

[2] Data and parameter estimates courtesy of Mr. Tom Woodward, MoDNR (Woodward, 2020)

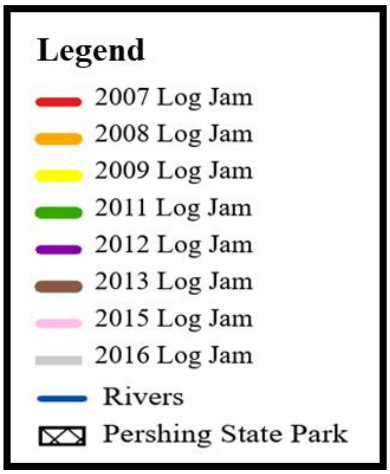

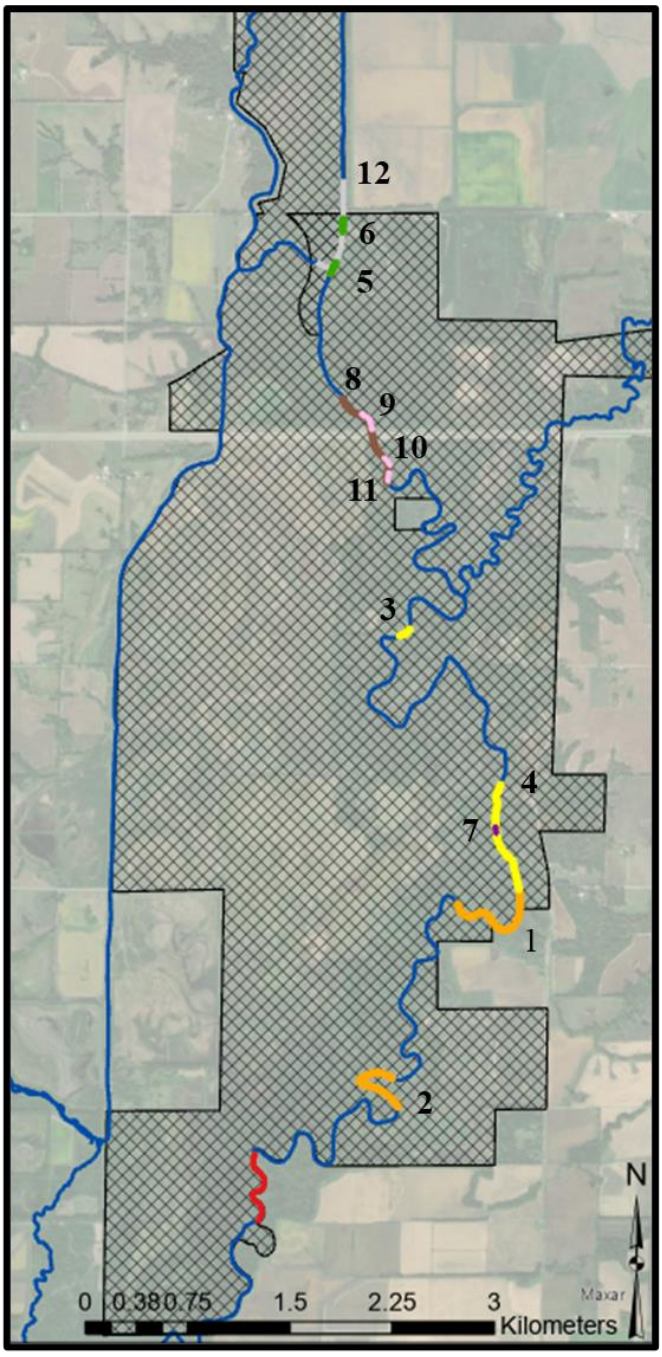

Figure 4:
Log Jams Identified by MoDNR and Google Earth from 2007 to 2018

Log jams were influential in changing stream hydraulics within the Locust Creek and Grand River watersheds. As previously indicated, changing upstream landcover and hydrology contributed to increased streamflow (Bradshaw et al., 2007; Clark, 1987; Laurance, 2007; O'Connell et al., 2007; Poff et al., 1997) which then, in turn, altered channel and floodplain hydraulics. These changes may be displayed as increased floodplain inundation, bank erosion, and sedimentation (Gellis et al., 2016; C. Hupp et al., 2013; Keys et al., 2018). In Locust Creek, the altered hydraulics impacted riparian communities, contributing to hardwood degradation (U.S. Army Corps of Engineers, 2020). The degradation then lead to fallen trees and increased LWD load and log jam formations which then altered channel and floodplain hydraulics, ultimately creating a cyclical process. Figure 5 displays the Locust Creek hydraulics and LWD cycle. Due to

the significant impact of LWD on altered hydraulics within Locust Creek and Pershing State Park, log jams were represented in the hydraulic model.

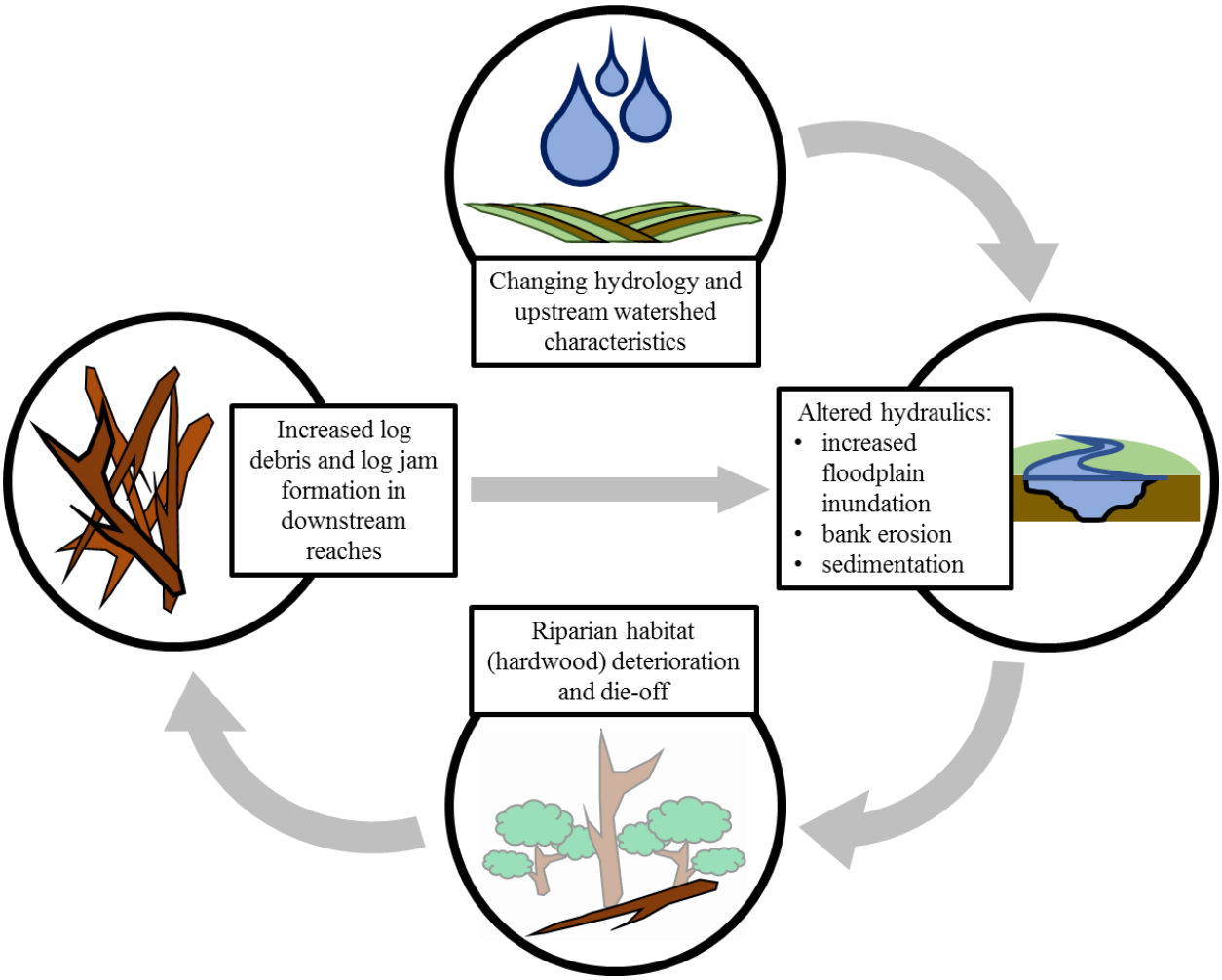

Figure 5:
Locust Creek Hydraulics and Woody Debris Life Cycle

This thesis investigated wetland community outcomes resulting from hydraulic influences and log jams. Sedimentation and erosion impacts were not included within the analysis.

Hydraulic Modeling Approach

This study utilized the HEC River Analysis System (RAS) to simulate 2D hydraulics within the Locust Creek floodplain and Pershing State Park from 2008 to 2018. Several HEC-RAS technical reference manuals provided detailed descriptions pertaining to the 2D theory and computation methodology including the USACE 2016 HEC-RAS Hydraulic Reference Manual and the USACE 2016 HEC-RAS 2D Modeling User's Manual (U.S. Army Corps of Engineers Hydrologic Engineering Center, 2016b, 2016a). In summary, 2D HEC-RAS utilized cells and cell faces to compute 2D hydraulics. Each cell face acted similar to a cross section in one-dimensional open channel hydraulics. The cell face topography was based off the underlying HEC-RAS terrain. Detailed hydraulic property tables were computed for each cell face including area, wetted perimeter, area roughness, and conveyance – elevation curves. Additionally, a volume-elevation curve was computed for every cell (U.S. Army Corps of Engineers Hydrologic Engineering Center, 2016b). These tables combined with the 2D Saint-Venant or Diffusion Wave equations were then used to compute the flow entering and leaving each cell. Both equation sets were simplified Navier-Stokes equations assuming incompressible flow, uniform density, and hydrostatic pressure. Additionally, the equations utilized mass conservation and momentum conservation (U.S. Army Corps of Engineers Hydrologic Engineering Center, 2016a). More detailed information related to the program calculations are available in the previously mentioned reference manuals.

Several files were required for a HEC-RAS simulation to run. Each simulation was primarily comprised of three files including a geometry file (.g0#), flow file (.f0# or .u0#), and plan file (.p0#). The geometry file contained all the information related to the computation grids including, but not limited to, the model spatial domain, cross section data or topography, channel

alignments, roughness coefficients, boundary condition locations, breaklines, and much more. Geometry files include associations with landcover datasets and topographic information. For 2D models, the spatially varied roughness coefficients were saved in a Landcover layer within RAS Mapper. RAS Mapper was a user interface for editing geometries and spatially displaying geometries, HEC-RAS terrains, and simulation results. Two types of flow files were available in HEC-RAS. A steady flow file, designated with a. f0# in the file name, was used to simulate temporally constant flows at the model boundary conditions. An unsteady flow file, designated with a. u0# in the file name, simulated temporally variable flows. These files referenced the HEC Data Storage System Visual Utility Engine (DSSVue) files containing developed time series discussed in Appendix A. Additionally, these files allowed the user to establish initial conditions and boundary condition characteristics. The plan file created an alternative or simulation by allowing the user to select combinations of geometry and flow files. The plan file also specified the simulation time frame, computational interval, computational tolerances, computation equation set, and other parameters.

Hydraulic Model Development

The analysis simulated 2D channel and floodplain hydraulics through the development of a HEC-RAS model. The model was adapted from an existing hydraulic model of the Lower Grand River (LGR model) documented in the 2020 Grand River Feasibility Study (U.S. Army Corps of Engineers, 2020). The model was maintained in HEC-RAS version 5.0.7. The vertical datum used in the HEC-RAS model was North American Vertical Datum 1988 (NAVD88) and the projection was North American Datum 1983 (NAD83) Universal Transverse Mercator (UTM) 15N U.S. Feet. Time series data was in Coordinated Universal Time (UTC).

HEC-RAS Terrain. The "2018_10_18_ExistingConditions(FWOP_Year0)" HEC-RAS terrain from USACE, documented in the 2020 Grand River Feasibility Report Appendix B, was used for the bathymetric data and floodplain topography (U.S. Army Corps of Engineers, 2020). The floodplain topography was developed from one-meter Light Detection and Ranging (LiDAR) data collected in February of 2017. The LiDAR was produced in NAD83 UTM Zone 15, NAVD88 Geoidl12B Survey Feet with a mean vertical error of -0.003 meter (Woolpert Inc., 2017). Channel bathymetry was represented with surveyed cross sections collected between fall 2016 and spring 2017 by USACE Kansas City District, River Engineering Section. Several survey methods were used to collect cross section information including hydrosurvey and range poles and virtual reference stations (VRS). The cross sections were then used to develop a HEC-RAS terrain representing the channel data that was then superimposed onto the LiDAR surface. Additional data pertaining to HEC-RAS terrain components and development are found in the USACE 2020 Grand River Feasibility Report Appendix B (U.S. Army Corps of Engineers, 2020).

Pershing State Park elevation changes were observed by project staff in the 10-year period of analysis between 2008 and 2018 in the form of sedimentation and erosion. However, insufficient data was available to quantify sedimentation amounts and incorporate temporally varying ground surface elevations into the model. Although 2009 and 2018 LiDAR datasets were available for comparison, there was insufficient commonality between survey conditions and collection methodology, preventing direct comparisons and elevation magnitude quantification. As a result, all hydraulic simulations, used a singular, stationary HEC-RAS terrain (described in the previous paragraph) for analysis. As a result, geomorphic and floodplain sedimentation impacts resulting from log jams and changing hydraulics were not captured in this analysis. Increased floodplain sedimentation can contribute to habitat zonation in floodplains (van Eck et al., 2006) by altering

floodplain elevations and associated flood frequency. Incorporation of dynamic sediment modeling would help to improve simulation of channel aggradation/degradation, log jam formations, and floodplain sedimentation which could be used to inform adjustments to flood frequency and predict sediment induced seedling mortality.

Model Domain. The adapted model domain or spatial boundary was determined by the location of the 2D perimeter. The 2D perimeter was a polygon within HEC-RAS used to generate cells for the model. The 2D perimeter was adjusted to encompass the entire Locust Creek floodplain from the USGS gage at Calico Road near Linneus, MO to the confluence with the Grand River. Additionally, the model domain included the Grand River floodplain from the USGS gage near Fountain Grove to the Burlington Northern Santa Fe (BNSF) railroad bridge near Sumner, MO. The Grand River was included in the model to account for Grand River backwater effects on Locust Creek. The model domain incorporated all of Pershing State Park including areas that received and lost flow over the past ten years. Where possible, the perimeter was oriented perpendicular to major inflow locations and was placed on elevated surfaces, such as bridges, oriented perpendicular to streams. The 2D perimeter extended approximately 335 meters north and west of the intersection of Ames Road and Crow Drive near Hickory Branch. On the east side of the floodplain, the perimeter extended to the Hannibal and St. Joseph railroad perpendicular to Muddy Creek, just north of Highway 36. Figure 6 displays the model domain.

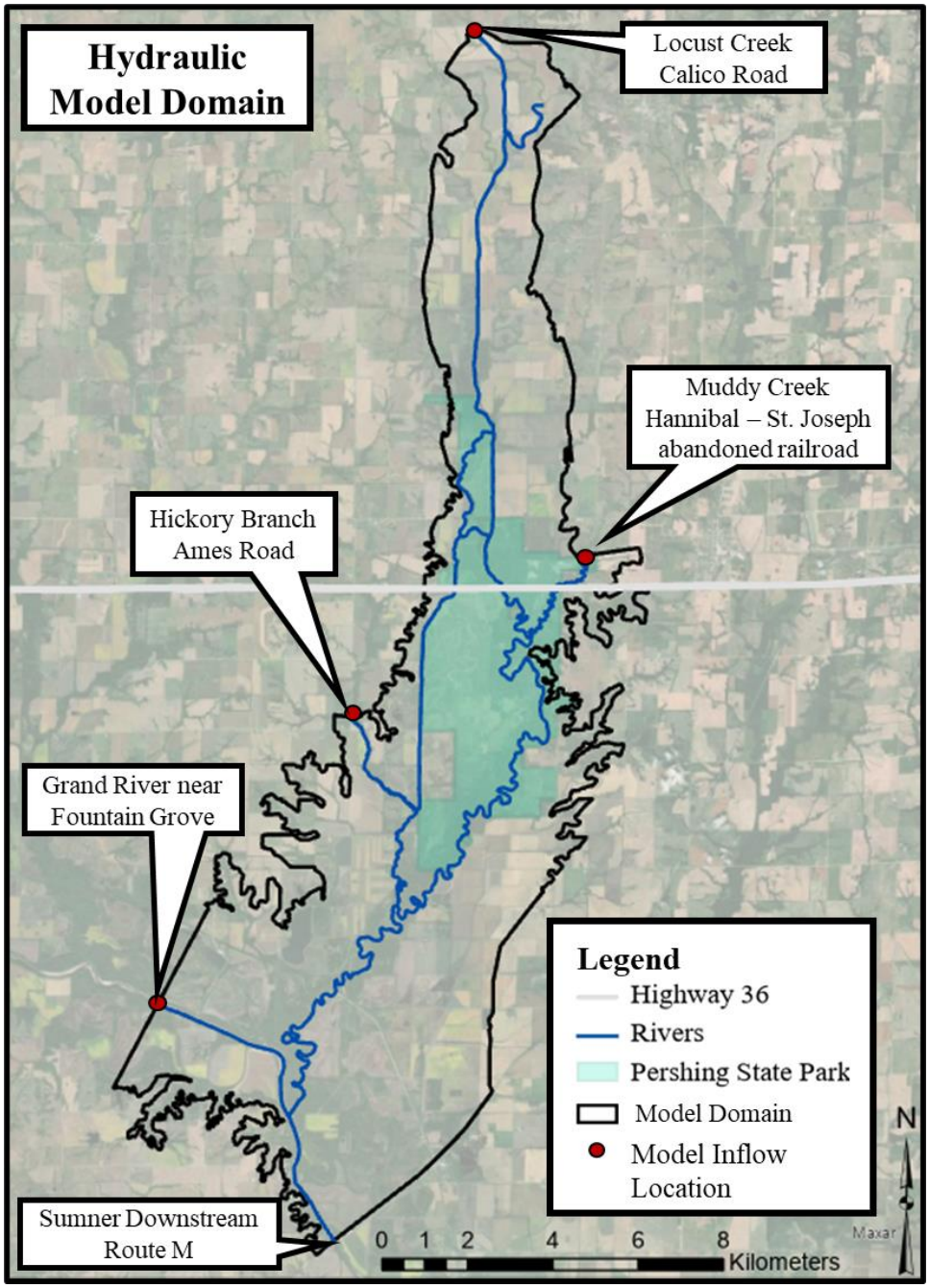

Figure 6:
Model Domain and Inflow Locations

Boundary Conditions. Inflows and outflows at domain boundaries were developed from a combination of USGS flow records, HEC-HMS generated flows, interpolated and factored flows. USGS flow records for Locust Creek at Linneus, MO and USACE Grand River HEC-HMS model outflows (U.S. Army Corps of Engineers, 2020) were used to simulate a continuous period of

record, as described in Appendix A, through the HEC-RAS model. The inflows were placed at various upstream boundaries including Grand River near Fountain Grove, Locust Creek near Linneus, MO, Muddy Creek at the Hannibal and St. Joseph railroad, and Hickory Branch 335 meters north and west of the intersection of Ames Road and Crow Drive. Normal depth was used for the downstream boundary condition located at the Grand River near Sumner, MO USGS gage. The hydrograph energy grade line (EG) slopes and normal depth friction slope were estimated by measuring the slope of the channel bed near the inflow location. Three channel slope measurements were extracted from the HEC-RAS terrain and the average of the measurements was used as the slope. Boundary conditions used in the model are summarized in Table 2. Boundary conditions were placed across the entire floodplain rather than being confined solely to the channel.

Table 2:
Boundary Condition Summary

Boundary Condition Name	Boundary Condition Type	EG Slope or Friction Slope, m/m
Hickory_Branch	Flow Hydrograph	0.001
Grand_FG	Flow Hydrograph	0.0001
Muddy Creek	Flow Hydrograph	0.0009
Locust Creek	Flow Hydrograph	0.0003
GR_Sumner	Normal Depth	0.0007

Continuous time series between 2008 and 2018 were developed for all model inflow locations and were used in the unsteady flow files. Detailed methodology pertaining to time series development was documented in Appendix A. The time series consisted of a combination of USGS instantaneous observed flows and HEC-HMS generated flows documented in the 2020 Grand River Feasibility Report. When available, 15-minute increment data (also known as instantaneous data) was used in the time series. Instantaneous data captured peaks of individual events whereas daily averaged data primarily focused on volume and can misrepresent hydrograph peaks. This is

especially true if typical event durations were less than one day. HEC-HMS generated flows were used to supplement periods of missing data in observed records and to simulate ungaged inflows. All inflow time series were converted to hourly time steps. Additional methods including interpolation and drainage-area ratios were used to extend records and supplement remaining missing values within the time series.

Computational Grid Details. Computational grids were adjusted to add additional detail and refine areas of analysis using breaklines and internal 2D area connections. Breaklines were added to the model to identify high ground or topographical components such as levees, roadways, and channel overbanks, that influence and control channel and floodplain hydraulics. Breaklines forced cell faces to align along the breakline, causing the cell to recognize the high ground and prevent water from passing through the elevated surfaces. Breaklines were placed along the banks and centerline of stream channels to align the cell faces within the channel, perpendicular to flow. The breaklines placed along the banks separated the channel from the floodplain, ensuring that water would only enter the floodplain when the water surface elevation exceeded bank elevations.

Internal 2D area connections allow the computational grids to override terrain elevations and model important hydraulic structures such as bridges and culverts to improve hydraulic connectivity. Internal 2D area connections were used to model culverts to simulate drainage from levee protected fields after levees were overtopped. Additionally, the internal 2D area connections were used to override false HEC-RAS terrain elevations, such as a levee breach. The same internal 2D area connection assumptions documented in the 2020 Grand River Feasibility Report were also applied within the model domain. The culverts included in the model were not surveyed. As a result, the culvert sizes may not be accurately portrayed and could impact inundation duration of

leveed areas. Internal 2D area connections were deleted if the structures were located outside of the adjusted modeling domain.

Since Dobbins Notch was created in 2010, in the middle of the analysis period, two different computation grids were developed for the two conditions. In addition, two computational grid resolutions were developed for each time period, resulting in four total computation grid configurations. One computation grid was developed for the 2008 to 2009 time periods and included an internal 2D area connection at Dobbins Notch. The Dobbins Notch internal 2D area connection adjusted the HEC-RAS terrain elevations such that the pre-existing levee was still intact. The second computation grid was developed for the 2010 to 2018 time periods and did not include an internal connection at Dobbins Notch. This was because the HEC-RAS terrain, representative of 2017 topography, already captured the notched levee computation grid. The four-computation grid configuration names and descriptions are provided in Table 3.

Table 3:
Base Computational Grids and Descriptions

Geometry Name	Description
LC_100ft_2008-2009	The computation grid utilized 30.5-meter by 30.5-meter (100-foot by 100-foot) cells throughout the entire model domain with slight cell size adjustments in isolated locations for model stability. An internal 2D area connection was placed along Dobbins Notch and the internal connection elevations were adjusted to reflect the existence of a completely intact levee.
LC_100ft_2010-2018	The computation grid utilized 30.5-meter by 30.5-meter (100-foot by 100-foot) cells throughout the entire model domain with slight cell size adjustments in isolated locations for model stability. No adjustments were made to the geometry to adjust Dobbins Notch since the HEC-RAS terrain already represented the notched levee.
LC_25ft_2008-2009	The computation grid utilized 7.62-meter by 7.62-meter (25-foot by 25-foot) cells within Pershing State Park areas of wetland community importance with slight cell size adjustments in isolated locations for model stability. An internal 2D area connection was placed along Dobbins Notch and elevations were adjusted to reflect the existence of a completely intact levee.
LC_25ft_2010-2018	The computation grid utilized 7.62-meter by 7.62-meter (25-foot by 25-foot) cells within Pershing State Park areas of wetland community importance with slight cell size adjustments in isolated locations for model stability. No adjustments were made to the geometry to adjust Dobbins Notch since the HEC-RAS terrain already represented the notched levee.

The base computation grids were then copied as needed to create a geometry files for each simulation year between 2008 and 2018.

Model Selection and Calibration

Model calibration was important to ensure that selected model parameters produced results that accurately portrayed observed conditions. As part of the model selection process, sensitivity to the computational methodology was investigated by comparing simulated results using both diffusion wave and full momentum equation sets. The simulated water surface elevations, depths, and downstream discharges were calibrated to available observational data by adjusting Manning's roughness coefficients, and downstream boundary friction slope. Two different events were used for calibration: one without a log jam and one with a log jam present. The first non-log jam calibration event occurred in April of 2017 and was used to calibrate the overall model characteristics such as roughness coefficients, friction slope at the normal depth downstream boundary. The resulting calibrated parameters were then applied to the log jam calibration event. The log jam calibration event occurred in March 2009 and was used to only calibrate a roughness coefficient associated with log jams based on inundation extent. Observational log jam data such as time of occurrence, length, and width were available from MoDNR, USGS SIR 2017-5120 (Heimann & Survey, 2017), Google Earth, and project staff (Woodward, 2020). Full calibration details are provided in Appendix B.

Calibration Data. Several sources of data were used to calibrate the model to the April 2017 and March 2009 events. The April 2017 event was calibrated to several sources of data including highwater marks (HWMs), USGS streamflow generated from a rating curve, and USGS instantaneous streamflow measurements. Surveyed HWMs were given the highest priority with respect to calibration because they were located within the Pershing State Park boundary. In other

words, calibrated parameters producing results that most closely represented the HWMs were used. HWMs included, but were not limited to, water lines on trees and debris lines. HWMs are impacted by wind wave action, super elevation, and debris which may push the water surface elevation to higher elevations in isolated locations. Additionally, due to the frequency of Locust Creek flood events, high water marks may be representative of different hydraulic events. As a result, HWMs can introduce error into the model. However, the HWMs provide a measurement of the floodplain hydraulics within Pershing State Park.

Log jam roughness was calibrated to aerial inundation extent imagery for the March 2009 event. Inundation extents and duration from aerial imagery were previously used to quantify wetland change in other studies (Martínez-Espinosa et al., 2021). Additional datasets including soil moisture and other sources of aerial imagery were used to quantify wetland change (Martínez-Espinosa et al., 2021); however, available datasets were too coarse to be applied to Pershing State Park. As a result, USGS Landsat 7 aerial imagery was used to calibrate the model for log jams. USGS Landsat 7 aerial imagery, available from the USGS LandLook web tool (U.S. Geological Survey, 2018), displayed inundation extents on March 14th, 2009 as a result of flooding from the March 2009 event. However, a timestep was not included. As a result, it was assumed that the image, collected during daylight hours, was collected at 1200 hours.

Analysis. The simulated downstream discharges, velocities, depths, and water surface elevations developed with the final calibration parameters were compared to USGS observed hydrographs, USGS field measurements, and USACE HWMs for the April 2017 event. The log jam model simulated inundation extents were visually compared to aerial inundation extent imagery for the March 2009 event.

Additionally, the Nash-Sutcliffe model efficiency (NSE), was used to compute how well the Grand River flows at Sumner predicted the USGS observed flows. NSE for each simulation was computed using Equation 1 where y_i was the observed USGS flow at a given time step, $y_{i,sim}$ was the simulated flow at a given time step, and $\bar{y}$ was the average observed USGS flow for the simulation period. In a perfect model, the NSE would equal 1.0.

Equation 1: $$NSE = 1 - \frac{\sum(y_i - y_{i,sim})^2}{\sum(y_i - \bar{y})^2}$$

Appendix B provides more detail pertaining to calibration parameters selection and analysis.

Model Validation

A validation process was applied to the model to ensure that the calibrated parameters produced results representative of observed datasets when applied to simulations that occurred outside of the calibration events. Similar to calibration, the model simulated results were validated against two different events: one without a log jam and one with a log jam present. However, parameters were not adjusted in order to analyze the effectiveness of the selected calibrated parameters in reproducing independent time series. The first validation event from October 7th, 2018 to October 15th, 2018 did not include a log jam and was used to validate overall model characteristics such as roughness coefficients, downstream boundary friction slope, and computation equation set. The second validation event occurred between March 24th and April 2nd of 2009 on Locust Creek during a year where a log jam was documented within Pershing State Park. Simulated water surface elevations were compared against observed inundation extents from the log jam event to validate the roughness coefficient associated with log jams. Appendix C provides detailed documentation pertaining to the validation process.

Validation Data. Several sources of data exist for model calibration including HWMs, USGS streamflow, and aerial imagery. The October 2018 event was selected for calibration because of data availability throughout the floodplain in Pershing State Park via HWMs. As previously discussed, HWMs may introduce error into the model. However, the HWMs provided a measurement of the floodplain hydraulics within Pershing State Park. Aerial imagery was used to validate the inundation extents in areas where HWMs and USGS measurements were unavailable. USGS Landsat 7 aerial imagery, available from the USGS LandLook web tool (U.S. Geological Survey, 2018), displayed inundation extents on October 24th, 2018 as a result of flooding from the October 2018 event. However, there was uncertainty associated with the time of day the Landsat 7 image was collected.

Simulated water surface elevations were validated against aerial imagery of observed inundation extents for the April 2009 event. Inundation extents and duration from aerial imagery were previously used to quantify wetland change in other studies (Martínez-Espinosa et al., 2021). Additional datasets including soil moisture and other sources of aerial imagery were used to quantify wetland change (Martínez-Espinosa et al., 2021); however, available datasets were too coarse to be applied to Pershing State Park. As a result, USGS Landsat 7 aerial imagery was used to validate the model for log jams. USGS Landsat 7 aerial imagery, available from the USGS LandLook web tool (U.S. Geological Survey, 2018), displayed inundation extents on April 7th, 2009 as a result of flooding from the April 2009 event. However, a timestep was not included. As a result, it was assumed that the image, collected during daylight hours, was collected at 1200 hours.

Analysis. The simulated downstream discharges, velocities, depths, water surface elevations, and inundation extents developed with the final calibration parameters were compared

to USGS observed hydrographs, USACE HWMs, and aerial imagery for the October 2018 event. The log jam model simulated inundation extents were visually compared to aerial inundation extent imagery for the April 2009 event. Additionally, the NSE, was used to compute how well the Grand River flows at Sumner predicted the USGS observed flows for the October 2018 event. NSE for each simulation was computed using Equation 1.

The simulated Grand River time series between 2008 and 2018 was compared to observed USGS peak event flows. For each year, the three highest peak Grand River hydrograph flows with corresponding observed USGS flows were extracted from the model at Sumner, MO and used to compute the NSE using Equation 1. Only peak flows were analyzed so that the NSE was representative of how well the model simulated peak flows not overall streamflow conditions. Three maximum peak event flows from each annual simulation were used to ensure flows from each annual simulation were included in the peak flow analysis. If, for instance, a bankfull threshold was used to filter peak flows instead of the three maximum peak event flows, data would not be included from 2012 and 2013 because those years simulated dry conditions.

Appendix C provides more detail pertaining to calibration parameters selection and analysis.

Habitat Analysis Methodology

In order to identify hydraulic metrics that could be used to forecast wetland risk and improve understanding of large-scale hydraulics on wetland trajectories, predicted wetland community transitions based on hydraulic metrics from model output were compared to observed actual transitions. Hydraulic parameters from the 2D unsteady flow model, included depth and duration, and were extracted annually. Annual changes in the hydraulic parameters including inundation duration and depth were compared and related to the wetland characteristics and habitat

metrics to determine changes in wetland classifications and land cover. The wetland change predictions based on the hydraulic model parameters were compared to observed wetland extents in 2011 and 2019 bottomland hardwood and wet prairie community. In order to identify monitored hydraulic metrics that could be used to forecast wetland risk and improve understanding of large-scale hydraulics on wetland trajectories.

Wetland Type Indicators

Initial values for hydraulic thresholds in inundation duration, inundation depth, and dry days were established for both bottomland hardwoods and wet prairies based on the existing literature. Inundation duration was representative of the number of consecutive days the wetland community could withstand being flooded. Long periods of continuous inundation can damage or kill both bottomland hardwood and wet prairie. Increases in inundation duration cause increases in seedling mortality (Kabrick et al., 2012; Krzywicka et al., 2017) via oxygen deprivation (Briscoe, 1961; Guo et al., 1998; Hall & Smith, 1955; Hook, 1984; Hosner, 1958, 1960). Inundation depth represented the maximum depth of water that the wetland community could withstand. When the inundation depth exceeds plant heights (tree saplings, leaves, etc.) the water column can impact nutrient and light availability (S. Kercher et al., 2007), negatively impacting both bottomland hardwoods and wet prairie. Dry days were representative of the number of days without flooding that was beneficial for the wetland communities. Historically, bottomland hardwoods and wet prairies were tolerant of both wet and dry conditions and benefited from seasonal drought and fire (Hanberry et al., 2014; Nelson, 2010; Slaughter & Kost, 2010). Reduction in the number of dry days or increasingly wetter conditions could negatively impact both bottomland hardwoods and wet prairies.

While habitat suitability metrics varied from species to species and were based on a wide variety of factors, general assumptions of community response were used to establish metrics for both bottomland hardwood forests and wet prairie. The metrics were largely based on assumptions determined by local conservation experts and state park managers familiar with Pershing State Park and Missouri ecosystems (USACE, 2020). Table 4 and Table 5 provide the initial metrics and descriptions of the criteria used for habitat analysis of bottomland hardwood forests and wet prairie, respectively.

Habitat suitability metrics for bottomland hardwood forests were largely related to seedling recruitment. Noticeable changes in bottomland hardwood forests resulting from mature specimen decay occurred over the course of several decades and, as a result, may not be apparent within the 10-year study period. Since seedlings were much smaller than mature trees, they were likely more sensitive to smaller inundation depths associated with more frequent events and had a better likelihood of being captured within the study period.

Habitat suitability metrics for wet prairies were largely related to summer growing conditions. The survival of wet prairie species during flooding conditions was largely dependent on the height of the vegetation and, thus, timing of flood events within the growing season. By July, wet prairie vegetation within Missouri was usually 0.6 to 0.9 meters tall and could withstand flood events producing depths less than the vegetation height (Nelson, 2010; Weaver, 1960).

Table 4:
Bottomland Hardwood Forest Habitat Suitability Metrics

Bottomland Hardwood Forest			
Hydraulic Parameter	**Metric (Ideal Conditions)**	**Description**	**References**
Inundation Duration	< 14 consecutive days between 7/1 - 9/30	Seedlings were largely impacted by flooding from mid-summer to early fall (7/1 - 9/30). During this time, seedlings could withstand two weeks of inundation. However, if flood	(Nelson, 2010; U.S. Army Corps of Engineers, 2020)

Bottomland Hardwood Forest			
Hydraulic Parameter	**Metric (Ideal Conditions)**	**Description**	**References**
		duration exceeded 14 consecutive days, then the seedlings drowned.	
Inundation/Flood Depth	< 0.15 meters between 7/1 - 9/30	Seedlings were largely impacted by flooding from mid-summer to early fall (7/1 - 9/30). During this time, flood depths exceeding 0.15 meters essentially drowned new seedlings, preventing recruitment.	(U.S. Army Corps of Engineers, 2020)
Dry Days	>214 dry days between 4/15 - 11/30	Seasonal drought was beneficial for bottomland hardwoods which, historically, were impacted by fire. Ideal dry conditions included approximately 93.33% dry days of the growing season (4/15 - 11/30), which translated to approximately 214 days of dry conditions.	(U.S. Army Corps of Engineers, 2020)
Key Species:	Bur Oak, Pin Oak, Pecan, Green Ash, Sugarberry, Slippery Elm, False Nettle, Goldenglow, Yellow Ironweed, Late Goldenrod, Sedges, Wood Reed Grass (Nelson, 2010)		

Table 5.
Wet Prairie Habitat Suitability Metrics

Wet Prairie			
Hydraulic Parameter	**Metric (Ideal Conditions)**	**Description**	**References**
Inundation Duration	< 30 consecutive days between 7/1 - 10/31	Wet prairie was largely impacted by flooding from mid-summer to mid-fall (7/1 - 10/31). During this time, plants could withstand 30 consecutive days of inundation. However, if flood duration exceeded 30 consecutive days more often than 4 out of 10 years, then the community may transition to emergent marsh (Nelson, 2010)	(Banach et al., 2009; S. Kercher et al., 2007; Nelson, 2010; Olmstead & Loope, 1984; U.S. Army Corps of Engineers, 2020)
Inundation/Flood Depth	< 0.61 meters between 7/1 - 10/31	Water was essential to the survival of wet prairie; however, the relationship between survival and water depth was largely dependent on plant height. Between mid-summer and mid-fall (7/1 - 10/31), plant heights were usually taller than 0.61 meters. As a	(Banach et al., 2009; Nelson, 2010; Olmstead & Loope, 1984; U.S. Army Corps of

Wet Prairie			
Hydraulic Parameter	**Metric (Ideal Conditions)**	**Description**	**References**
		result, wet prairie could survive water depths less than 0.61 meters during this time.	Engineers, 2020; Weaver, 1960)
Dry Days	>75 dry days between 7/15 - 10/31	Seasonal drought is beneficial for wet prairies which, historically, lack standing water by the end of summer for approximately eight to ten years. Ideal dry conditions include approximately 68.85% dry days between mid-summer and mid-fall (7/15 - 10/31), which translates to approximately 75 days of dry conditions.	(Nelson, 2010; U.S. Army Corps of Engineers, 2020)
Key Species:	Prairie Cordgrass, bluejoint, smartweeds, sedges, swamp milkweed, asters, false aster, sawtooth sunflower, ironweed, southern blue flag, water parsley, rice cutgrass, tickseed sunflower, false indigo, buttonbush (Nelson, 2010)		

Depth Threshold: Duration and Recession Maps

Duration, arrival time, and recession map results were extracted from RAS Mapper using a depth threshold calculated for each wetland community type. Since HEC-RAS 5.0.7 did not account for gridded infiltration process, the depth threshold selected was based off a representative soil infiltration rate for each wetland community type. The depth threshold was calculated using the hydraulic conductivity associated with the most prominent soil type located within the wetland community of interest spatial extents. More specifically, county soil data collected between 1998 and 2020 from the Soil Survey Geographic (SSURGO) database were overlaid by the 2019 ecosystem extents for bottomland hardwood forest and wet prairie in Aeronautical Reconnaissance Coverage Geographic Information System (ArcGIS) Pro version 2.6.1. The area of each soil texture classification within the respective Pershing State Park ecosystem boundaries was computed with the "Tabulate Area" geoprocessing tool. These areas were then divided by the total

wetland community area within Pershing State Park to determine the percentages of soil type comprising each habitat. The results are provided in Table 6.

Table 6:
Percentage of Soil Classification within Pershing State Park Wetland Communities

Wetland Community	Total Area, km^2	Clay Loam	Silt Loam	Silty Clay Loam	Clay	Water
Bottomland Hardwood	2.15	0.00%	7.60%	92.3%	0.07%	0.00%
Wet Prairie	5.70	0.00%	5.21%	25.2%	69.6%	0.00%

Based on the results, silty clay loam and clay were the dominant soil textures within bottomland hardwood and wet prairie communities, respectively. The associated hydraulic conductivities for silty clay loam and clay were 0.10 centimeters (cm) per hour and 0.03 cm per hour, respectively (Rawls et al., 1983). Since the HEC-RAS model used a mapping output interval of two hours, the hourly hydraulic conductivity rates were multiplied by two to represent the depth of water that would possibly move through the soil column within the mapping output interval. The computed depths of 0.20 cm and 0.06 cm were used as the final duration depth thresholds for bottomland hardwood forest and wet prairie, respectively.

Inundation Duration

Simulations. The number of consecutive days of inundation duration was computed for both the bottomland hardwood and wet prairie growing seasons for each year of simulation. RAS Mapper computed duration as the difference between recession time and arrival time. Recession time was defined as the time water in a cell last fell below the specified depth threshold in a simulation. Arrival time was defined as the time water in a cell first exceeded the specified depth threshold in a simulation. With this methodology, RAS Mapper did not calculate the consecutive number of days a cell was inundated or the amount of time the water depth is above the specified threshold. Instead, duration computations in RAS Mapper was based on the assumption of a single

event and disregarded the time between events when water fell below the depth threshold and then rose above the threshold again (Figure 7). As a result, the consecutive number of days inundated could not be directly exported from RAS Mapper.

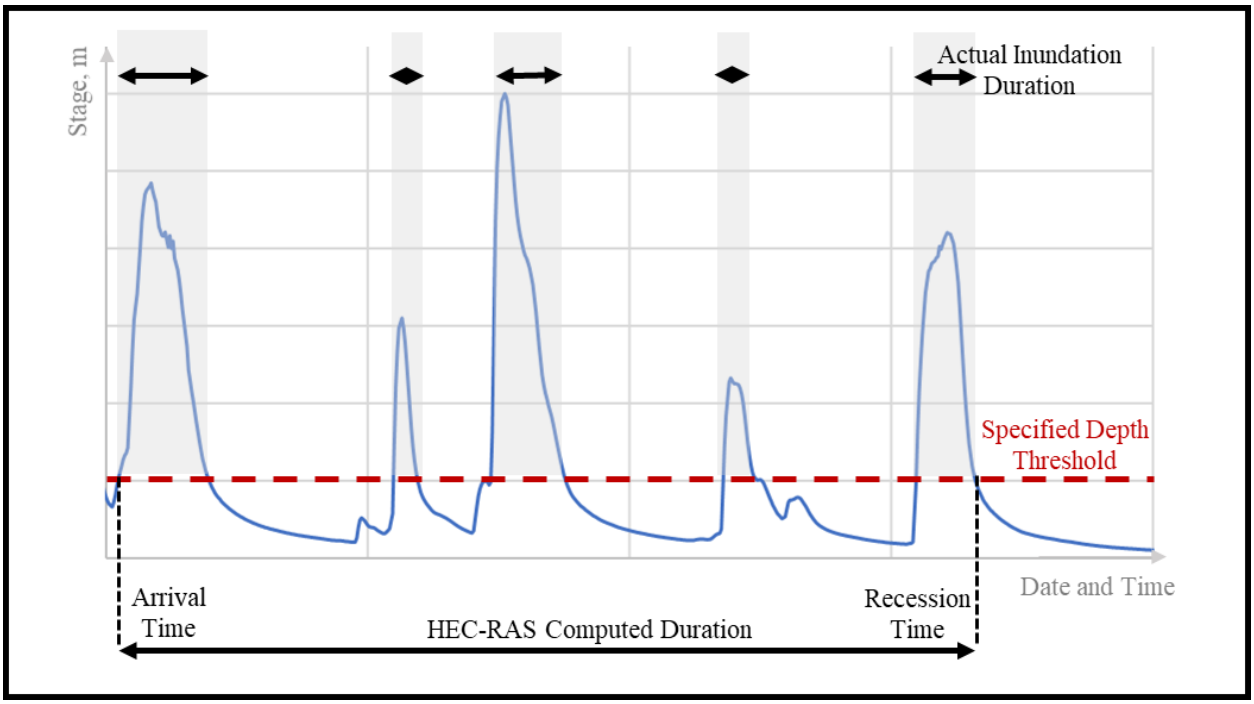

Figure 7:
Comparison Between HEC-RAS Computed Duration and the Actual Inundation Duration of a Cell

Since RAS Mapper did not account for possible dry days between multiple events, multiple simulations were created to isolate each hydrograph peak. The hydrograph peak or event resulting in the largest inundation was the primary focus for the simulations. More specifically, inundation extent for the growing seasons for each year were visually examined in RAS Mapper and engineering judgement was used to identify the event that contributed to the largest widespread flooding and took the longest amount of time to drain. Usually, the start of the rising limb associated with this event was set as the start time of the first simulation. The simulation end date and time were adjusted to at least include the minimum number of days specified in Table 4 and Table 5 (14 consecutive days for bottomland hardwood and 30 consecutive days for wet prairie).

If needed, additional consecutive simulations were added to ensure that the total combined simulation time of the consecutive simulations met or exceeded the number of days associated with the inundation duration thresholds.

For some years, several consecutive events occurred within the simulation time discussed in the previous paragraph. When this occurred, several shorter simulations were generated to ensure that only one hydrograph peak occurred during each simulation. More specifically, the start of a simulation coincided with the end of the receding waters and the start of the next inundation wave as seen in Figure 8. Additionally, if the largest flood event exceeded the bottomland hardwood season of analysis, a break between simulations was placed at 01 October 00:00. This allowed for separation of results at the end of the bottomland hardwood period of analysis, while allowing results computed before the cutoff date to be applied to both bottomland hardwood and wet prairie analysis. If needed, additional simulations were added after 01 October 00:00 to be used for the wet prairie period of analysis. The final simulation start and end dates and times are provided in Table 7.

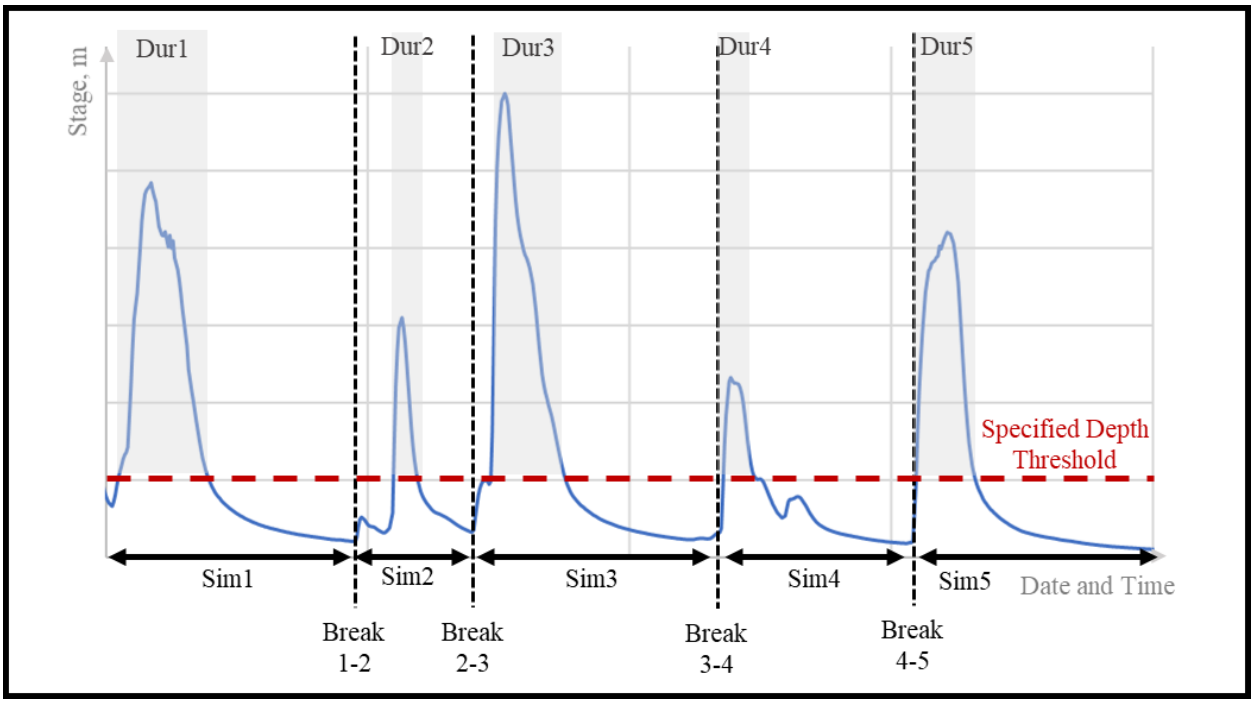

Figure 8:
Breakdown of Consecutive Simulations

Table 7:
Consecutive Day Simulations

Year	Sim 1		Sim 2		Sim 3		Sim 4		Sim 5	
	Start Date	End Date	Start Date	End Date	Start Date	End Date	Start Date	End Date	Start Date	End Date
2008	9/12/2008 20:00	10/1/2008 0:00	10/1/2008 0:00	10/15/2008 16:00						
2009	8/27/2009 4:00	10/1/2009 0:00								
2010	9/16/2010 0:00	9/19/2010 4:00	9/19/2010 4:00	9/22/2010 6:00	9/22/2010 6:00	9/24/2010 10:00	9/24/2010 10:00	10/1/2010 0:00	10/1/2010 0:00	10/24/2010 0:00
2011	8/19/2011 0:00	8/30/2011 16:00	8/30/2011 16:00	10/1/2011 0:00						
2012	7/1/2012 0:00	10/1/2012 0:00								
2013	7/1/2013 0:00	10/1/2013 0:00								
2014	9/10/2014 0:00	10/1/2014 0:00	10/1/2014 0:00	10/13/2014 16:00						
2015	7/19/2015 12:00	7/26/2015 16:00	7/26/2015 16:00	7/29/2015 2:00	7/29/2015 2:00	8/4/2015 10:00	8/4/2015 10:00	8/9/2015 14:00	8/9/2015 14:00	9/8/2015 8:00
2016	8/27/2016 6:00	10/1/2016 0:00								
2017	7/13/2017 8:00	8/14/2017 0:00								
2018	9/7/2018 8:00	10/1/2018 0:00	10/1/2018 0:00	11/1/2018 0:00						

In order to ensure that the consecutive simulations started from the end of the previous simulation, restart files were used. A restart file, also known as a hotstart file, was generated at the end of the first simulation. The restart file, containing the inundation conditions from the end of the previous simulation, was then imported as the initial conditions for the next simulation. This was accomplished by creating additional unsteady flow files that referenced a specific hotstart file. This process was repeated when consecutive simulations occurred. Restart files were applied to all consecutive simulations with the exception of 2010 Sim2 which used a warmup period to establish initial conditions.

Individual plans were created for each simulation. The plans used the respective geometry associated with the year of analysis and the unsteady flow file. The plan names included the start and end dates of the simulation. Once the simulations were complete, duration and recession maps were generated for each simulation and exported from RAS Mapper as tagged image file format (TIFF) files.

Results Processing: Consecutive Days. The resulting TIFF files had several cells without any data that were assigned "null values". The null values corresponded to locations that were never inundated during the simulations meaning that the duration and recession time were equal to zero days. In order to perform the calculations in ArcGIS Pro for all areas that were inundated, the null values were reassigned to represent values using the raster calculator conditional operations in ArcGIS Pro. Duration and recession null values were reassigned to zero days. Null values had to be reassigned to perform raster calculations such as addition and multiplication. When null values were not reassigned and raster calculations were applied, the resulting raster produced null values at the same locations as the source rasters. Even if one source raster had a cell value and the other contained a null value, the null value persisted. As a result, the null values

were reassigned so all inundation extents for every year could be fully analyzed and multiplied against one another without reducing the extents of the overall results. The rasters were then clipped to Pershing State Park extents to reduce computation time using the clip raster data management tool in ArcGIS Pro. If a singular event occurred and there was only one simulation needed, then the duration map layer was equivalent to the number of consecutive days inundated. However, if multiple simulations were required, additional processing was required.

For consecutive simulations, terminology needed to be established. Each simulation was referred to as "sim" followed by a number designating the order of the simulation in the period of analysis for that year. "Break" refers to the transition from one simulation to the next. Breaks were designated with numbers identifying which simulations the break fell between. For instance, a break between sim1 and sim2 was referred to as break1-2. The computed inundation duration for each simulation was referred to as "dur" followed by the simulation number the duration was associated with (Figure 8).

The following process was followed. For the example described below, a total of five consecutive simulations were analyzed (sim1 through sim5). If fewer simulations were used, then steps associated with the number of consecutive simulations present within a given year were followed. The ArcGIS Pro raster calculator tool with conditional operations were used to perform these calculations on the imported TIFF files.

Break Analysis. First, each break between each simulation was analyzed. As part of this process, the recession time of the first simulation and the total simulation time frame were compared. If the recession time of sim1 was equal to the total simulation time (indicated the cell was wet at the beginning of the second simulation), then the cell

associated with break1-2 was assigned a value of one. This indicated that the cell remained wet from sim1 to sim2.

Two Consecutive Simulations. Then, two consecutive simulations were analyzed. If a cell associated with break1-2 was assigned a value of one, then dur1 and dur2 were summed producing dur1-2. In ArcGIS Pro, the raster calculator tool was used to compute the dur1-2 raster. Specifically, the break1-2 raster (in ones and zeros) was multiplied against the sum of dur1 and dur2. This process was repeated for all two consecutive simulation combinations producing maps for dur2-3, dur3-4, and dur4-5.

Three Consecutive Simulations. Next, three consecutive simulations were analyzed. If a cell associated with break1-2 and break2-3 was assigned a value of one for both break maps, then duration maps associated with the three simulations were summed (dur1 + dur2 + dur3) to get the resulting duration map dur1-3. In the raster calculator ArcGIS Pro tool, the break1-2 and break2-3 rasters (in ones and zeros) were multiplied against the sum of dur1, dur2, and dur3. This process was repeated for the other three consecutive simulations producing duration maps dur2-4 and dur3-5.

Four Consecutive Simulations. Four consecutive simulations were then analyzed. If a cell associated with break1-2, break2-3, and break3-4 was assigned a value of one for all three break maps, then the duration maps associated with the four consecutive simulations were summed (dur1 + dur2 + dur3 + dur4) to get the resulting duration map, dur1-4. In the raster calculator ArcGIS Pro tool, the break1-2, break2-3, and break3-4 rasters (in ones and zeros) were multiplied against the sum of dur1, dur2, dur3, and dur4. This process was repeated for the other four consecutive simulations producing an additional duration map, dur2-5

Five Consecutive Simulations. Finally, five consecutive simulations were analyzed. If a cell associated with break1-2, break2-3, break3-4, and break4-5 was assigned a value of one for all break maps, then the duration maps associated with the five consecutive simulations were summed (dur1 + dur2 + dur3 +dur4 +dur5) to get the resulting duration map, dur1-5. In the raster calculator ArcGIS Pro tool, the break1-2, break2-3, break3-4, and break4-5 rasters (in ones and zeros) were multiplied against the sum of dur1, dur2, dur3, dur4, and dur5.

All of the generated duration (dur) maps were then combined in ArcGIS Pro using maximum duration values and the mosaic raster tool to generate one TIFF or raster dataset. This raster was representative of the maximum number of consecutive days a cell was inundated over the course of the entire simulation period between the first and last consecutive simulation of that given year.

Results Processing: Habitat Metrics. Once a combined raster was computed for each habitat analysis year, the habitat metric thresholds were applied. The maximum consecutive day raster datasets were opened in ArcGIS Pro. Then, conditional reassignment was applied to each raster using the conditional function within the raster calculator tool. The following conditional reassignment was specified in the raster calculator tool.

Equation 2: $$Con(\text{“}raster\text{”}, 1, 0, \text{“}VALUE < param\text{”})$$

Where,

$raster$ = the clipped raster for a given year

1 = the value to assign if the value meets the parameter requirement

0 = the value to assign if the cell value does not meet the parameter requirement

$Value < param$ = the parameter threshold used for the analysis, specified in Table 4 and Table 5 for each wetland community type.

Using the inundation duration thresholds identified for each specific wetland community, cells for each year were assigned either a value of one or zero. Cells were assigned values of one if the cell consecutive days of inundation fell below the maximum inundation duration threshold. Cells were assigned values of zero if the maximum number of consecutive days exceeded the specified inundation duration threshold. The conditionally reassigned rasters for each year of analysis associated with one wetland community were then multiplied together using the raster calculator tool. The resulting map had each cell either assigned a value of one or zero. A value of one indicated that the consecutive days of inundation duration between 2008 and 2018 never reached a duration great enough to kill the wetland community, indicating that conditions were ideal for community growth. Varying inundation duration thresholds were applied to identify better thresholds to be used in future analyses. This same process was applied to results for both wetland communities. Inundation duration thresholds of 14, 10, and 7 days and 30, 15, and 10 days were analyzed for bottomland hardwood and wet prairie, respectively.

Once the inundation duration habitat metric maps were developed, areas associated with the map values of one and zero were computed for three wetland community outcomes. The first wetland community outcome was representative of community gains or an expansion of new communities from the 2011 MoDNR spatial extents to the 2019 USACE spatial extents. The spatial extent of the wetland community gains occurred when the 2019 communities did not overlap the 2011 communities. The second wetland community outcome was representative of

persistent communities. In other words, wetland community spatial extents did not change between the 2011 and 2019 surveys. Persistent communities occurred where both the 2011 and 2019 ecosystem surveys overlapped. The third community outcome was representative of community losses or a reduction of past community spatial extents. Community loss occurred where the 2011 ecosystem survey did not overlap the 2019 ecosystem survey. The areas were computed in ArcGIS Pro using the tabulate area spatial analyst tool. Percentages of the total area associated with each community outcome and growing condition (one or zero) were computed for both bottomland hardwood forests and wet prairie. Correctly simulated percentages were computed by dividing the total area of ones within each individual community outcome by the respective, observed community outcome area (Equation 3). Likewise, incorrectly simulated percentages were computed with the same methodology with the exception of using the total area of zeros instead of ones.

Equation 3:

$$\%\ Simulated_i = \frac{A_{1,0_i}}{A_{T_i}}$$

Where,

i = a single community outcome (gain, persistence, or loss)

$A_{1,0}$ = the simulated area of the assigned value (either 1 or 0), within an observed community outcome area

A_T = the observed total area of an individual community outcome (gain, persistence, or loss)

Inundation Depth

Simulations. Plan files developed for analysis of annual peak flows, discussed in Appendix C, were copied and used for the inundation depth simulations. The start and end dates/times were adjusted to reflect the analysis period for each wetland community: 01 July 00:00 to 30 September 24:00 for bottomland hardwood and 01 July 00:00 to 31 October 24:00 for wet prairie. All other parameters remained the same, only the simulation time frame was adjusted.

HEC-RAS Map Generation. The inundation depth was generated in RAS Mapper using the maximum "Depth" map. The maximum depth option reported the maximum water depth recorded in a cell at any point during the simulation. In other words, the maximum depth in one cell may have occurred at a different time than the maximum depth in another cell. The maximum depth maps were only generated for the simulations that utilized the simulation time periods corresponding with the period of analysis in Table 4 and Table 5. A HEC-RAS maximum depth map was generated for each year of analysis for each wetland community and was exported as a TIFF file.

Habitat Metric Application. The maximum depth TIFFs were uploaded to ArcGIS Pro as raster datasets and null values were reassigned to zero depths using the raster calculator tool and conditional operations. Then, the rasters were clipped to Pershing State Park extents to reduce computation time. The conditional reassignment process detailed for inundation duration was followed with one exception: the maximum depth habitat metric thresholds were used for conditional reassignment. Using the maximum depth thresholds identified for each specific wetland community and Equation 2, cells for each year were assigned either a value of one or zero. Cells were assigned values of one if the cell maximum depth fell below the maximum depth threshold. Cells were assigned values of zero if the maximum depth exceeded the specified depth

threshold. The conditionally reassigned rasters for each year of analysis associated with one wetland community were then multiplied together using the raster calculator tool. The resulting map had each cell either assigned a value of one or zero. A value of one indicated that the maximum depth between 2008 and 2018 never reached a depth great enough to kill the community, indicating that conditions were ideal for community growth. Additionally, varying inundation depth thresholds were applied to identify better thresholds to be used in future analyses. This same process was applied to results for both wetland communities. Inundation duration thresholds of 0.15 meters, 0.30 meters and 0.61 meters, and 0.61 meters, 1.22 meters, and 1.83 meters were analyzed for bottomland hardwood forests and wet prairie, respectively.

Once the inundation depth habitat metric maps were developed, areas associated with the map values of one and zero were computed for three community outcomes: community gain, community persistence, and community loss. The community outcomes were discussed in more detail in Chapter 2. The areas were computed in ArcGIS Pro using the tabulate area spatial analyst tool. Percentages of the total area associated with each habitat outcome and growing condition (one or zero) were also computed using methodology detailed in Chapter 2, Habitat Analysis Methodology, Inundation Depth.

Dry Days

Simulations. The annual peak plan files discussed in Appendix C were copied and used for the dry day simulations. The start and end dates/times were adjusted to reflect the analysis period for each wetland community: 15 April 00:00 to 30 November 24:00 for bottomland hardwood forests and 15 July 00:00 to 31 October 24:00 for wet prairie. All other parameters remained the same. Only the simulation time frame was adjusted.

HEC-RAS Map Generation. Using the associated depth thresholds for each wetland community, duration maps were generated in RAS Mapper. If the simulation end dates/times matched the end of the period of analysis associated with the wetland community, then the duration map was generated with respect to the start of the period of analysis. For wet prairie, the duration maps were generated with respect to a start date and time of July 15th 00:00. By specifying the date and time at which the duration map starts the computation, the resulting map did not include the time inundated before the specified date and time. Instead, the duration was computed from the specified start date and time to the end of the simulation. For bottomland hardwood forest, the simulation time frame for each year differed from the dry day period of analysis. Since the bottomland hardwood forest period of analysis for dry days was from April 15th 00:00 to November 30th 24:00, two duration maps were generated with respect to those dates and times. Since the duration was computed to the end of the simulation, the April 15th duration included duration measurements after the November 30th cutoff. As a result, the total duration between April 15th and November 30th was then computed by subtracting the November 30th duration from the April 15th duration.

Habitat Metric Application. The resulting TIFF files had several cells without any data that were assigned "null values". The null values corresponded to locations that were never inundated during the simulations meaning that the duration was equal to zero days. The ArcGIS Pro spatial analysis reclassify tool was used to reassign the null values a value of zero days. A conditional reassignment process similar to the maximum depth conditional reassignment was applied. After the null values (cells that were never inundated) were reclassified to zero duration days for all generated duration maps, the November 30th duration map was subtracted from the April 15th duration map. Then, all rasters were clipped to Pershing State Park extents. After the

rasters were clipped, the computed duration maps were subtracted from the total number of days within the habitat dry day period of analysis (230 days for bottomland hardwood forest and 109 days for wet prairie) using the raster calculator tool. The resulting maps displayed the number of dry days within the dry day period of analysis. After the dry day maps were generated, conditional reassignment was applied (Equation 2) using the dry day thresholds (T) for each wetland community. For each wetland community, the resulting conditionally reassigned dry day rasters for each year were multiplied together using the raster calculator tool. The resulting map had each cell either assigned a value of one or zero. A value of one indicated that the number of dry days for each year between 2008 and 2018 met or exceeded the number of dry days identified as beneficial to the community, indicating that conditions were ideal for community growth. Additionally, varying habitat metric thresholds including short (T/4), medium (T/2), and long (T) dry days were applied to identify better thresholds to be used in future analyses. This same process was applied to results for both communities.

Once the dry day habitat metric maps were developed, areas associated with the map values of one and zero were computed for three community outcomes: community gain, persistence, and loss. The community outcomes were discussed in more detail in Chapter 2. The areas were computed in ArcGIS Pro using the tabulate area spatial analyst tool. Percentages of the total area associated with each community outcome and growing condition (one or zero) were computed.

However, due to model limitations in HEC-RAS 5.0.7 when computing duration for sub-simulation time frames, the maps did not produce correct duration estimates. As a result, the dry day maps could not be generated, and the dry day habitat thresholds could not be further analyzed.

Chapter 3: Results and Discussion

The following sections provide the results from the analyses described above. Results are discussed in detail with respect to their interpretation, application, uncertainty, and limitations.

Hydraulic Model Calibration and Validation

Calibration and validation results are discussed in the following sections. Calibration results were used to evaluate if the selected parameters produced results that accurately portrayed observed conditions. Validation results were evaluated to ensure that the calibrated parameters produced results representative of observed datasets when applied to simulations outside of the calibration events.

Calibration Results

Based on detailed comparisons and discussions provided in Appendix B, the final calibrated model used a computation grid where boundary conditions spanned the entire floodplain and a downstream normal depth friction slope of 0.0007 m/m was used. The diffusion wave approximation of the Navier-Stokes equation was used for modeling due to better model performance in comparison to the full momentum equation including decreased computation time and lower occurrence of large, unrealistic velocities. Figure 9 displays the spatial variation and calibrated roughness coefficients used in the final calibration model.

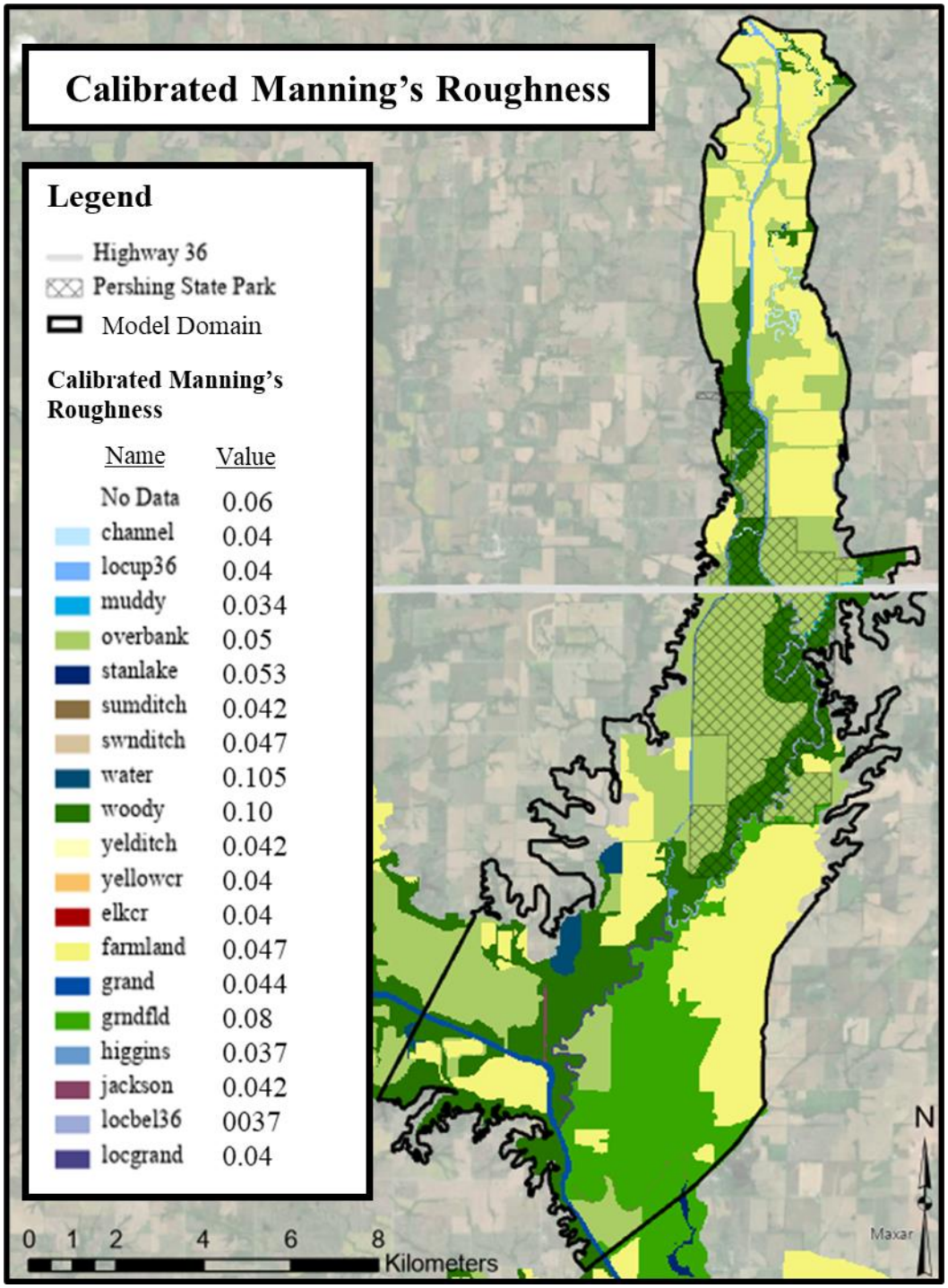

Figure 9:
Final Calibrated Manning's n Roughness Coefficients

The calibrated parameter set simulated a Grand River peak flow of 2,061 cubic meters per second (cms) at Sumner, MO. When compared to the USGS peak discharge of 2,540 cms, the simulated peak flow produced a percent error of -19% indicating that the selected parameters underestimated peak flows. Underestimating peak flows may underpredict inundation depths and duration of stressed wetland communities. Additionally, peak flow underestimation will likely have a greater impact on deteriorating fringe communities where negative impacts will not be captured in the hydraulic analysis due to lower simulated water surface elevations.

Figure 10 displays the simulated Grand River hydrograph at Sumner for the individual April 2017 event and Table 8 compares the simulated discharges and velocities to instantaneous USGS measurements at Sumner. Overall, the simulated hydrograph shape was similar to the observed hydrograph. The selected calibration parameters also portrayed the best estimate of instantaneous USGS flow measurements in the main channel when compared to other calibration iterations (Appendix B).

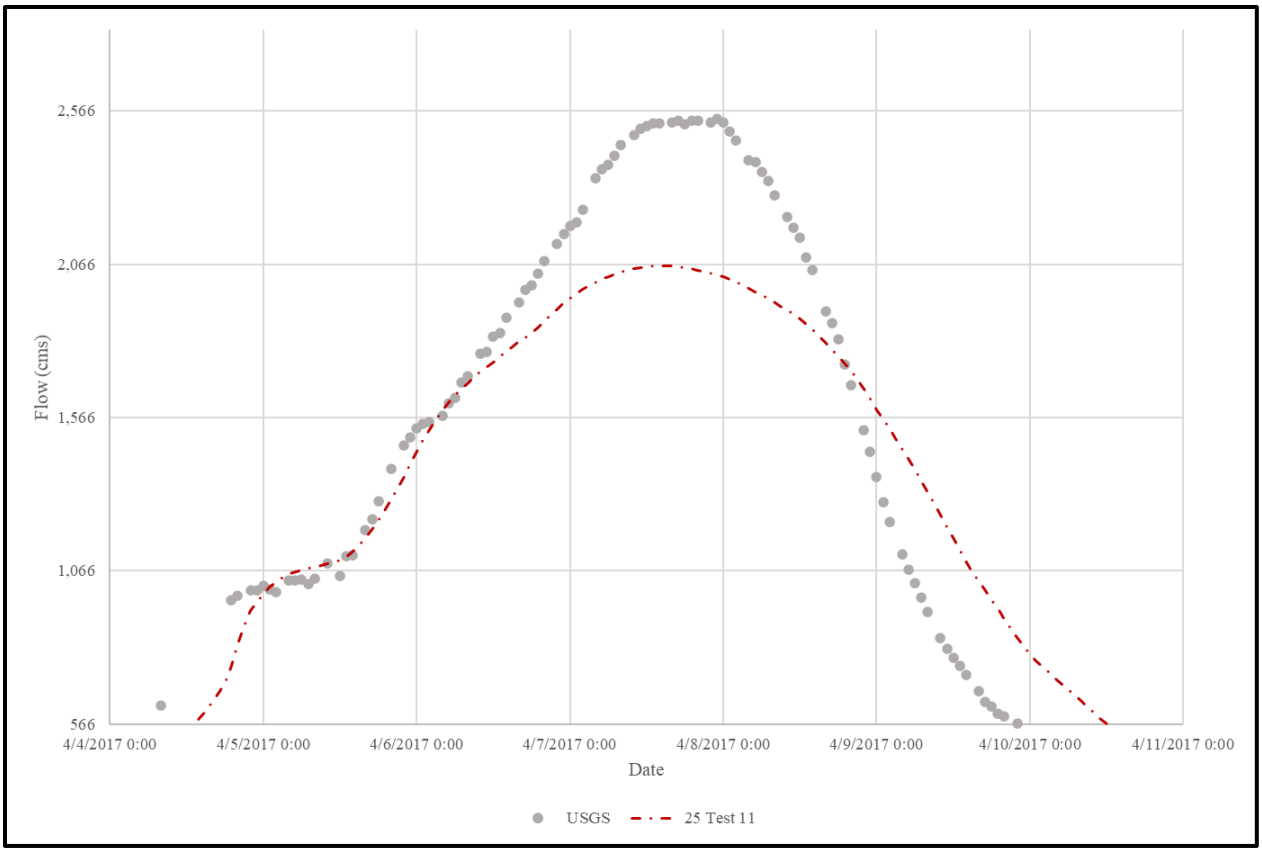

Figure 10:
Simulated Flows at Sumner using Final Calibrated Parameters Compared to USGS Flows

Table 8:

Grand River at Sumner, MO Simulated Main Channel and Overflow Discharge and Average Channel Velocity Comparisons with USGS Measurements Recorded at 4/6/2017 16:24:48 UTC.

Simulation	**Discharge, cms**		**Average Channel Velocity, meters per second (mps)**	
	Main Channel	*Overflow*	*Main Channel*	*Overflow*
USGS	1,543	382	1.71	0.56
25 Test11	1,463	340	2.00	0.76

The simulated NSE for the April 2017 event was 0.958. An NSE close to 1.0 indicates a good calibration. However, the NSE calculation was biased as the NSE calculation used every time step within the April 2017 event simulation. By accounting for all time steps, more datapoints

reflective of baseflow conditions were incorporated into the calculations which reduced the overall impact of the underestimated peaks in the NSE calculation.

Next, the calibration simulation results were compared to observed HWMs. Table 9 displays the simulated water surface elevations and differences with respect to USACE surveyed HWMs. The final calibration parameters produced simulated water surface elevations that largely underestimated the HWMs from 0.35 meters to 0.71 meters, further indicating that the model underpredicted peak flows and stages.

Table 9:
Simulated Water Surface Elevations Compared to USACE Surveyed HWMs using Final Parameters

Simulation	**Simulated Elevation in m-NAVD88** Water Surface Elevation Difference between Simulation Results and Observed in meters Pershing State Park					Grand River			
USACE Surveyed HWM	211.56	211.54	209.16	206.04	205.40	205.38	205.42	205.59	205.11
25 Test11	210.99	211.00	208.52	205.70	205.03	204.85	204.78	204.89	204.73
	-0.57	-0.55	-0.64	-0.35	-0.37	-0.52	-0.64	-0.71	-0.38

Lastly, a log jam roughness coefficient of 1.0 produced the most representative inundation extents, fell within the acceptable range of roughness coefficients, and thus, was used for all log jam roughness coefficients in annual simulations and habitat analyses. However, a log jam roughness coefficient of 1.0 still underpredicted inundation extents. Underestimation of the inundation extents may result in fewer hydraulic impacts (shallower depths and smaller inundation durations) to key wetland communities, resulting in underestimation of wetland community changes. However, the underestimation of the simulated inundation extents may be a result of changes in topography due to floodplain sedimentation that occurred between 2009 and 2018.

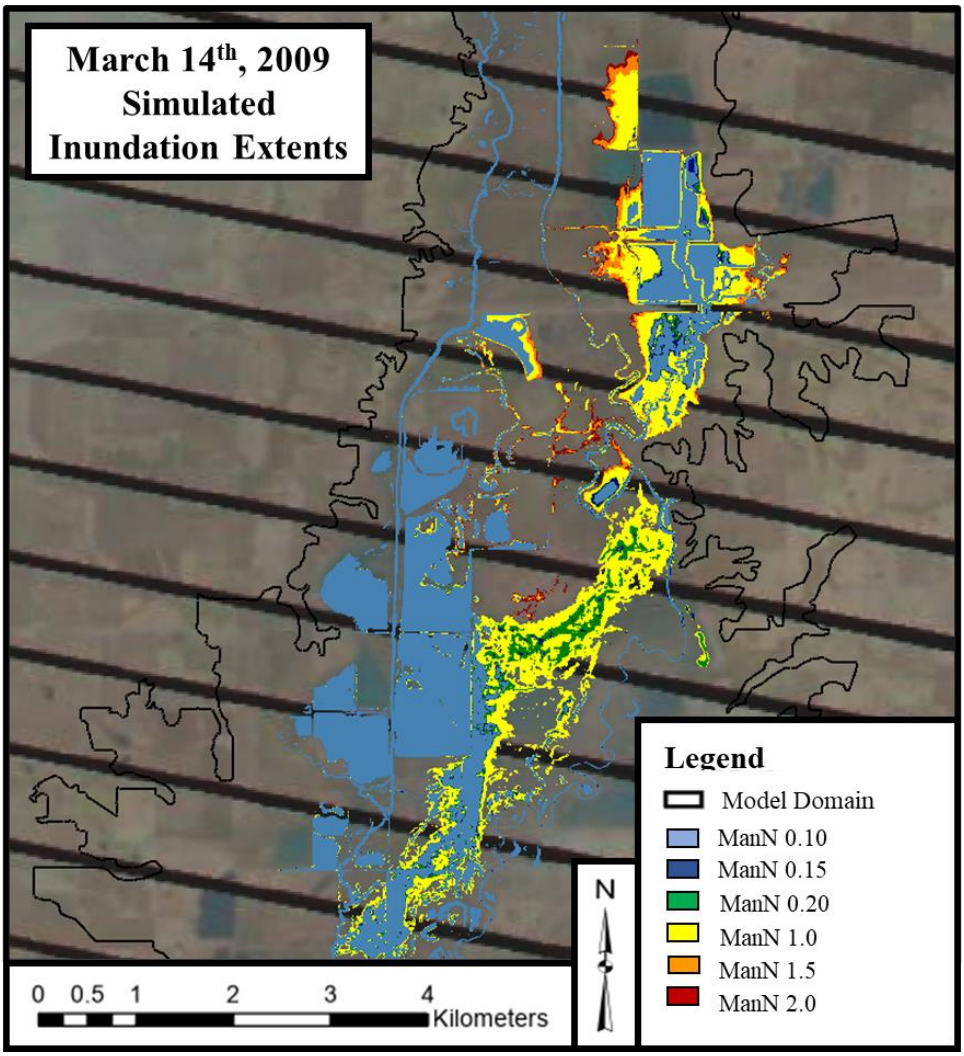

Figure 11:
Log Jam Roughness Coefficient Calibration March 2009 Inundation Extents

Validation Results

Appendix C provides detailed documentation pertaining to the validation results. Validation results indicated that the selected parameters reflected observed hydrograph timing with respect to the October 2018 event and October annual simulation (Figure 12). However, the peak discharge of the October event was underestimated by approximately 7.4%. Additionally, the hydrograph volume for the October 2018 event appeared to be underestimated on the falling limb

possibly due to increased floodplain attenuation in the Grand River floodplain. The annual simulation indicated that peak discharges were routinely underestimated for events ranging in magnitude of peak flows. Again, underpredicting peak flows may underpredict inundation extents, depths, and durations, thus underpredicting wetland community degradation and other community impacts.

October 2018 HWM comparisons showed that water surfaces within Pershing State Park differed from observed by as much as 0.45 meters on Locust Creek near Highway 36 and as little as 0.07 meters along the old Locust Creek channel downstream of the Muddy Creek confluence. Table 10 displays the 2018 simulated water surface elevations and the differences between the simulated water surface elevations and HWMs. Overestimation of the water surfaces may over predict inundation durations and impacts to wetland communities. Only one HWM remained in Fountain Grove for comparison against simulated water surface elevations as all other locations remained dry in the simulation. The simulated water surface elevations were approximately 0.53 meters lower than the surveyed HWM. This may indicate that lower than observed peak volumes were simulated at Grand River at Fountain Grove due to methodologies used to develop a continuous flow record.

Table 10:
2018 Validation Simulation Water Surface Elevations Compared to USACE Surveyed HWMs

Dataset	**Simulated Water Surface Elevation in m-NAVD88** Water Surface Elevation Difference between Simulation Results and Observed in meters Pershing State Park			Grand River
USACE Surveyed HWM	210.84	208.50	208.50	205.31
25 Test11	211.29 0.45	208.57 0.07	208.56 0.06	204.79 -0.53

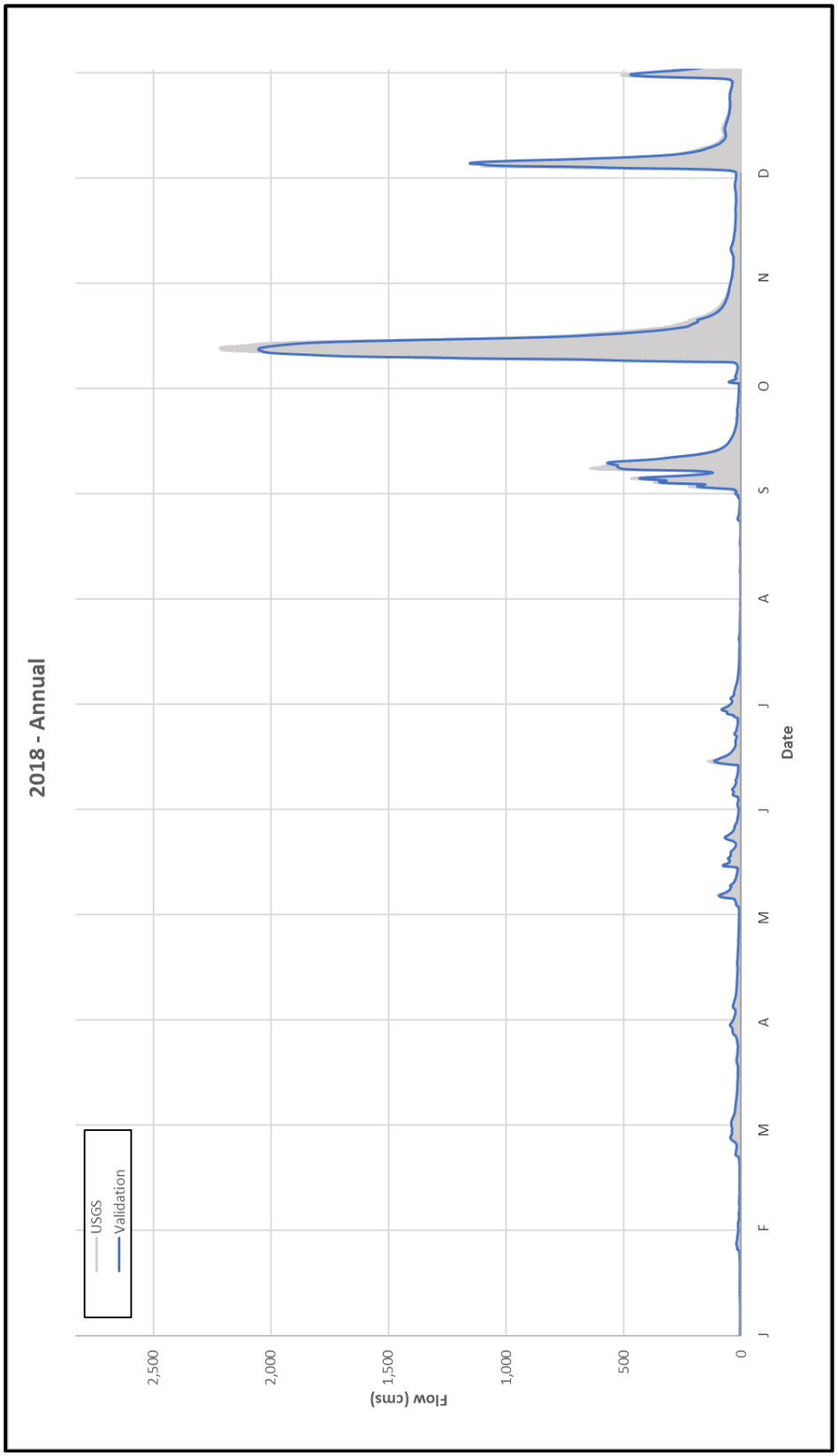

Figure 12:
Simulated Grand River Flows at Sumner for the 2018 Annual Simulation Compared to USGS Observed Flows

October 2018 inundation extents agreed with observed satellite images within Pershing State Park (Figure 13) apart from areas near Fountain Grove. The overestimation of Fountain Grove inundation was attributed to the placement of the Grand River Fountain Grove boundary condition. The boundary condition was placed such that it extended across the entire floodplain to allow for flow distribution across the entire floodplain during larger flows. As part of that methodology, the boundary condition extended through a levee system which likely reduced the amount of flow entering the leveed overbank areas in real world scenarios. Additionally, the areas circled in red appeared to drain slowly, contributing to increased inundation duration and extents. This may be a result of inaccurate culvert data used in the model. However, the areas along Locust Creek are the primary areas of interest and appeared to reflect the inundation extents observed in the satellite imagery.

The log jam roughness coefficient of 1.0 and log jam validation simulation underestimated the inundation extents in the areas of existing wet prairie (Figure 14). Underestimation of the inundation extents may result in fewer hydraulic impacts (shallower depths and smaller inundation durations) to key wetland communities, resulting in underestimation of wetland community changes. However, the underestimation of the simulated inundation extents may be a result of changes in topography due to floodplain sedimentation that occurred between 2009 and 2018.

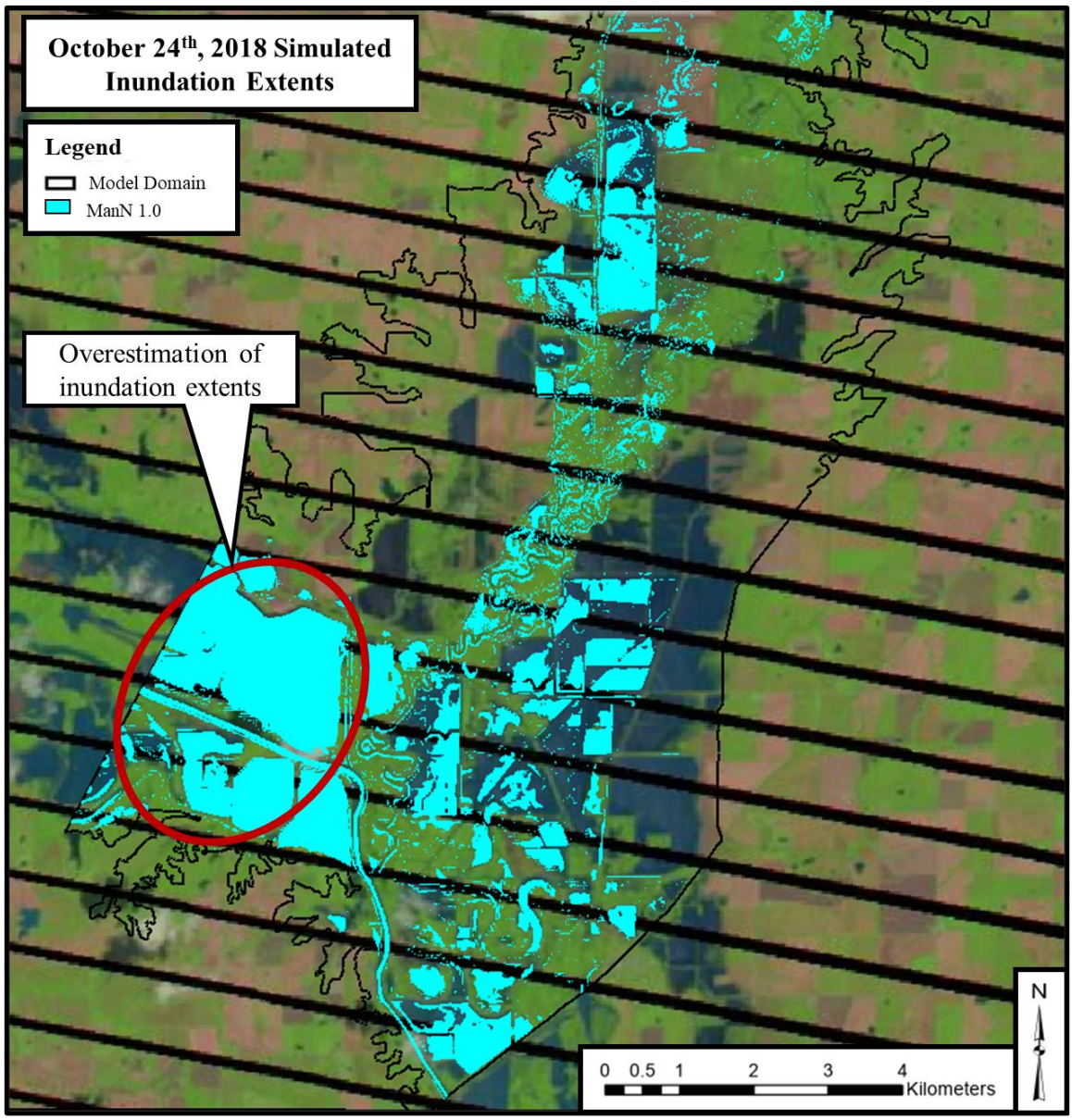

Figure 13:
2018 Event Inundation Extent Validation

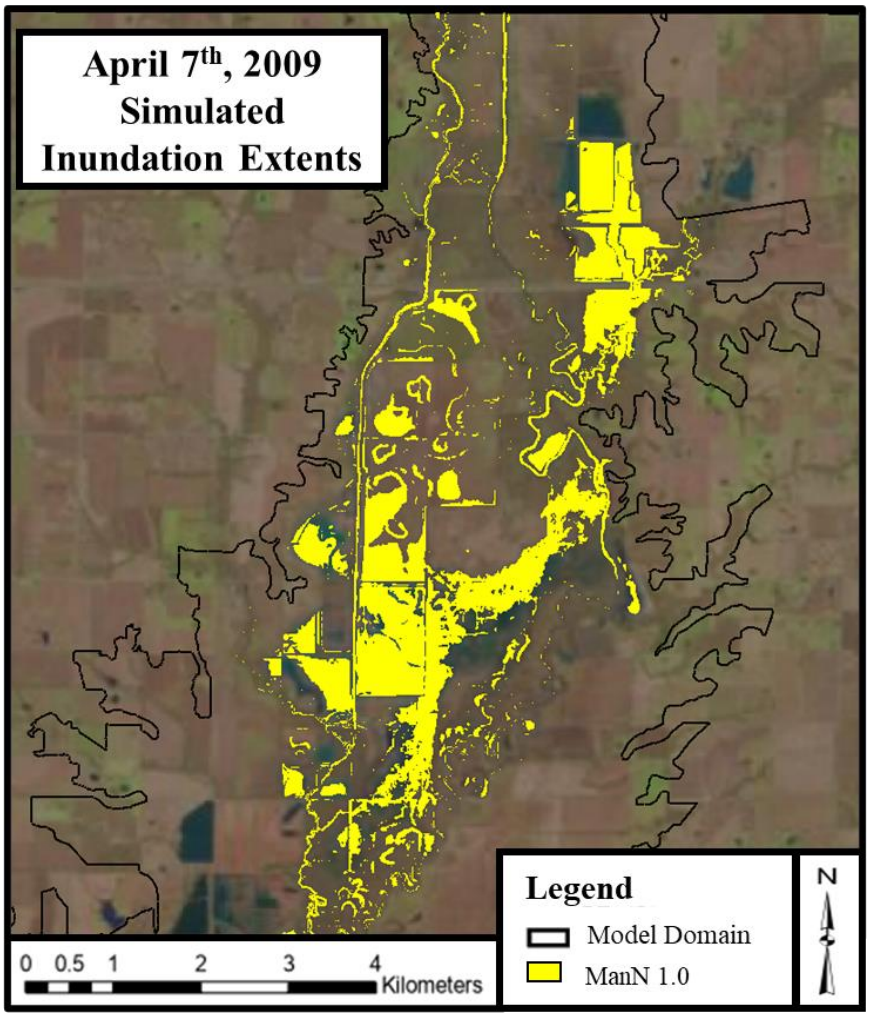

Figure 14:
Log Jam Roughness Coefficient Validation April 2009 Inundation Extents

The three largest simulated Grand River event discharges at Sumner, MO for each year of analysis were used to compute the NSE for peak event flows. Simulated discharges ranged from 515 to 3,990 cms. The estimated bankfull flow for the Grand River at Sumner was 8,230 cms (USACE, 2020), indicating that 91% of the analyzed simulated flows exceeded bankfull discharges. The resulting peak flow NSE was 0.30. The computed NSE of 0.30 was low and indicated that the hydraulic model did not accurately simulate Grand River peak discharges at the Sumner, MO gage location. In a perfect model, the NSE would equal 1.0. Only peak flows were included in the NSE computation and, as a result, the NSE was representative of how well the

model simulated peak flows. When comparing the thirty-three simulated peak flows to USGS instantaneous peak flows, the simulated flows routinely overestimated Grand River streamflows near Sumner, producing an average overestimation of 166 cms and maximum overestimation of 18,800 cms in 2014. Annual simulations including 2008, 2009, 2010, and 2014 were primarily responsible for the overestimations of peak event streamflows. Inflows for these years used larger percentages of HEC-HMS flows to develop the Locust Creek inflow time series (Appendix A). Additionally, these years completely used HEC-HMS generated flows for Grand River inflows. As discussed in Appendix A, the HEC-HMS generated flows tended to overestimate flows when compared to observed USGS flows. Overestimated flows may contribute to increased simulated inundation depths and duration, overestimating negative impacts to both wet prairie and bottomland hardwood forests.

Viability of Hydraulic Metrics to Predict Wetland Community Transitions

Two hydraulic metrics at three values were tested for their ability to predict change in wetland community extent. Figure 15 through Figure 18 display the combined habitat metric threshold maps for both bottomland hardwood forest and wet prairie for the 2008 to 2018 analysis period. Blue areas (value of one) on the cumulative threshold maps indicated that the habitat metric between 2008 and 2018 never reached a threshold great enough to kill the wetland community, meaning conditions were ideal for community growth. Orange areas (value of zero) indicated that the habitat metric exceeded the threshold, creating conditions that were not ideal for community growth. Vertically and horizontally hatched areas represented the 2011 ecosystem and 2019 ecosystem survey extents, respectively. Figure 19 and Table 11 provide the areas and percentages of the growing conditions computed for the bottomland hardwood forest habitat metric thresholds for each community outcome. Likewise, Figure 20 and Table 12 provide the areas and percentages

of the growing conditions computed for the wet prairie habitat metric thresholds for each community outcome.

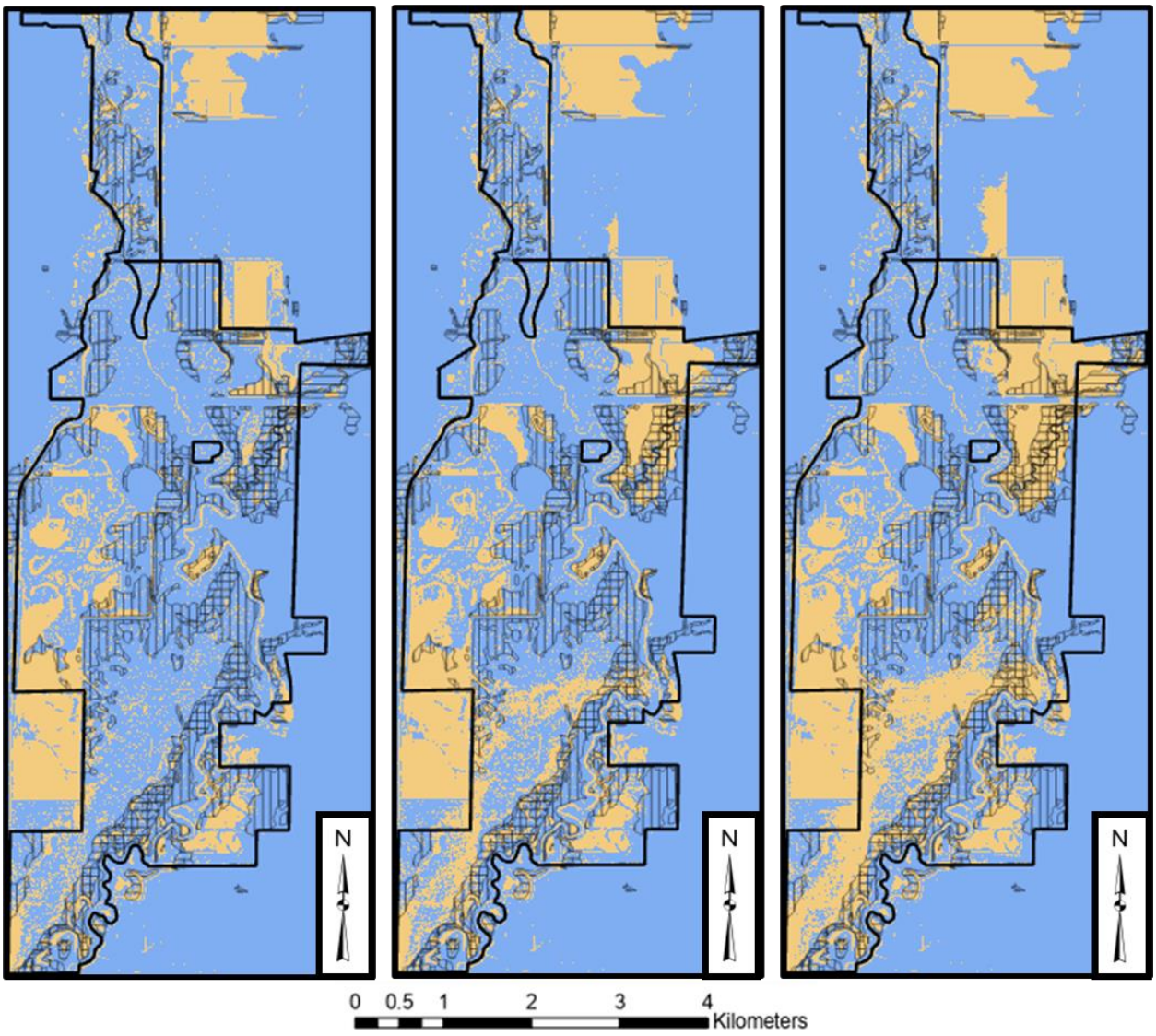

Figure 15:

Bottomland Hardwood Forest Combined Inundation Durations from 2008 to 2018 for Varying Inundation Duration Thresholds.
a) Inundation duration threshold of 14 days. b) Inundation duration threshold of 10 days. c) Inundation duration threshold of 7 days. Blue indicates that the inundation duration between 2008 and 2018 did not exceed the threshold. Orange indicates that at least once during the study period, inundation duration exceeded the threshold, creating conditions that were not ideal for community growth. Vertically hatched areas represent the 2011 bottomland hardwood forest ecosystem survey extents and the horizontally hatched areas represent the 2019 bottomland hardwood forest ecosystem extents.

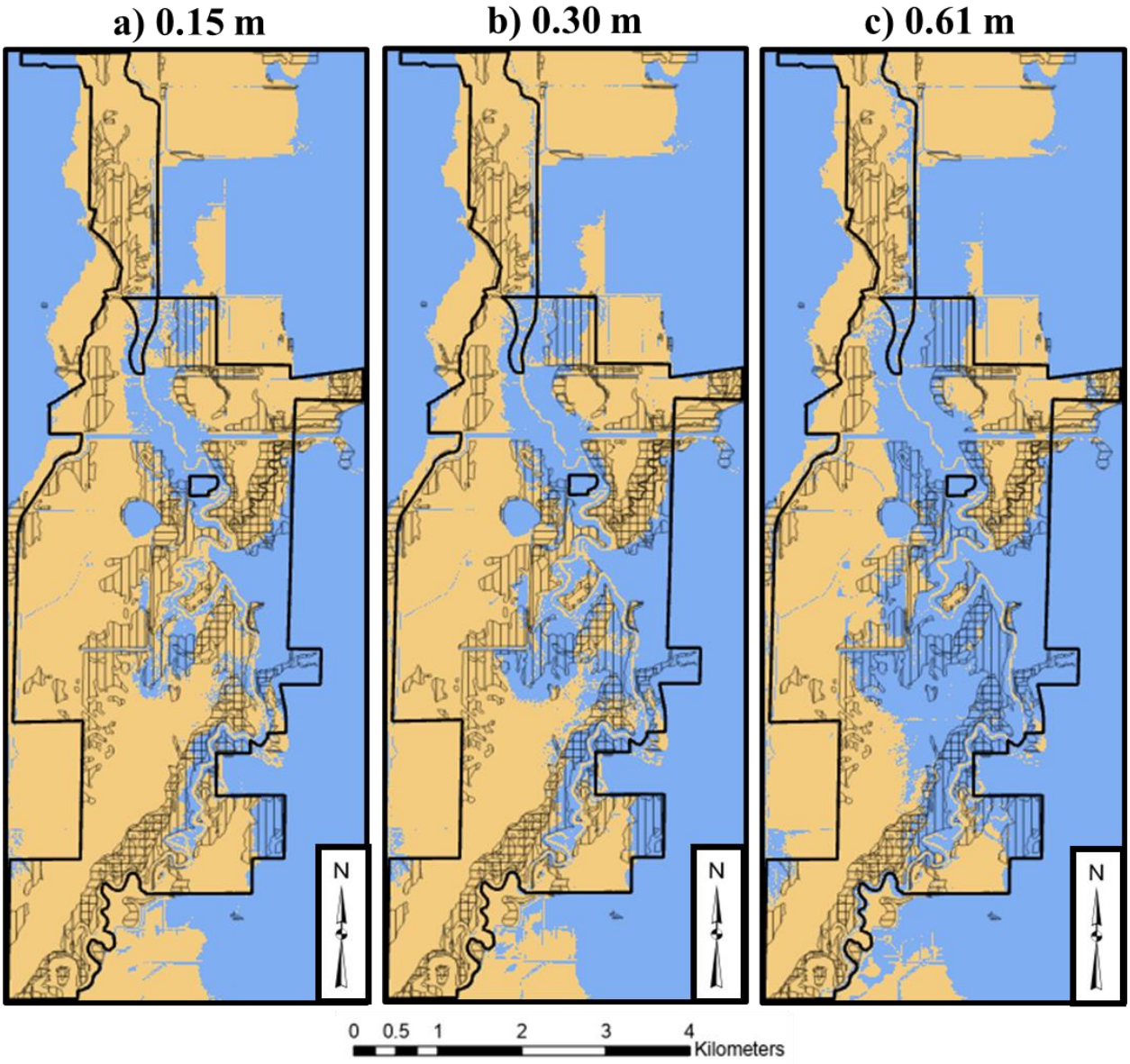

Figure 16:

Bottomland Hardwood Forest Combined Maximum Inundation Depths from 2008 to 2018 for Varying Inundation Depth Thresholds.
a) Inundation depth threshold of 0.15 meters. b) Inundation depth threshold of 0.30 meters. c) Inundation depth threshold of 0.61 meters. Blue indicates that the maximum inundation depths between 2008 and 2018 did not exceed the depth threshold. Orange indicates that at least once during the study period, inundation depth exceeded the threshold, creating conditions that were not ideal for community growth. Vertically hatched areas represent the 2011 bottomland hardwood forest ecosystem survey extents and the horizontally hatched areas represent the 2019 bottomland hardwood forest ecosystem extents.

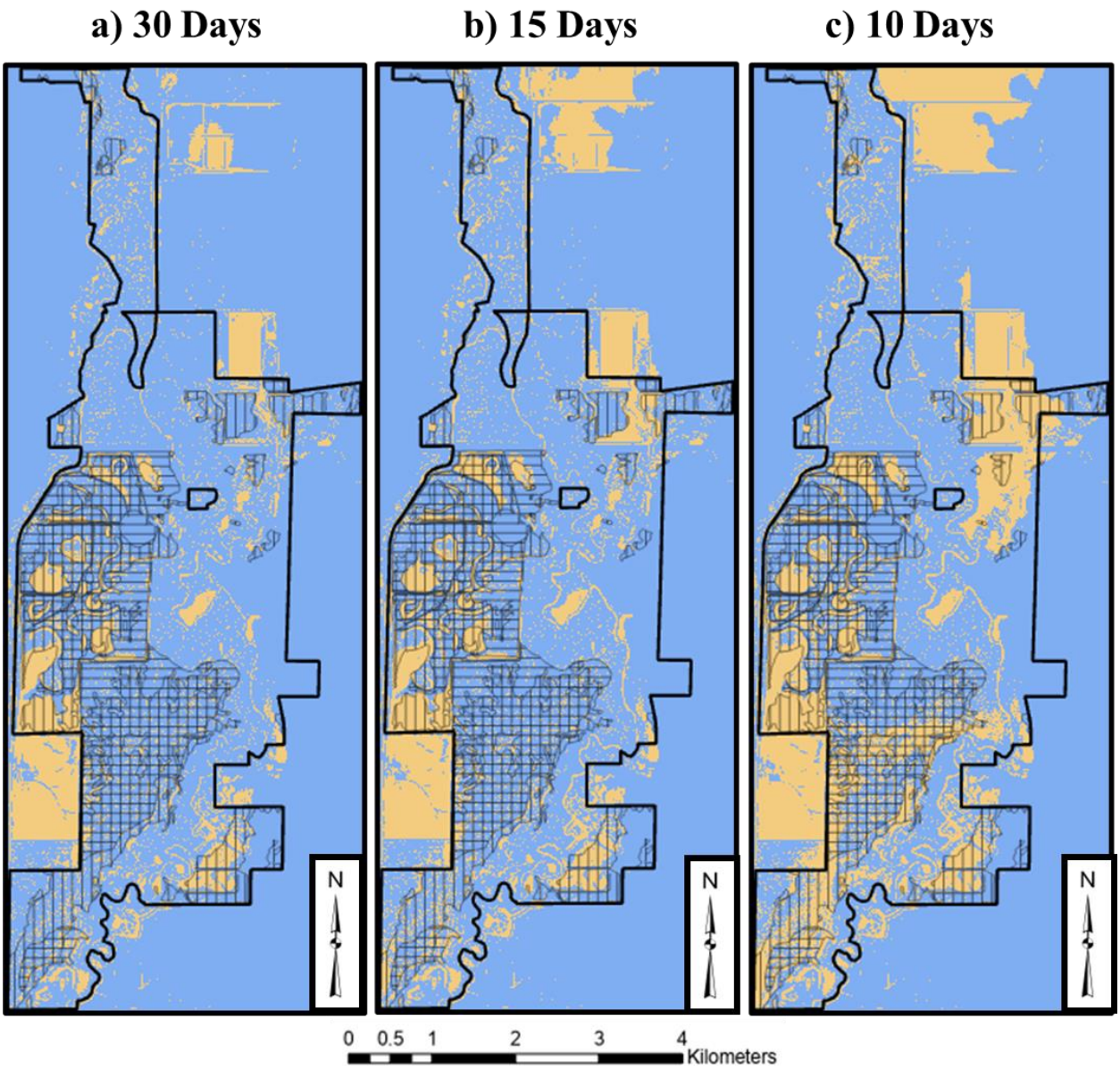

Figure 17:

Wet Prairie Combined Inundation Durations from 2008 to 2018 for Varying Inundation Duration Thresholds. a) Inundation duration threshold of 30 days. b) Inundation duration threshold of 15 days. c) Inundation duration threshold of 10 days. Blue indicates that the inundation duration between 2008 and 2018 did not exceed the threshold. Orange indicates that at least once during the study period, inundation duration exceeded the threshold, creating conditions that were not ideal for community growth. Vertically hatched areas represent the 2011 wet prairie ecosystem survey extents and the horizontally hatched areas represent the 2019 wet prairie ecosystem extents.

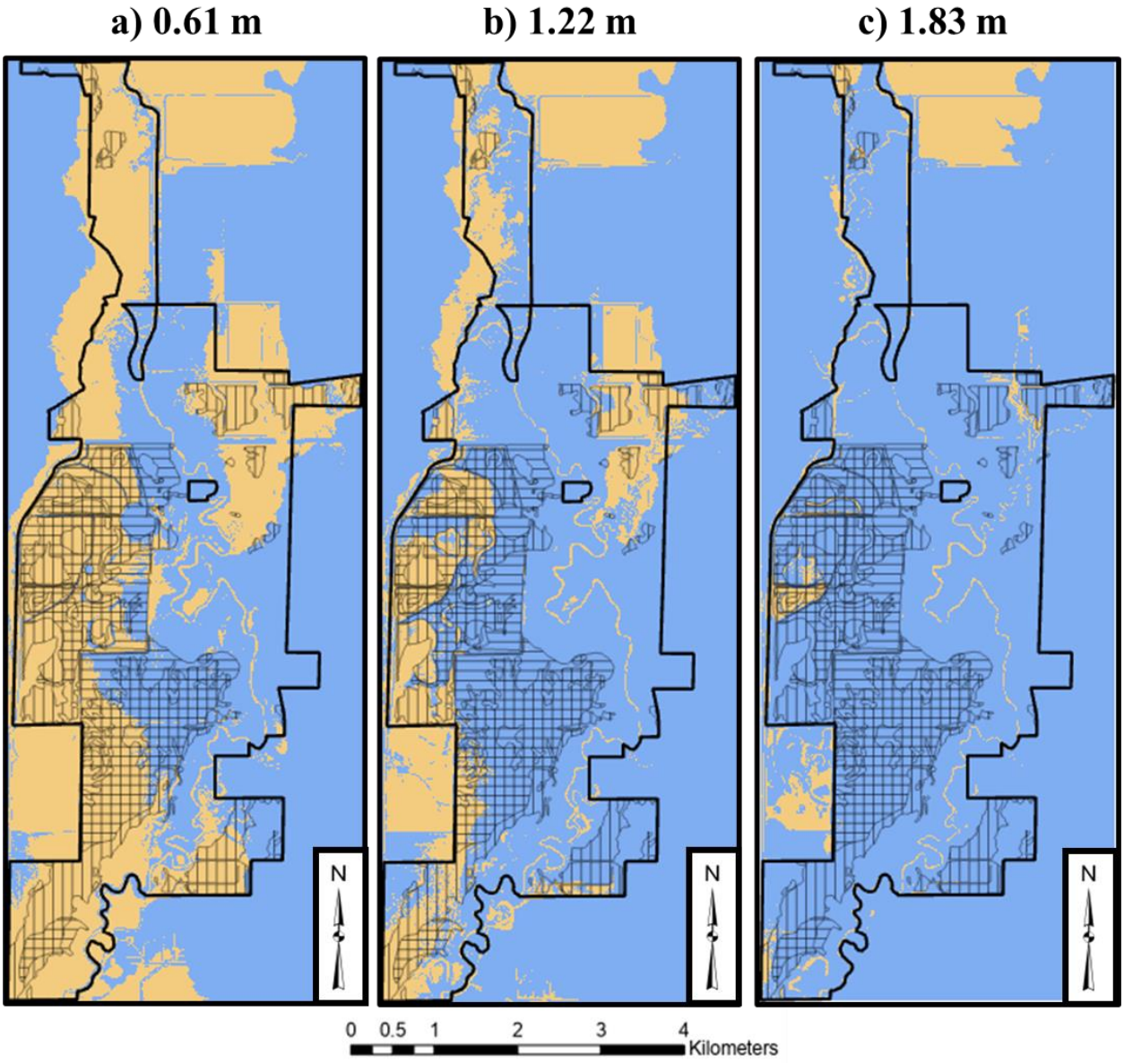

Figure 18:

Wet Prairie Combined Maximum Inundation Depths from 2008 to 2018 for Varying Inundation Depth Thresholds. a) Inundation depth threshold of 0.61 meters. b) Inundation depth threshold of 1.22 meters. c) Inundation depth threshold of 1.83 meters. Blue indicates that the maximum inundation depths between 2008 and 2018 did not exceed the depth threshold. Orange indicates that at least once during the study period, inundation depth exceeded the threshold, creating conditions that were not ideal for community growth. Vertically hatched areas represent the 2011 wet prairie ecosystem survey extents and the horizontally hatched areas represent the wet prairie ecosystem extents.

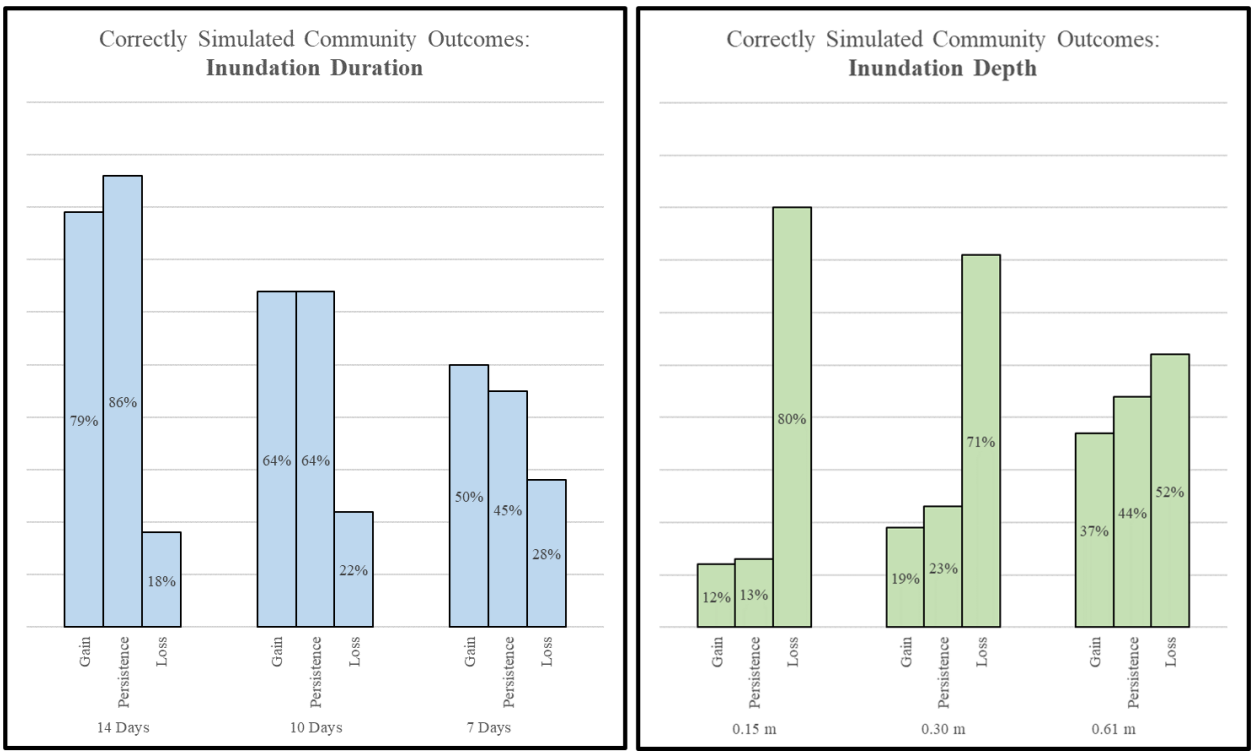

Figure 19:
Bottomland Hardwood Forest Percentages of Total Area Associated with Community Outcomes

Table 11:
Bottomland Hardwood Forest Computed Areas for Community Gain, Persistence, and Loss

Hydraulic Parameter	Habitat Metric Threshold	**Computed Areas of Habitat Gain, Persistence, and Loss in km²** Percentage of Total Area (%)					
		Community Gain		*Community Persistence*		*Community Loss*	
		Incorrectly Simulated Community Loss (Orange)	Correctly Simulated Community Gain (Blue)	Incorrectly Simulated Community Loss (Orange)	Correctly Simulated Community Persistence (Blue)	Correctly Simulated Community Loss (Orange)	Incorrectly Simulated Community Gain (Blue)
Total Area, km²		16.6		13.4		54.3	
BH Inundation Duration, days	14	3.4	13.2	1.9	11.5	9.8	44.5
		21%	79%	14%	86%	18%	82%
	10	6.0	10.6	4.9	8.5	12.0	42.4
		36%	64%	36%	64%	22%	78%
	7	8.3	8.3	7.3	6.1	15.0	39.3
		50%	50%	55%	45%	28%	72%
BH Inundation Depth, m	0.15	14.6	2.0	11.6	1.8	43.6	10.7
		88%	12%	87%	13%	80%	20%
	0.30	13.4	3.2	10.3	3.1	38.5	15.8
		81%	19%	77%	23%	71%	29%
	0.61	10.6	6.1	7.5	5.9	28.3	26.0
		63%	37%	56%	44%	52%	48%

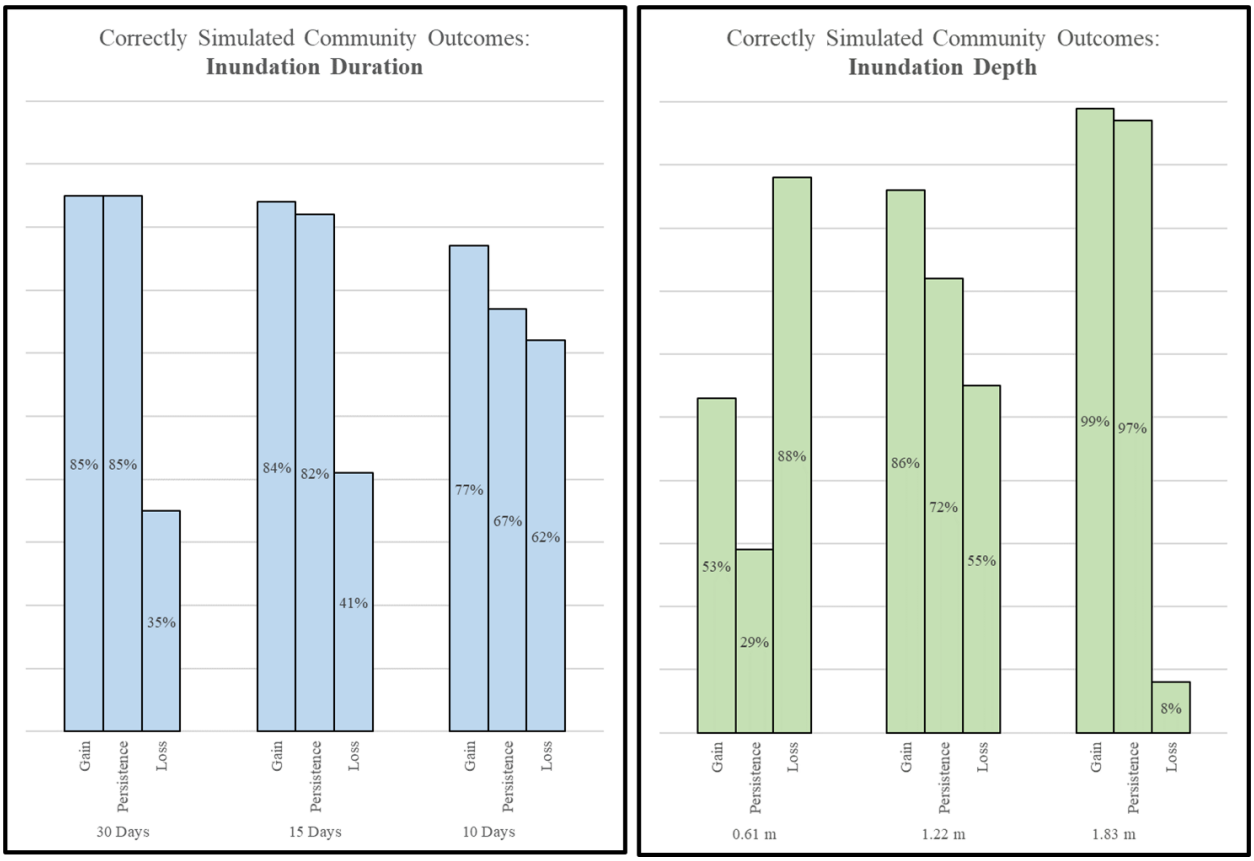

Figure 20:
Wet Prairie Percentages of Total Community Area Associated with Community Outcomes

Table 12:
Wet Prairie Computed Areas for Community Gain, Persistence, and Loss

Hydraulic Parameter	Habitat Metric Threshold	**Computed Areas of Community Gain, Persistence, and Loss in km²** Percentage of Total Area (%)					
		Community Gain		*Community Persistence*		*Community Loss*	
		Incorrectly Simulated Community Loss (Orange)	Correctly Simulated Community Gain (Blue)	Incorrectly Simulated Community Loss (Orange)	Correctly Simulated Community Persistence (Blue)	Correctly Simulated Community Loss (Orange)	Incorrectly Simulated Community Gain (Blue)
Total Area, km²		21.8		39.6		38.2	
WP Inundation Duration, days	30	3.2	18.6	5.9	33.8	13.4	24.8
		15%	85%	15%	85%	35%	65%
	15	3.6	18.3	7.1	32.5	15.8	22.4
		16%	84%	18%	82%	41%	59%
	10	5.1	16.7	13.0	26.7	23.7	14.5
		23%	77%	33%	67%	62%	38%
WP Inundation Depth, m	0.61	10.2	11.7	28.2	11.5	33.5	4.7
		47%	53%	71%	29%	88%	12%
	1.22	3.0	18.8	11.3	28.4	21.0	17.2
		14%	86%	28%	72%	55%	45%
	1.83	0.3	21.6	1.0	38.6	2.9	35.3
		1%	99%	3%	97%	8%	92%

Bottomland hardwood and wet prairie results were compared to identify general trends. Based on the results, no single metric was sufficient for predicting all bottomland hardwood community outcomes. Inundation duration thresholds better predicted bottomland hardwood gain and persistence, demonstrated by higher percentages of correctly simulated outcomes (Figure 19). Likewise, inundation depth only successfully predicted community loss (Figure 19). Unlike bottomland hardwood, one metric threshold for wet prairie was reasonable for community outcome predictions. Specifically, an inundation duration of 10 days for wet prairie was reasonable for all community outcomes with respect to across-the-board predictions even though it was not the highest performer for any singular outcome (gain, persistence, loss) (Figure 20).

The following sections discuss results for each habitat metric type (inundation duration, inundation depth, and dry days). As previously discussed, failure to generate sub-simulation duration maps from HEC-RAS 5.0.7 prevented further analysis of the dry day habitat metric thresholds.

Inundation Duration

Inundation duration metrics were analyzed for bottomland hardwood forests and wet prairie. Area distributions indicated that inundation duration metrics overestimated community gain and underestimated community loss for both bottomland hardwood forest and wet prairie. More specifically, the inundation duration appeared to overestimate community gain within areas of observed community loss. For bottomland hardwood forests, the inundation duration thresholds incorrectly identified community loss for 72% to 82% of the observed community loss area. For wet prairies, the inundation duration threshold incorrectly identified community loss for 38% to 65% of the total observed community loss area. However, an inundation duration of 10 days for wet prairie was reasonable for all community outcomes with respect to across-the-board predictions even though it was not the highest performer for any singular outcome (gain, persistence, loss) (Figure 20).

Out of the bottomland hardwood forest inundation duration thresholds, 14 days appeared to best predict community gain as it correctly identified 79% of observed community gain and 86% of persistent communities (Figure 19). However, the high percentages of correctly identified community gain and persistence may be attributed to the fact that 14 days indicated ideal community conditions for all observed community outcomes (Figure 15). Out of the wet prairie inundation duration thresholds, 30 days appeared to best predict community gain as it correctly identified 85% of observed community gain and 85% of persistent communities (Figure 20). Once again, the high percentages of correctly identified community gain and persistence may be attributed to the fact that 30 days indicated ideal community conditions everywhere, rather than just the targeted observed community gain areas (Figure 17). Although the inundation duration

metric thresholds provided estimates for predicting community gain, they were not good indicators for community loss predictions.

Community outcome area percentages for bottomland hardwood forests appeared to be sensitive to inundation duration threshold adjustments. Halving of the bottomland hardwood forests inundation depth threshold resulted in a 29% and 46% reduction in correctly identifying community gains and persistent communities, respectively. Reducing the inundation duration metric threshold for bottomland hardwood forest reduced the percentages of correctly identified community gains and persistent communities. However, halving the initial metric threshold for wet prairie resulted in a 1% and 3% reduction in correctly identifying community gains and persistent communities, respectively.

Inundation Depth

With respect to bottomland hardwood forests, inundation depth appeared to overestimate community loss, incorrectly estimating community loss for 63% to 88% of observed community gains and 56% to 87% of observed persistent communities. The bottomland hardwood forest inundation depth threshold of 0.15 meters best predicted community loss by correctly identifying 80% of observed community loss (Figure 19). As a result, the application of the bottomland hardwood forest inundation depth thresholds may be applied to bottomland hardwood forest to predict community loss but may lead to overpredictions.

Wet prairie inundation depth thresholds did not appear to inherently overpredict or underpredict community gain like bottomland hardwood forest or inundation duration thresholds. While the inundation depth threshold of 0.61 meters predicted community loss, increases to the inundation depth threshold significantly reduced community loss estimates and began overpredicting community gains. Wet prairie results appeared more sensitive to varying threshold

depths than bottomland hardwood forest. Doubling the initial metric threshold for wet prairie resulted in correctly identifying community gains by an additional 33% and correctly identifying persistent communities by 43% (Figure 20). Doubling of the bottomland hardwood forest inundation depth threshold correctly identified an additional 7% of community gain and 10% of persistent communities (Figure 19).

Since wet prairie depth thresholds both overpredicted community gain and loss, different wet prairie depth thresholds could be used to predict the different community outcomes. For instance, a depth threshold of 1.22 meters was a good metric for predicting community gain as it correctly identified 86% of observed community gain, 72% of persistent communities, and 55% of habitat loss (Figure 20). The 1.83 meters depth threshold was also considered for use in predicting community gain as it correctly identified 99% of observed community gain. However, the 1.83 meters depth threshold metric only correctly simulated 8% of community loss, indicating that this metric threshold significantly overestimated community gain. As a result, the 1.22 meters threshold was recommended for predicting community gain (Figure 18). A depth threshold of 0.61 meters was a better metric for predicting wet prairie loss as it correctly identified 88% of observed community loss (Figure 20). All other wet prairie depth thresholds underpredicted habitat loss. As a result, the 0.61 meters threshold was recommended for predicting wet prairie loss.

Literature Comparison

The recommended inundation duration and inundation depth thresholds were compared to previously identified thresholds from the literature review. Table 13 provides identified thresholds from past studies.

Table 13:
Comparison of Recommended Thresholds

Community Type	Source	Inundation Duration, days	Inundation Depth, m	Notes
Wet Prairie	*Recommended Threshold*	*30*	*0.61 - 1.22*	
	(Olmstead & Loope, 1984)	30-90	0.3	
	(Weaver, 1960)	30	0.6 - 0.9	
	(Banach et al., 2009)	21	0.6	
	(Gattringer et al., 2017)	14	---	
Bottomland Hardwood	*Recommended Threshold*	*14*	*0.15*	
	(Nelson, 2010)	14		
	(Hodges, 1997)	30	0.3 - 0.7	Water depths that exceeded the thresholds produced 80%-90% mortality
	(Kabrick et al., 2012)	21	---	Inundation durations of three weeks resulted in mortality rates of approximately 24%
	(U.S. Army Corps of Engineers, 2020)	14	0.15	The thresholds identified were not measured or determined from observations, but instead were identified from a literature review
	(McCurry et al., 2010)	15	---	Durations less than the threshold provided benefits
	(Allen et al., 2001)		0.6	Species specific. Species may be more water tolerant than Missouri BH species

The recommended inundation duration thresholds for both wet prairie and bottomland hardwood reflected reported thresholds. A wet prairie inundation threshold of 30 days fell within the upper limits of other inundation thresholds (Olmstead & Loope, 1984; Weaver, 1960), indicating 30 days was a reasonable inundation duration habitat metric for wet prairie. However, the 10 day threshold fell below recommended limits. The recommended inundation duration metric for bottomland hardwood forests was within past threshold ranges but was more representative of the lower limit of the acceptable threshold range. Although the recommended 14 days was on the lower end of the acceptable threshold range, the simulated loss rates (18%) associated with the 14-day inundation duration threshold were similar to mortality rates (24%) obtained using a 21-day

threshold (Kabrick et al., 2012), indicating that the simulated loss percentages for a bottomland hardwood inundation threshold of 14 days were reasonable.

The recommended wet prairie depth threshold of 0.61 meters for community loss predictions was in the middle of acceptable threshold ranges from other studies. However, the 1.22-meter inundation depth threshold exceeded the threshold ranges identified in the literature review, indicating that 1.22 meters may not be the best habitat metric threshold to predict wet prairie gains. As a result, when estimating community gains for wet prairie, emphasis should be placed on inundation duration rather than inundation depth. Additional research involving physical analysis of wet prairie communities and response to varying inundation depth could be used to verify which depth thresholds are more representative of wet prairie community transitions and if the 1.22-meter depth threshold is indeed applicable.

The inundation depth threshold recommended for bottomland hardwood was below previously used thresholds. Although the recommended 0.15-meter threshold was below the acceptable threshold range, the simulated loss rates (80%) associated with the 0.15-meter inundation depth threshold were similar to mortality rates (80%) obtained using a 0.3-meter threshold (Hodges, 1997). The similar mortality rates indicated that the bottomland hardwood inundation depth threshold of 0.15 meters produced reasonable loss estimates.

Summary and Application

While several metrics overestimated wetland community loss or community gains, no singular hydraulic parameter produced area distributions representative of all observed community outcomes. Inundation duration less than the specified threshold was a better metric than inundation depth for predicting both bottomland hardwood forest and wet prairie community gains or spatial expansion. Inundation durations of 14 days and 30 days fell within acceptable threshold ranges

documented in past studies and could be used to predict community gains for bottomland hardwood and wet prairie, respectively. An inundation duration of 10 days fell below acceptable threshold ranges but best simulated all community outcomes for wet prairie. Inundation depth exceeding a specified threshold of 0.15 meters was a better metric than inundation duration for predicting bottomland hardwood forest loss but fell below threshold ranges identified in the literature. Finally, wet prairie inundation depth thresholds could be used to predict both community gains and community losses depending on the selection of the habitat threshold magnitude. An inundation duration threshold of 1.22 meters could be used to predict wetland prairie gains and an inundation depth threshold of 0.61 meters could be used to predict wet prairie loss. However, the wet prairie inundation depth threshold of 1.22 meters exceeded acceptable thresholds, indicating inundation duration may generate replicable results in future wet prairie analyses rather than inundation depth. As a result, both inundation duration and inundation depth should be used together to predict gains and loss for all communities, but inundation duration should receive higher priority when used to predict wet prairie community gain.

While this research confirmed the utility of hydraulic metrics for predicting wetland community transitions, understanding of large-scale hydraulics could be improved. This research analyzed the impacts of individual hydraulic parameters resulting from continuous simulation of a complicated hydraulic system on wetland communities, contributing to overall understanding of wetland community response in large-scale hydraulic systems. However, since the analysis only focused on relationships with specific hydraulic parameters such as inundation duration and inundation depth, the parameters analyzed may not completely portray the complexity of the entire hydraulic system. Additional hydraulic parameters and associated habitat metrics may be required to fully understand floodplain hydraulic behavior and resulting wetland community transitions.

For example, further research is needed to identify additional hydraulic parameters and associated habitat metric thresholds related to other parameters such as sedimentation and soil characteristics for bottomland hardwood forests and wet prairie. Additionally, analysis related to the interaction between different hydraulic habitat metrics such as inundation duration and sedimentation could further improve understanding of large-scale hydraulic impacts on wetland community response.

This research, with respect to bottomland hardwoods and wet prairie communities, may be transferable to other basins located within the Midwestern United States with similar characteristics as Locust Creek Basin. For instance, the analysis may be applied to an agricultural, unregulated basin. This is because changes in basin location, hydrology, and upstream basin characteristics may result in changes to downstream species composition within wet prairie and bottomland hardwood communities. Alteration in species and community composition may create changes in overall hydraulic tolerances in wet prairie or bottomland hardwood communities, contributing to identification of different metric thresholds.

Limitations and Future Research

Several sources of uncertainty existed within the hydraulic model and analysis that could be improved with additional information or future analysis.

Local Inflows: Local inflows from bluff drainage and rainfall within the model domain were not included in the simulations. Accounting for the missing drainage area may introduce larger volumes to the floodplain and alter timing of hydrograph peaks. As a result, the existing model may underrepresent the changes to the floodplain wetland communities. Incorporation of bluff drainage and smaller drainage areas to better account for the full volume entering the floodplain could improve overall floodplain volume estimates. A possible source of error in the results may result from not including all flows contributing to the wetlands. The missing additional

drainage areas may introduce larger volumes to the floodplain and alter timing of hydrograph peaks. As a result, the existing model may underrepresent the changes to the floodplain wetland communities.

Log Jams. Several assumptions were made when modeling log jams. The exact dates for initial development and final removal for log jams were not known. For the purpose of the model, it was assumed the log jams persisted for the entire year of analysis. However, log jams may have only formed after a major event within that given year or been removed early within the year. By keeping the log jams in place for an entire year, the hydraulic effects of a log jam (increased water surface elevation, reduced flow, etc.) may be over or underrepresented in the model simulations. Future surveys of log jams documenting the initial formation, log jam dimensions, and removal date would provide additional data to better model the log jams to ensure log jam assumptions don't contribute to overestimation of changing wetland community spatial extents. High resolution remote sensing data could be used in future work to identify log jam characteristics.

Stationary Landcover: Other than adjustments made to account for in-channel log jams on an annual basis, additional adjustments to landcover were not included. As a result, the hydraulic results do not show seasonality impacts resulting from decreased roughness due to leaf-off periods, harvesting, and tilling operations. Additionally, the hydraulic results do not show impacts resulting from gradual growth and die-off of varying communities. For example, the hardwood riparian zones may thin and reduce the floodplain roughness with increased inundation as trees die. Incorporation of temporally and spatially varying roughness coefficients would provide the ability to better simulate varying landcover changes.

Infiltration and Evaporation. At the time of analysis, HEC-RAS 5.0.7 did not include methods to simulate infiltration and evaporation within 2D area cells. Cells within the 2D area

permanently held water if the cells contained lower elevations than surrounding cells. Depending on soil moisture status, the permanently ponded water may overestimate inundation duration and overestimate negative impacts to bottomland hardwood forest and wet prairie communities. Infiltration and evaporation process would allow these permanently ponded areas to drain to a water depth of zero and return to a dry state. Within the HEC-RAS modeling framework, further advancements have been made to incorporate hydrologic processes within 2D hydraulic simulations. The model should be updated to a newer version of HEC-RAS to account for soil infiltration and evaporation. Doing so would provide better estimates of inundation duration times and impacts to wetland communities.

2011 Ecosystem Survey. The 2011 ecosystem survey was largely based on an analysis that used soil classifications and other parameters to identify bottomland hardwood forest and wet prairie spatial extents supplemented with ground truthing. As a result, the 2011 ecosystem survey may not have been completely representative of observed wetland community locations. Future wetland community transitional analyses should incorporate an additional ecosystem survey to provide another reference for community spatial extents and reduce spatial extent uncertainty.

Wetland Community Quality. This analysis applied thresholds with the assumption that community loss may be represented by locations that exceeded the specified habitat metric thresholds. However, the thresholds analyzed may be an indicator of community quality rather than a strict life and death factor. Additional research involving ground surveys and specimen samples of bottomland hardwood forests and wet prairies in Pershing State Park is recommended to verify the quality of the wetland community within the predicted community outcome areas.

Evaluation of HEC-RAS 2D for Application

Inundation duration, inundation depth, and dry days were identified from the literature review as three hydraulic parameters with potential to predict wetland community or ecosystem transitions. Several hydraulic results such as inundation duration and inundation depth were easily simulated, exported from HEC-RAS, and used to identify wetland community transitional trends, indicating HEC-RAS was a beneficial tool for wetland management.

However, limitations in computing duration maps for sub-simulation time frames complicated duration map analysis. In RAS Mapper, the duration map was computed by subtracting the arrival time from the recession time for each cell. By default, the duration maps were generated using the full simulation time period. An option existed to specify the start date and time or apply a start date and time offset when generating the duration maps. When this option was selected, the arrival time and recession calculation computations should begin at the specified start date and time. However, HEC-RAS continued to calculate the recession map with respect to the start of the entire simulation time period.

For example, wet prairie dry depth simulations were run from 01July 00:00 to 31October 24:00 of each analysis year, resulting in a total simulation period of 123 days. Duration maps were extracted from HEC-RAS using a specified start date and time of 15July 00:00 resulting in a duration analysis period of 109 days, meaning that the exported durations should range from zero to 109 days. However, once the duration maps were opened in ArcGIS Pro, several of the resulting durations contained negative days, indicating that the initial arrival of water occurred after water last receded below the specified depth threshold. To further investigate, the recession and arrival time maps were generated using a start date and time of 15July 00:00. Arrival times started at zero and did not exceed the 109-day period of analysis. However, it was still unclear if the arrival time

maps were generated from the start of the simulation time period or the specified start date and time. The recession map results contained maximum values of 123 days, indicating that the recession maps ignored the specified date and time and continued to use the simulation start time for recession time computations. Due to these uncertainties associated with the development of duration maps for sub-simulation time frames, dry day habitat metric thresholds were not analyzed using the sub-simulation time frames. Additional analysis could be completed by rerunning the dry day simulations with the start and end days of the simulation corresponding to the dry day period of analysis for each wetland community. As long as the simulation time frame corresponds to the specified period of analysis and a start date offset is not used when generating the maps, HEC-RAS will report correct duration values.

This outcome, although not informative for the thesis research objective, was important, nonetheless. HEC-RAS is a widely used hydraulic modeling package and HEC-RAS 2D will be used in future analysis. Identifying and correcting potential issues with sub-simulation analysis will be crucial for simulation of continuous time series in two-dimensional modeling.

Chapter 4: Conclusions

This thesis used a two-dimensional hydraulic model to simulate flow over a 10-year period and tested whether common hydraulic parameters, including inundation duration, depth, and dry day duration, could be used to predict shifts in riparian wetland ecosystem boundaries. The goal of this effort was to identify easily monitored hydraulic metrics that could be used to forecast wetland risk and, overall, to improve understanding of large-scale hydraulics on wetland trajectories.

This thesis represented an exciting and novel application of a 2D HEC-RAS model for continuous annual simulations and wetland community response. Through this application of 2D HEC-RAS, it was identified that, together, inundation duration and inundation depth habitat metrics were overall predictive of wetland community transitions for bottomland hardwood forest and wet prairie. Inundation duration less than the specified threshold was a better metric than inundation depth for predicting both bottomland hardwood forest and wet prairie community gains or spatial expansion. Conversely, inundation depth exceeding the specified threshold was a better metric than inundation duration for predicting bottomland hardwood forest loss. Finally, wet prairie inundation depth thresholds could be used to predict both community gains and community losses depending on the selection of the habitat threshold magnitude. Overall, this thesis demonstrated that there was no singular hydraulic habitat metric that captured both community gains and losses.

The overall predictive trends associated with inundation duration and inundation depth habitat metrics could be used in future applications. Wetland resource managers can simulate projected hydrologic inflows and use the hydraulic results with habitat metrics to adapt monitoring, sampling, and rehabilitation efforts to effectively target rehabilitation locations in areas of

simulated, ideal growing conditions. Additionally, scientists interested in studying individual species could measure these hydraulic habitat metrics to develop relationships between the metric thresholds and species response.

References

Abbe, T. (2006). *Conceptual design guidelines: Application of engineered logjams.*

Aberle, J., & Järvelä, J. (2013). Flow resistance of emergent rigid and flexible floodplain vegetation. *Journal of Hydraulic Research*, *51*(1), 33–45. https://doi.org/10.1080/00221686.2012.754795

Addy, S., & Wilkinson, M. E. (2019). Representing natural and artificial in-channel large wood in numerical hydraulic and hydrological models. *WIREs Water*, *6*(6), e1389. https://doi.org/https://doi.org/10.1002/wat2.1389

Alberto, A., St-Hilaire, A., Courtenay, S. C., & van den Heuvel, M. R. (2016). Monitoring stream sediment loads in response to agriculture in Prince Edward Island, Canada. *Environmental Monitoring and Assessment*, *188*(7). https://doi.org/10.1007/s10661-016-5411-3

Allen, J. A., Keeland, B. D., Stanturf, J. A., Clewell, A. F., & Kennedy, H. E. , Jr. (2001). *A Guide to Bottomland Hardwood Restoration*. U.S. Geological Survey, Biological Resources Division Information and Technology Report USGS/BRD/ITR-2000-0011, U.S. Department of Agriculture, Forest Service, Southern Research Station, General Technical Report SRS-40. https://pubs.usgs.gov/itr/2000/0011/report.pdf

Angel, J. R., Swanson, C., Boustead, B. M., Conlon, K., Hall, K. R., Jorns, J. L., Kunkel, K. E., Lemos, M. C., Lofgren, B. M., Ontl, T., Posey, J., Stone, K., Takle, E., & Todey, D. (2018). *Chapter 21 : Midwest. Impacts, Risks, and Adaptation in the United States: The Fourth National Climate Assessment, Volume II*. https://doi.org/10.7930/NCA4.2018.CH21

Banach, K., Banach, A. M., Lamers, L. P. M., de Kroon, H., Bennicelli, R. P., Smits, A. J. M., & Visser, E. J. W. (2009). Differences in flooding tolerance between species from two wetland

habitats with contrasting hydrology: implications for vegetation development in future floodwater retention areas. *Annals of Botany*, *103*(2), 341–351. https://doi.org/10.1093/aob/mcn183

Baptist, M. J., Babovic, V., Rodríguez Uthurburu, J., Keijzer, M., Uittenbogaard, R. E., Mynett, A., & Verwey, A. (2007). On inducing equations for vegetation resistance. *Journal of Hydraulic Research*, *45*(4), 435–450. https://doi.org/10.1080/00221686.2007.9521778

Bates, B., Kundzewicz, Z. W., Wu, S., Burkett, V., Doell, P., Gwary, D., Hanson, C., Heij, B., Jiménez, B., Kaser, G., Kitoh, A., Kovats, S., Kumar, P., Magadza, C. H. D., Martino, D., Mata, L., Medany, M., Miller, K., & Arnell, N. (2008). *Climate Change and Water. Technical Paper of the Intergovernmental Panel on Climate Change*.

Beck, W. J., Moore, P. L., Schilling, K. E., Wolter, C. F., Isenhart, T. M., Cole, K. J., & Tomer, M. D. (2019). Changes in lateral floodplain connectivity accompanying stream channel evolution: Implications for sediment and nutrient budgets. *Science of The Total Environment*, *660*, 1015–1028. https://doi.org/https://doi.org/10.1016/j.scitotenv.2019.01.038

Berhane, T. M., Lane, C. R., Mengistu, S. G., Christensen, J., Golden, H. E., Qiu, S., Zhu, Z., & Wu, Q. (2020). Land-Cover Changes to Surface-Water Buffers in the Midwestern USA: 25 Years of Landsat Data Analyses (1993–2017). *Remote Sensing*, *12*(5). https://doi.org/10.3390/rs12050754

Bradshaw, C. J. A., Sodhi, N. S., Peh, K. S. H., & Brook, B. W. (2007). Global evidence that deforestation amplifies flood risk and severity in the developing world. *Global Change Biology*, *13*(11), 2379–2395. https://doi.org/10.1111/j.1365-2486.2007.01446.x

Brierley, G., & Stankoviansky, M. (2002). Geomorphic responses to land use change: lessons from different landscape settings. *Earth Surface Processes and Landforms*, *27*(4), 339–341. https://doi.org/10.1002/esp.330

Briscoe, C. B. (1961). Germination of Cherrybark and Nuttal Oak Acorns Following Flooding. *Rio Piedras, Puerto Rico: U.S. Forest Service, Tropical Forest Research Center*. *Ecology*, *42*(2), 430–431.

Brummer, C. J., Abbe, T. B., Sampson, J. R., & Montgomery, D. R. (2006). Influence of vertical channel change associated with wood accumulations on delineating channel migration zones, Washington, USA. *Geomorphology*, *80*(3), 295–309. https://doi.org/https://doi.org/10.1016/j.geomorph.2006.03.002

Burke, M., King, S., Gartner, D., & Eisenbies, M. (2003). Vegetation, Soil, and Flooding Relationships in a Blackwater Floodplain Forest. *Wetlands*, *23*, 988–1002. https://doi.org/10.1672/0277-5212(2003)023[0988:VSAFRI]2.0.CO;2

Byun, K., & Hamlet, A. F. (2018). Projected changes in future climate over the Midwest and Great Lakes region using downscaled CMIP5 ensembles. *International Journal of Climatology*, *38*(S1), e531–e553. https://doi.org/https://doi.org/10.1002/joc.5388

Camporeale, C., Perucca, E., Ridolfi, L., & Gurnell, A. M. (2013). Modeling the interactions between river morphodynamics and riparian vegetation. *Reviews of Geophysics*, *51*(3), 379–414. https://doi.org/10.1002/rog.20014

Camporeale, C., & Ridolfi, L. (2006). Riparian vegetation distribution induced by river flow variability: A stochastic approach. *Water Resources Research*, *42*(10). https://doi.org/https://doi.org/10.1029/2006WR004933

Chow, V. te. (1959). *Open-Channel Hydraulics*. McGraw Hill.

Claassen, R., Carriazo, F., Cooper, J., Hellerstein, D., & Udea, K. (2011). *Grassland to Cropland Conversion in the Northern Plains: The Role of Crop Insurance, Commodity, and Disaster Programs*. https://www.ers.usda.gov/webdocs/publications/44876/7477_err120.pdf?v=0

Clark, C. (1987). Deforestation and Floods. *Environmental Conservation*, *14*(1), 67–69. https://doi.org/10.1017/S0376892900011127

Collins, B. D., Montgomery, D. R., Fetherston, K. L., & Abbe, T. B. (2012). The floodplain large-wood cycle hypothesis: A mechanism for the physical and biotic structuring of temperate forested alluvial valleys in the North Pacific coastal ecoregion. *Geomorphology*, *139–140*, 460–470. https://doi.org/10.1016/j.geomorph.2011.11.011

Covino, T. (2017). Hydrologic connectivity as a framework for understanding biogeochemical flux through watersheds and along fluvial networks. *Geomorphology*, *277*, 133–144. https://doi.org/https://doi.org/10.1016/j.geomorph.2016.09.030

Dahl, T. E. (1990). *Wetlands losses in the United States, 1780's to 1980's*. U.S. Dept. of the Interior, Fish and Wildlife Service. //catalog.hathitrust.org/Record/002477298

Dahl, T. E. (2011). *Status and Trends of Wetlands in the Conterminous United States 2004 to 2009*.

Davidson, S. L., & Eaton, B. C. (2013). Modeling channel morphodynamic response to variations in large wood: Implications for stream rehabilitation in degraded watersheds. *Geomorphology*, *202*, 59–73. https://doi.org/https://doi.org/10.1016/j.geomorph.2012.10.005

Dijkstra, J. T., & Uittenbogaard, R. E. (2010). Modeling the interaction between flow and highly flexible aquatic vegetation. *Water Resources Research*, *46*(12). https://doi.org/https://doi.org/10.1029/2010WR009246

Douglas, E. M., Vogel, R. M., & Kroll, C. N. (2000). Trends in floods and low flows in the United States: impact of spatial correlation. *Journal of Hydrology*, *240*(1), 90–105. https://doi.org/https://doi.org/10.1016/S0022-1694(00)00336-X

Emerson, D. G., Vecchia, A. v, Dahl, A. L., & Survey, U. S. G. (2005). Evaluation of drainage-area ratio method used to estimate streamflow for the Red River of the North Basin, North Dakota and Minnesota. In *Scientific Investigations Report* (Online only). https://doi.org/10.3133/sir20055017

Environmental Protection Agency. (2016). *What Climate Change Means for Missouri*. *EPA 430-F-16-027*.

Fraaije, R. G. A., ter Braak, C. J. F., Verduyn, B., Breeman, L. B. S., Verhoeven, J. T. A., & Soons, M. B. (2015). Early plant recruitment stages set the template for the development of vegetation patterns along a hydrological gradient. *Functional Ecology*, *29*(7), 971–980. https://doi.org/10.1111/1365-2435.12441

Funk, J. C., & Ruhr, C. E. (1971). Stream channelization in the midwest. In *Stream Channelization: A Symposium. AFS Special Publication #2*.

Galat, D. L., Fredrickson, L. H., Humburg, D. D., Bataille, K. J., Bodie, J. R., Dohrenwend, J., Gelwicks, G. T., Havel, J. E., Helmers, D. L., Hooker, J. B., Jones, J. R., Knowlton, M. F., Kubisiak, J., Mazourek, J., McColpin, A. C., Renken, R. B., & Semlitsch, R. D. (1998). Flooding to restore connectivity of regulated, large-river wetlands: Natural and controlled flooding as complementary processes along the lower Missouri River. *BioScience*, *48*(9), 721–733. https://doi.org/10.2307/1313335

Garssen, A. G., Baattrup-Pedersen, A., Riis, T., Raven, B. M., Hoffman, C. C., Verhoeven, J. T. A., & Soons, M. B. (2017). Effects of increased flooding on riparian vegetation: Field

experiments simulating climate change along five European lowland streams. *Global Change Biology*, *23*(8), 3052–3063. https://doi.org/10.1111/gcb.13687

Garssen, A. G., Baattrup-Pedersen, A., Voesenek, L. A. C. J., Verhoeven, J. T. A., & Soons, M. B. (2015). Riparian plant community responses to increased flooding: a meta-analysis. *Global Change Biology*, *21*(8), 2881–2890. https://doi.org/10.1111/gcb.12921

Gattringer, J. P., Donath, T. W., Eckstein, R. L., Ludewig, K., Otte, A., & Harvolk-Schöning, S. (2017). Flooding tolerance of four floodplain meadow species depends on age. *PLOS ONE*, *12*(5), e0176869-. https://doi.org/10.1371/journal.pone.0176869

Gellis, A., Myers, M. K., Noe, G., Hupp, C., Schenk, E., & Myers, L. (2016). Storms, channel changes, and a sediment budget for an urban-suburban stream, Difficult Run, Virginia, USA. *Geomorphology*, *278*. https://doi.org/10.1016/j.geomorph.2016.10.031

Groves, J., Williams, D., Caley, P., Norris, R., & Caitcheon, G. (2009). Modelling of floating seed dispersal in a fluvial environment. *River Research and Applications*, *25*, 582–592. https://doi.org/10.1002/rra.1229

Guo, Y., Shelton, M., & Lockhart, B. R. (1998). Effects of flood duration and season on germination of black, cherrybark, northern red, and water oak acorns. *New Forests*, *15*(1), 69–76. https://doi.org/10.1023/A:1006535619398

Hafs, A. W., Harrison, L. R., Utz, R. M., & Dunne, T. (2014). Quantifying the role of woody debris in providing bioenergetically favorable habitat for juvenile salmon. *Ecological Modelling*, *285*, 30–38. https://doi.org/https://doi.org/10.1016/j.ecolmodel.2014.04.015

Hall, T. F., & Smith, G. E. (1955). Effects of Flooding on Woody Plants, West Sandy Dewatering Project, Kentucky Reservoir. *Journal of Forestry*, *53*(4), 281–285. https://doi.org/10.1093/jof/53.4.281

Hanberry, B. B., Dey, D. C., & He, H. S. (2014). The history of widespread decrease in oak dominance exemplified in a grassland–forest landscape. *Science of The Total Environment*, *476–477*, 591–600. https://doi.org/https://doi.org/10.1016/j.scitotenv.2014.01.048

Heimann, D. C., & Survey, U. S. G. (2017). Assessment of an in-channel redistribution technique for large woody debris management in Locust Creek, Linn County, Missouri. In *Scientific Investigations Report*. https://doi.org/10.3133/sir20175120

Heitmeyer, M. E., Nigh, T. A., Mengel, D. C., Blanchard, P. E., & Nelson, F. A. (2011). *An evaluation of ecosystem restoration and management options for floodplains in the Lower Grand River Region, Missouri. Greenbrier Wetland Services Report 11-01*.

Hodges, J. D. (1997). Development and ecology of bottomland hardwood sites. *Forest Ecology and Management*, *90*(2), 117–125. https://doi.org/https://doi.org/10.1016/S0378-1127(96)03906-0

Hook, D. (1984). Adaptations to Flooding with Fresh Water. In *Flooding and Plant Growth* (pp. 265–294). https://doi.org/10.1016/B978-0-12-424120-6.50013-4

Hooke, J. M., Brookes, C. J., Duane, W., & Mant, J. M. (2005). A simulation model of morphological, vegetation and sediment changes in ephemeral streams. *Earth Surface Processes and Landforms*, *30*(7), 845–866. https://doi.org/10.1002/esp.1195

Hosner, J. F. (1958). The Effects of Complete Inundation upon Seedlings of Six Bottomland Tree Species. *Ecology*, *39*(2), 371–373. https://doi.org/10.2307/1931886

Hosner, J. F. (1960). Relative Tolerance to Complete Inundation of Fourteen Bottomland Tree Species. *Forest Science*, *6*(3), 246–251. https://doi.org/10.1093/forestscience/6.3.246

Hupp, C., Noe, G., Schenk, E., & Benthem, A. (2013). Recent and historic sediment dynamics along Difficult Run, a suburban Virginia Piedmont stream. *Geomorphology, s 180–181*, 156–169. https://doi.org/10.1016/j.geomorph.2012.10.007

Hupp, C. R., & Osterkamp, W. R. (1985). Bottomland Vegetation Distribution along Passage Creek, Virginia, in Relation to Fluvial Landforms. *Ecology*, *66*(3), 670–681. https://doi.org/10.2307/1940528

Hydrologic Engineering Center. (2009). *HEC-DSSVue: HEC Data Storage System Visual Utility Engine User's Manual*.

Hydrologic Engineering Center. (2020). *HEC-RAS River Analysis System User's Manual*.

Jacobson, R., & Faust, T. (2014). Hydrologic connectivity of floodplains, northern missouri-implications for management and restoration of floodplain forest communities in disturbed landscapes. *River Research and Applications*, *30*(3), 269–286. https://doi.org/10.1002/rra.2636

Jacques, R., Stovall, J., Comer, C., Williams, H., & Symmank, M. (2021). Herbivory and flooding impacts on planted bottomland hardwood seedlings. *Forestry: An International Journal of Forest Research*, cpab043. https://doi.org/10.1093/forestry/cpab043

Järvelä, J. (2004). Determination of flow resistance caused by non-submerged woody vegetation. *International Journal of River Basin Management*, *2*(1), 61–70. https://doi.org/10.1080/15715124.2004.9635222

Johnston, C. A. (2003). Shrub Species as Indicators of Wetland Sedimentation. *Wetlands*, *23*(4), 911–920. https://doi.org/10.1672/0277-5212(2003)023[0911:SSAIOW]2.0.CO;2

Kabrick, J., Dey, D., Sambeek, J., Coggeshall, M., & Jacobs, D. F. (2012). Quantifying flooding effects on hardwood seedling survival and growth for bottomland restoration. *New Forests, 43*, 695–710.

Kercher, S., Herr-Turoff, A., & Zedler, J. (2007). Understanding invasion as a process: The case of Phalaris arundinacea in wet prairies. *Biological Invasions*, *9*, 657–665. https://doi.org/10.1007/s10530-006-9066-9

Kercher, S. M., & Zedler, J. B. (2004). Flood tolerance in wetland angiosperms: a comparison of invasive and noninvasive species. *Aquatic Botany*, *80*(2), 89–102. https://doi.org/https://doi.org/10.1016/j.aquabot.2004.08.003

Keys, T. A., Govenor, H., Jones, C. N., Hession, W. C., Hester, E. T., & Scott, D. T. (2018). Effects of large wood on floodplain connectivity in a headwater Mid-Atlantic stream. *Ecological Engineering*, *118*, 134–142. https://doi.org/https://doi.org/10.1016/j.ecoleng.2018.05.007

Knox, J. C. (2006). Floodplain sedimentation in the Upper Mississippi Valley: Natural versus human accelerated. *Geomorphology*, *79*(3), 286–310. https://doi.org/https://doi.org/10.1016/j.geomorph.2006.06.031

Kothyari, U., Hashimoto, H., & Hayashi, K. (2009). Effect of tall vegetation on sediment transport by channel flows. *Journal of Hydraulic Research*, *47*, 700–710. https://doi.org/10.3826/jhr.2009.3317

Krzywicka, A. E., Pociask, G. E., Grimley, D. A., & Matthews, J. W. (2017). Hydrology and soil magnetic susceptibility as predictors of planted tree survival in a restored floodplain forest. *Ecological Engineering*, *103*, 275–287. https://doi.org/https://doi.org/10.1016/j.ecoleng.2017.04.011

Kushlan, J. A. (1990). Freshwater Marshes. In R. L. Myers & J. J. Ewel (Eds.), *Ecosystems of Florida* (pp. 324–363). University of Central Florida Press.

Lark, T. J., Spawn, S. A., Bougie, M., & Gibbs, H. K. (2020). Cropland expansion in the United States produces marginal yields at high costs to wildlife. *Nature Communications*, *11*(1), 4295. https://doi.org/10.1038/s41467-020-18045-z

Laurance, W. F. (2007). Forests and floods. *Nature*, *449*(7161), 409–410. https://doi.org/10.1038/449409a

Liu, X., Zeng, Y., & Huai, W. (2018). Modeling of Interactions Between Floating Particles and Emergent Stems in Slow Open Channel Flow. *Water Resources Research*, *54*(9), 7061–7075. https://doi.org/https://doi.org/10.1029/2018WR022617

Luhar, M., & Nepf, H. (2013). From the blade scale to the reach scale: A characterization of aquatic vegetative drag. *Advances in Water Resources*, *51*, 305–316. https://doi.org/10.1016/j.advwatres.2012.02.002

Lukács, B. A., E-Vojtkó, A., Erős, T., Molnár V., A., Szabó, S., & Götzenberger, L. (2019). Carbon forms, nutrients and water velocity filter hydrophyte and riverbank species differently: A trait-based study. *Journal of Vegetation Science*, *30*(3), 471–484. https://doi.org/10.1111/jvs.12738

Mahoney, J. M., & Rood, S. B. (1998). Streamflow requirements for cottonwood seedling recruitment—An integrative model. *Wetlands*, *18*(4), 634–645. https://doi.org/10.1007/BF03161678

Martínez-Espinosa, C., Sauvage, S., al Bitar, A., Green, P. A., Vörösmarty, C. J., & Sánchez-Pérez, J. M. (2021). Denitrification in wetlands: A review towards a quantification at global

scale. *Science of The Total Environment*, *754*, 142398. https://doi.org/https://doi.org/10.1016/j.scitotenv.2020.142398

McCurry, J. R., Gray, M. J., & Mercker, D. C. (2010). Early Growing Season Flooding Influence on Seedlings of Three Common Bottomland Hardwood Species in Western Tennessee. *Journal of Fish and Wildlife Management*, *1*(1), 11–18. https://doi.org/10.3996/JFWM-015

McKenney, R., Jacobson, R. B., & Wertheimer, R. C. (1995). Woody vegetation and channel morphogenesis in low-gradient, gravel-bed streams in the Ozark Plateaus, Missouri and Arkansas. *Geomorphology*, *13*(1), 175–198. https://doi.org/https://doi.org/10.1016/0169-555X(95)00034-3

McMillan, H., Krueger, T., & Freer, J. (2012). Benchmarking observational uncertainties for hydrology: rainfall, river discharge and water quality. *Hydrological Processes*, *26*(26), 4078–4111. https://doi.org/https://doi.org/10.1002/hyp.9384

Meinert, D. M., Steele, A., & Horton, J. (2011). *Pershing State Park: Geology-Landform-Soils Relationships*.

Meli, P., Rey Benayas, J. M., Balvanera, P., & Martínez Ramos, M. (2014). Restoration Enhances Wetland Biodiversity and Ecosystem Service Supply, but Results Are Context-Dependent: A Meta-Analysis. *PLOS ONE*, *9*(4), e93507-. https://doi.org/10.1371/journal.pone.0093507

Merritt, D. M., & Wohl, E. E. (2002). PROCESSES GOVERNING HYDROCHORY ALONG RIVERS: HYDRAULICS, HYDROLOGY, AND DISPERSAL PHENOLOGY. *Ecological Applications*, *12*(4), 1071–1087. https://doi.org/https://doi.org/10.1890/1051-0761(2002)012[1071:PGHARH]2.0.CO;2

Montgomery, D. R. (1999). Process domains and the river continuum. *Journal of the American Water Resources Association*, *35*(2), 397–410. https://doi.org/10.1111/j.1752-1688.1999.tb03598.x

Montgomery, D. R., & Buffington, J. M. (1997). Channel-reach morphology in mountain drainage basins. *Geological Society of America Bulletin*, *109*(5), 596–611. https://doi.org/10.1130/0016-7606(1997)109<0596:CRMIMD>2.3.CO;2

Montgomery, D. R., Collins, B. D., Buffington, J. M., & Abbe, T. B. (2003). Geomorphic effects of wood in rivers. *American Fisheries Society Symposium*, *37*, 21–47.

Mueller, D. S. (2009). *Measuring discharge with acoustic doppler current profilers from a moving boat* (C. R. Wagner, C. R. Wagner, Geological Survey (U.S.), U.S.G.S, U.S. Geological Survey, USGS, Servicio Geológico de los Estados Unidos, United States. Department of the Interior. Geological Survey, & United States. Geological Survey, Eds.). U.S. Dept. of the Interior, U.S. Geological Survey.

Multi-Resolution Land Characteristics Consortium. (2019, January). *NLCD 2016 Land Cover (CONUS)*. https://www.mrlc.gov/data/nlcd-2016-land-cover-conus

Nahlik, A. M., & Fennessy, M. S. (2016). Carbon storage in US wetlands. *Nature Communications*, *7*(1), 13835. https://doi.org/10.1038/ncomms13835

Naiman, R., & Decamps, H. (1997). The Ecology of Interfaces: Riparian Zones. *Annual Review of Ecology and Systematics*, *28*. https://doi.org/10.1146/annurev.ecolsys.28.1.621

Nelson, P. (2010). *The Terrestrial Natural Communities of Missouri*. Missouri Department of Conservation.

Nepf, H. M. (2011). Flow and transport in regions with aquatic vegetation. *Annual Review of Fluid Mechanics*, *44*, 123–142. https://doi.org/10.1146/annurev-fluid-120710-101048

Nepf, H. M. (2012). Hydrodynamics of vegetated channels. *Journal of Hydraulic Research*, *50*(3), 262–279. https://doi.org/10.1080/00221686.2012.696559

NOAA. (2013). *Technical Report NESDIS 142-3: Regional Climate Trends and Scenarios for the U.S. National Climate Assessment*. Department of Commerce, National Oceanic and Atmospheric Administration, National Environmental Satellite, Data, and Information.

Noe, G. B., Hupp, C. R., & Rybicki, N. B. (2013). Hydrogeomorphology Influences Soil Nitrogen and Phosphorus Mineralization in Floodplain Wetlands. *Ecosystems*, *16*(1), 75–94. https://doi.org/10.1007/s10021-012-9597-0

NRCS USDA. (2020). *Web Soil Survey*. Natural Resources Conservation Service, United States Department of Agriculture. https://websoilsurvey.sc.egov.usda.gov/App/WebSoilSurvey.aspx

O'Connell, P. ~E., Ewen, J., O'Donnell, G., & Quinn, P. (2007). Is there a link between agricultural land-use management and flooding? *Hydrology and Earth System Sciences*, *11*(1), 96–107.

Olmstead, I. C., & Loope, Lloyd. L. (1984). Plant communities of Everglades National Park. *Environments of South Florida: Present and Past II*, 167–184.

Osterkamp, W. R., & Hupp, C. R. (1984). Geomorphic and vegetative characteristics along three northern Virginia streams. *Geological Society of America Bulletin*, *95*(9), 1093. https://doi.org/10.1130/0016-7606(1984)95<1093:GAVCAT>2.0.CO;2

Pagliara, S., & Carnacina, L. (2011). Influence of large woody debris on sediment scour at bridge piers. *International Journal of Sediment Research*, *26*(2), 121–136. https://doi.org/https://doi.org/10.1016/S1001-6279(11)60081-4

Parker, C., Henshaw, A. J., Harvey, G. L., & Sayer, C. D. (2017). Reintroduced large wood modifies fine sediment transport and storage in a lowland river channel. *Earth Surface Processes and Landforms*, *42*(11), 1693–1703. https://doi.org/https://doi.org/10.1002/esp.4123

Pekel, J.-F., Cottam, A., Gorelick, N., & Belward, A. S. (2016). High-resolution mapping of global surface water and its long-term changes. *Nature*, *540*(7633), 418–422. https://doi.org/10.1038/nature20584

Phillips, J. D. (2012). Log-jams and avulsions in the San Antonio River Delta, Texas. *Earth Surface Processes and Landforms*, *37*(9), 936–950. https://doi.org/https://doi.org/10.1002/esp.3209

Piliouras, A., Kim, W., & Carlson, B. (2017). Balancing Aggradation and Progradation on a Vegetated Delta: The Importance of Fluctuating Discharge in Depositional Systems. *Journal of Geophysical Research: Earth Surface*, *122*(10), 1882–1900. https://doi.org/10.1002/2017JF004378

Pizzuto, J., Skalak, K., Pearson, A., & Benthem, A. (2016). Active overbank deposition during the last century, South River, Virginia. *Geomorphology*, *257*, 164–178. https://doi.org/https://doi.org/10.1016/j.geomorph.2016.01.006

Poff, N. L., Allan, J. D., Bain, M. B., Karr, J. R., Prestegaard, K. L., Richter, B. D., Sparks, R. E., & Stromberg, J. C. (1997). The Natural Flow Regime. *BioScience*, *47*(11), 769–784. https://doi.org/10.2307/1313099

Poff, N. L., Bledsoe, B. P., & Cuhaciyan, C. O. (2006). Hydrologic variation with land use across the contiguous United States: Geomorphic and ecological consequences for stream

ecosystems. *Geomorphology*, *79*(3), 264–285. https://doi.org/https://doi.org/10.1016/j.geomorph.2006.06.032

Pryor, S., Barthelmie, R., & Schoof, J. (2013). High-resolution projections of climate-related risks for the Midwestern USA. *Climate Research*, *56*, 61–79. https://doi.org/10.3354/cr01143

Qiao, L., Pan, Z., Herrmann, R. B., & Hong, Y. (2014). Hydrological Variability and Uncertainty of Lower Missouri River Basin Under Changing Climate. *JAWRA Journal of the American Water Resources Association*, *50*(1), 246–260. https://doi.org/10.1111/jawr.12126

Rasche, D., Reinhardt-Imjela, C., Schulte, A., & Wenzel, R. (2019). Hydrodynamic simulation of the effects of stable in-channel large wood on the flood hydrographs of a low mountain range creek, Ore Mountains, Germany. *Hydrology and Earth System Sciences*, *23*(10). https://doi.org/10.5194/hess-23-4349-2019

Rawls, W. J., Brakensiek, D. L., & Miller, N. (1983). Green-ampt Infiltration Parameters from Soils Data. *Journal of Hydraulic Engineering*, *109*(1), 62–70. https://doi.org/10.1061/(ASCE)0733-9429(1983)109:1(62)

Richardson, D. M., Holmes, P. M., Esler, K. J., Galatowitsch, S. M., Stromberg, J. C., Kirkman, S. P., Pyšek, P., & Hobbs, R. J. (2007). Riparian vegetation: degradation, alien plant invasions, and restoration prospects. *Diversity and Distributions*, *13*(1), 126–139. https://doi.org/10.1111/j.1366-9516.2006.00314.x

Rojas, M., Quintero, F., & Young, N. (2020). Analysis of Stage–Discharge Relationship Stability Based on Historical Ratings. *Hydrology*, *7*(2), 31. https://doi.org/http://dx.doi.org/10.3390/hydrology7020031

Roni, P., Beechie, T., Pess, G., & Hanson, K. (2014). Wood placement in river restoration: fact, fiction, and future direction. *Canadian Journal of Fisheries and Aquatic Sciences*, *72*(3), 466–478. https://doi.org/10.1139/cjfas-2014-0344

Schumm, S. A. (1969). River Metamorphosis. *Journal of the Hydraulics Division*, *95*(1), 255–274.

Searcy, J. K. (1955). *Floods in Missouri: Magnitude and Frequency*. https://pubs.usgs.gov/circ/1955/0370/report.pdf

Sear, D. A., Millington, C. E., Kitts, D. R., & Jeffries, R. (2010). Logjam controls on channel:floodplain interactions in wooded catchments and their role in the formation of multi-channel patterns. *Geomorphology*, *116*(3), 305–319. https://doi.org/https://doi.org/10.1016/j.geomorph.2009.11.022

Shankman, D., & Samson, S. (1991). Channelization effects on Obion River flooding, Western Tennessee. *JAWRA Journal of the American Water Resources Association*, *27*, 247–254. https://doi.org/10.1111/j.1752-1688.1991.tb03129.x

Shields Jr, F., Knight, S., Morin, N., & Blank, J. (2003). Response of fishes and aquatic habitats to sand-bed stream restoration using large woody debris: The Interactions between Sediments and Water (Guest Editor: Brian Kronvang). *Hydrobiologia*, *494*. https://doi.org/10.1023/A:1025434920429

Silvertown, J., Dodd, M. E., Gowing, D. J. G., & Mountford, J. O. (1999). Hydrologically defined niches reveal a basis for species richness in plant communities. *Nature*, *400*(6739), 61–63. https://doi.org/10.1038/21877

Simon, A. (1989). A model of channel response in disturbed alluvial channels. *Earth Surface Processes and Landforms*, *14*(1), 11–26. https://doi.org/10.1002/esp.3290140103

Simon, A. (1994). *Gradation processes and channel evolution in modified West Tennessee streams; process, response, and form*.

Slaughter, B. S., & Kost, M. A. (2010). *Natural community abstract for wet prairie* (No. 12). https://mnfi.anr.msu.edu/abstracts/ecology/Wet_Prairie.pdf

Soons, M. B., de Groot, G. A., Cuesta Ramirez, M. T., Fraaije, R. G. A., Verhoeven, J. T. A., & de Jager, M. (2017). Directed dispersal by an abiotic vector: wetland plants disperse their seeds selectively to suitable sites along the hydrological gradient via water. *Functional Ecology*, *31*(2), 499–508. https://doi.org/10.1111/1365-2435.12771

Ström, L., Jansson, R., Nilsson, C., Johansson, M. E., & Xiong, S. (2011). Hydrologic effects on riparian vegetation in a boreal river: an experiment testing climate change predictions. *Global Change Biology*, *17*(1), 254–267. https://doi.org/10.1111/j.1365-2486.2010.02230.x

Tealdi, S., Camporeale, C., Perucca, E., & Ridolfi, L. (2010). Longitudinal dispersion in vegetated rivers with stochastic flows. *Advances in Water Resources*, *33*, 562–571. https://doi.org/10.1016/j.advwatres.2010.03.003

Teskey, R. O., Hinckley, T. M., & Service, U. S. F. and W. (1977). Impact of water level changes on woody riparian and wetland communities. Volume I, plant and soil responses. In *FWS/OBS*. http://pubs.er.usgs.gov/publication/fwsobs77_58

Tomer, M. D., & Schilling, K. E. (2009). A simple approach to distinguish land-use and climate-change effects on watershed hydrology. *Journal of Hydrology*, *376*(1), 24–33. https://doi.org/https://doi.org/10.1016/j.jhydrol.2009.07.029

Twedt, D., & Mini, A. (2019). *Forest Area to Support Landbird Population Goals for the Mississippi Alluvial Valley (MAV)*.

U.S. Army Corps of Engineers. (1932). *Report from the Chief of Engineers on Grand River, Missouri and Iowa, covering navigation, flood control, power development, and irrigation*. U.S. Army Corps of Engineers.

U.S. Army Corps of Engineers. (2020). *Grand River Ecosystem Restoration Study: Final Integrated Feasibility Report and Environmental Assessment, Lower Grand River Sub-Basin, Missouri*.

U.S. Army Corps of Engineers Hydrologic Engineering Center. (2016a). *HEC-RAS 5.0 Reference Manual*.

U.S. Army Corps of Engineers Hydrologic Engineering Center. (2016b). *HEC-RAS River Analysis System 2D Modeling User's Manual*. www.hec.usace.army.mil

U.S. Fish and Wildlife Service. (n.d.). *Freshwater Marshes and Wet Prairies: Multi-Species Recovery Plan for South Florida*.

U.S. Fish and Wildlife Service. (2011). *Swan Lake National Wildlife Refuge Comprehensive Conservation Plan and Environmental Assessment*.

U.S. Geological Survey. (2018). *USGS LandLook.* https://landlook.usgs.gov/landlook/viewer.html

Valverde, R. (2013). *Roughness and geometry effects of engineered log jams on 1-D flow characteristics*. https://ir.library.oregonstate.edu/concern/graduate_thesis_or_dissertations/gh93h224f

van Eck, W. H. J. M., Lenssen, J. P. M., van de Steeg, H. M., Blom, C. W. P. M., & de Kroon, H. (2006). Seasonal Dependent Effects of Flooding on Plant Species Survival and Zonation: a Comparative Study of 10 Terrestrial Grassland Species. *Hydrobiologia*, *565*(1), 59–69. https://doi.org/10.1007/s10750-005-1905-7

Verhoeven, J. T. A., Soons, M. B., Janssen, R., & Omtzigt, N. (2008). An Operational Landscape Unit approach for identifying key landscape connections in wetland restoration. *Journal of Applied Ecology, 45*(5), 1496–1503. https://doi.org/10.1111/j.1365-2664.2008.01534.x

Verry, E. S., Dolloff, C. A., & Manning, M. E. (2004). Riparian ecotone: A functional definition and delineation for resource assessment. *Water, Air, and Soil Pollution: Focus*, *4*, 67–94.

Weaver, J. E. (1960). *Flood Plain Vegetation of the Central Missouri Valley and Contact of Woodland and Prairie*. https://digitalcommons.unl.edu/cgi/viewcontent.cgi?article=1496&context=agronomyfacpub

Webster, A. J., Groffman, P. M., & Cadenasso, M. L. (2018). Controls on denitrification potential in nitrate-rich waterways and riparian zones of an irrigated agricultural setting. *Ecological Applications*, *28*(4), 1055–1067. https://doi.org/10.1002/eap.1709

Westerberg, I. K., Wagener, T., Coxon, G., McMillan, H. K., Castellarin, A., Montanari, A., & Freer, J. (2016). Uncertainty in hydrological signatures for gauged and ungauged catchments. *Water Resources Research*, *52*(3), 1847–1865. https://doi.org/https://doi.org/10.1002/2015WR017635

Wilby, R. L., Clifford, N. J., de Luca, P., Harrigan, S., Hillier, J. K., Hodgkins, R., Johnson, M. F., Matthews, T. K. R., Murphy, C., Noone, S. J., Parry, S., Prudhomme, C., Rice, S. P., Slater, L. J., Smith, K. A., & Wood, P. J. (2017). The 'dirty dozen' of freshwater science: detecting then reconciling hydrological data biases and errors. *WIREs Water*, *4*(3), e1209. https://doi.org/https://doi.org/10.1002/wat2.1209

Wohl, E. (2011). Threshold-induced complex behavior of wood in mountain streams. *Geology*, *39*(6), 587–590. https://doi.org/10.1130/G32105.1

Wohl, E., & Beckman, N. D. (2014). Leaky rivers: Implications of the loss of longitudinal fluvial disconnectivity in headwater streams. *Geomorphology, 205*, 27–35. https://doi.org/https://doi.org/10.1016/j.geomorph.2011.10.022

Woodward, T. (2020). *Email correspondence with Zac Corrum regarding Pershing State Park logjam areas*. Pershing State Park Superintendent, Missouri Department of Natural Resources.

Woolpert Inc. (2017). *Airborne LiDAR Report: KC COE TO 0006 Lower Grand River. Contract Number W912DQ-14-D-1006, Task Number 0006. Collected on behalf of USACE Kansas City District*.

Yager, E. M., & Schmeeckle, M. W. (2013). The influence of vegetation on turbulence and bed load transport. *Journal of Geophysical Research: Earth Surface*, *118*(3), 1585–1601. https://doi.org/https://doi.org/10.1002/jgrf.20085

Yang, J. Q., Chung, H., & Nepf, H. M. (2016). The onset of sediment transport in vegetated channels predicted by turbulent kinetic energy. *Geophysical Research Letters*, *43*(21), 11,261-11,268. https://doi.org/10.1002/2016GL071092

Yin, Y., Nelson, J. C., & Lubinski, K. S. (1997). Bottomland Hardwood Forests along the Upper Mississippi River. *Natural Areas Journal*, *17*(2), 164–173. http://www.jstor.org/stable/43911662

Zong, L., & Nepf, H. (2011). Spatial distribution of deposition within a patch of vegetation. *Water Resources Research - WATER RESOUR RES*, *47*. https://doi.org/10.1029/2010WR009516

Appendix A: Time Series Development

Inflow time series were needed to simulate flows through the hydraulic model and were thus developed to ensure a continuous flow time series was simulated between 2008 and 2018. The methods used to create a continuous time series are documented within this appendix.

The model was calibrated and validated using publicly available monitoring data. When available, 15-minute increment data (also known as instantaneous data) was used to complete the time series. Instantaneous data captured peaks of individual events whereas daily averaged data primarily focused on volume and can misrepresent hydrograph peaks. This is especially true if typical event durations were less than one day. Instantaneous streamflow data was downloaded from USGS for 2007 to 2019. Within the model domain, there were three USGS gages with flow and stage measurements: Locust Creek at Linneus, MO; Grand River at Fountain Grove, MO; and Grand River near Sumner, MO. The Fountain Grove gage was installed January 2017, indicating that the period of record only contained a few years of observed data. However, the Fountain Grove gage was included in the model to simulate Grand River backwater impacts on Locust Creek and was largely only relevant to the habitat analysis area during large events. Figure A.1 displays the gage locations relative to the model domain and Table A.1 summarizes available gage datasets.

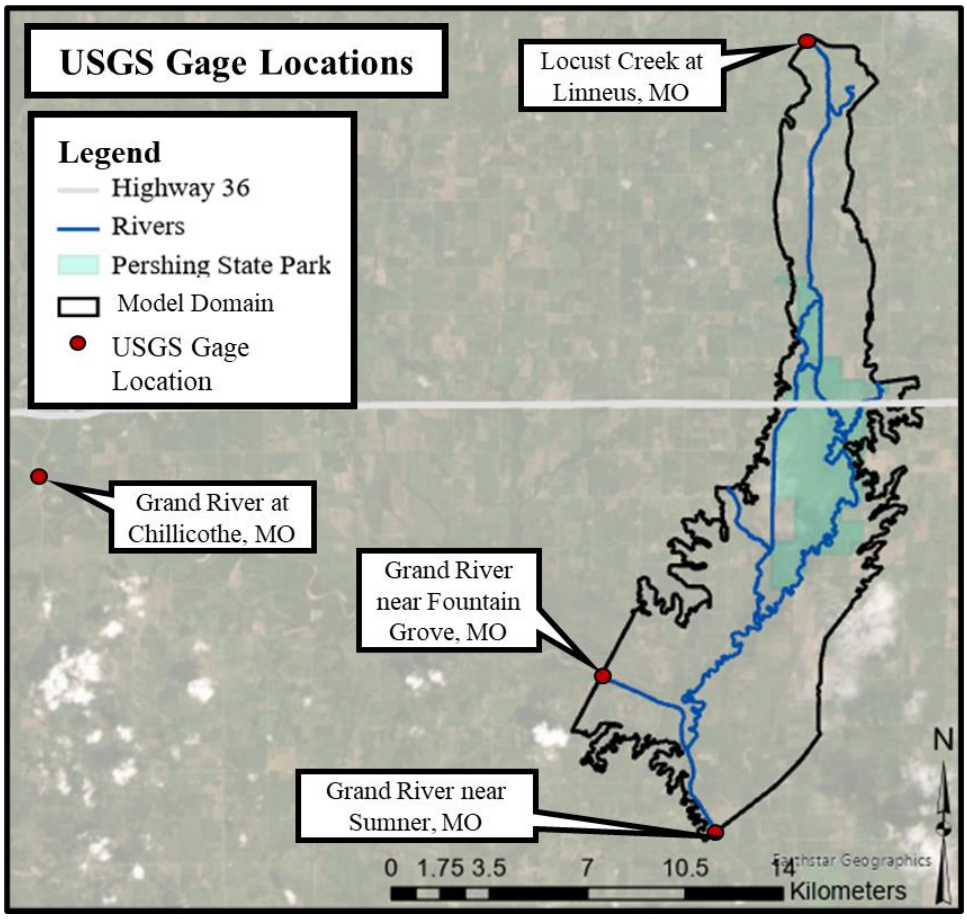

Figure A.1:
USGS Gage Locations Relative to Model Domain

Table A.1:
Observed Gage Data

USGS Gage Name	Gage Number	USGS Basin Area at Gage, km²	Period of Record	Gage Zero Datum NAVD88, m	Data Type
Locust Creek at Linneus, MO	06901500	1,424	01Oct2000 - present	211.13	Instantaneous
Grand River at Chillicothe, MO	06899680	12,665	01Feb2017 - present	200.87	Instantaneous
Grand River near Fountain Grove, MO	06900800	16,162	18Jan2017 - present	194.43	Instantaneous
Grand River near Sumner, MO	06902000	17,819	11Nov1995 - present	194.42	Instantaneous

Inflows at USGS Locations

The instantaneous flow datasets for all four gages were downloaded from USGS. All data was imported into HEC Data Storage System Visual Utility Engine (HEC-DSSVue) in UTC through the USGS Data Import Toolbox (Hydrologic Engineering Center, 2009). UTC was used to prevent shifts in data due to Daylight Savings Time. UTC is six hours ahead of Central Standard Time (CST) and five hours ahead of Central Daylight Time (CDT). All gage datasets had data gaps within the model period which is problematic for HEC-RAS function. In order to prevent errors at the boundary conditions, HEC-RAS required inflows and outflows formatted in regular timesteps. Hourly data was extracted from the 15-minute data using the "Change Time Interval" HEC-DSSVue math function. Missing data between hours was interpolated using DSSVue "estimate" editing function. Where data was missing for over 24 consecutive hours or the missing data appeared to represent the peak of an event (regardless of the number of missing hours), the data was not interpolated and was classified as "missing" and subsequently filled using the procedure described in the next paragraph. 24 hours was selected as the interpolation threshold because typical event durations for Locust Creek and Grand River were between one to two days and seven to ten days, respectively (U.S. Army Corps of Engineers, 2020). In other words, if there was no indication of an event (rising limb or falling limb) at the beginning of a data gap less than or equal to 24 consecutive hours, it was unlikely that interpolation would miss a hydrograph/event.

In order to develop a continuous period of record, the missing values between 2007 and 2018 were supplemented with flow datasets generated in the USACE Grand River HEC-HMS model documented in Appendix A Section 1 Attachment 2 of the USACE Grand River Feasibility Study (U.S. Army Corps of Engineers, 2020) hereby referred to as HEC-HMS flows. As seen in this thesis and Figure A.2, the HEC-HMS flows routinely overestimated large events. As a result,

the HEC-HMS flows may overestimate flood volumes, stages, inundation extents, and inundation duration during the simulations. Hourly HEC-HMS flows were available for the Chillicothe, Linneus, and Sumner gages from 01 August 1948 00:00 to 29 October 2018 00:00. Special consideration was given to the missing data for the Grand River near Fountain Grove gage. While the other gages had an HEC-HMS node at the same location, Fountain Grove did not. As a result, the Chillicothe HEC-HMS flows were factored by USGS drainage area to generate an HEC-HMS flow record at the Fountain Grove gage location. The drainage area factor used was computed by dividing the Fountain Grove drainage area by the Chillicothe drainage area. Table A.2 displays the drainage areas and the resulting drainage area factor. The Chillicothe HEC-HMS dataset was then multiplied by the drainage area factor to create the Fountain Grove HEC-HMS flow dataset. Figure A.3 compares the generated Fountain Grove HEC-HMS dataset with the instantaneous data. Overall, it appeared that the factored HEC-HMS flows generally matched the observed peak flows with some HEC-HMS events overestimating observed peak flows.

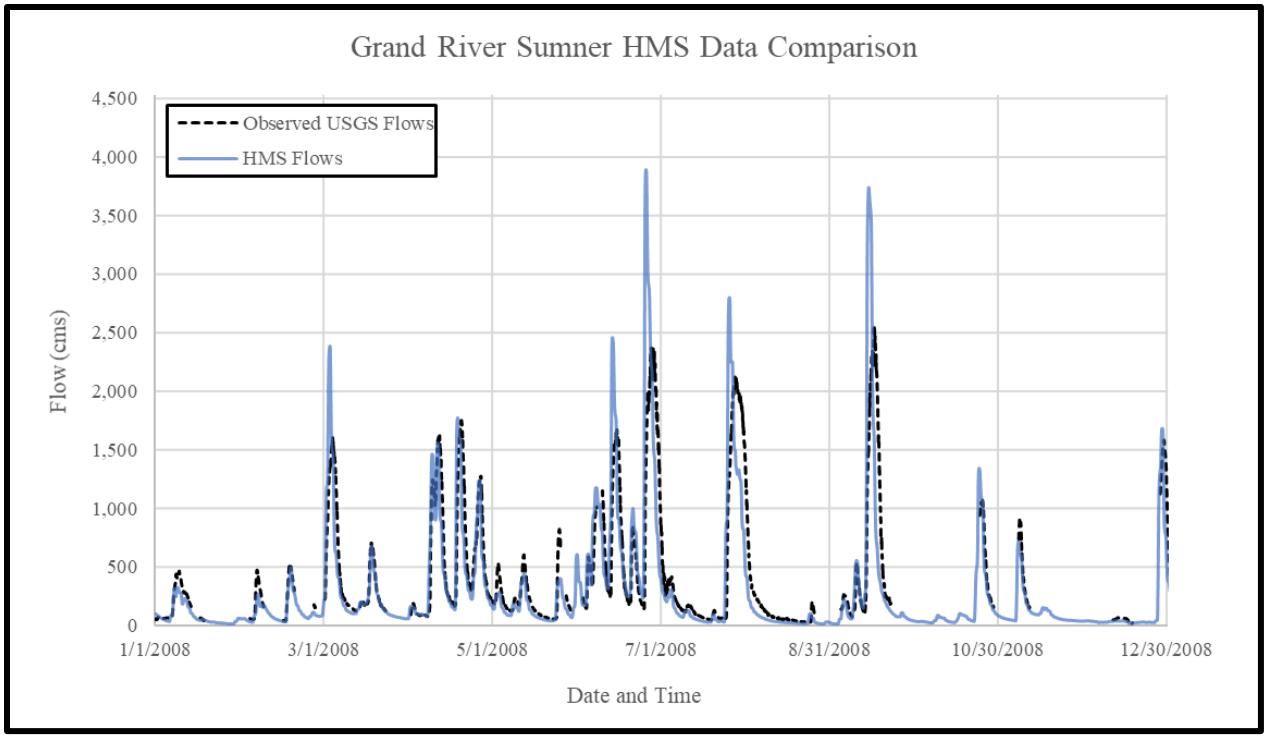

Figure A.2:
Grand River at Sumner HEC-HMS Flows (blue) Compared to Observed Instantaneous Flows (black, dashed) for 2008

Table A.2:
Drainage Areas and Drainage Area Factor Used to Generate Fountain Grove HEC-HMS Flow

Gage	USGS Drainage Area, km^2
Chillicothe	12,665
Fountain Grove	16,162
Drainage Area Factor	1.28

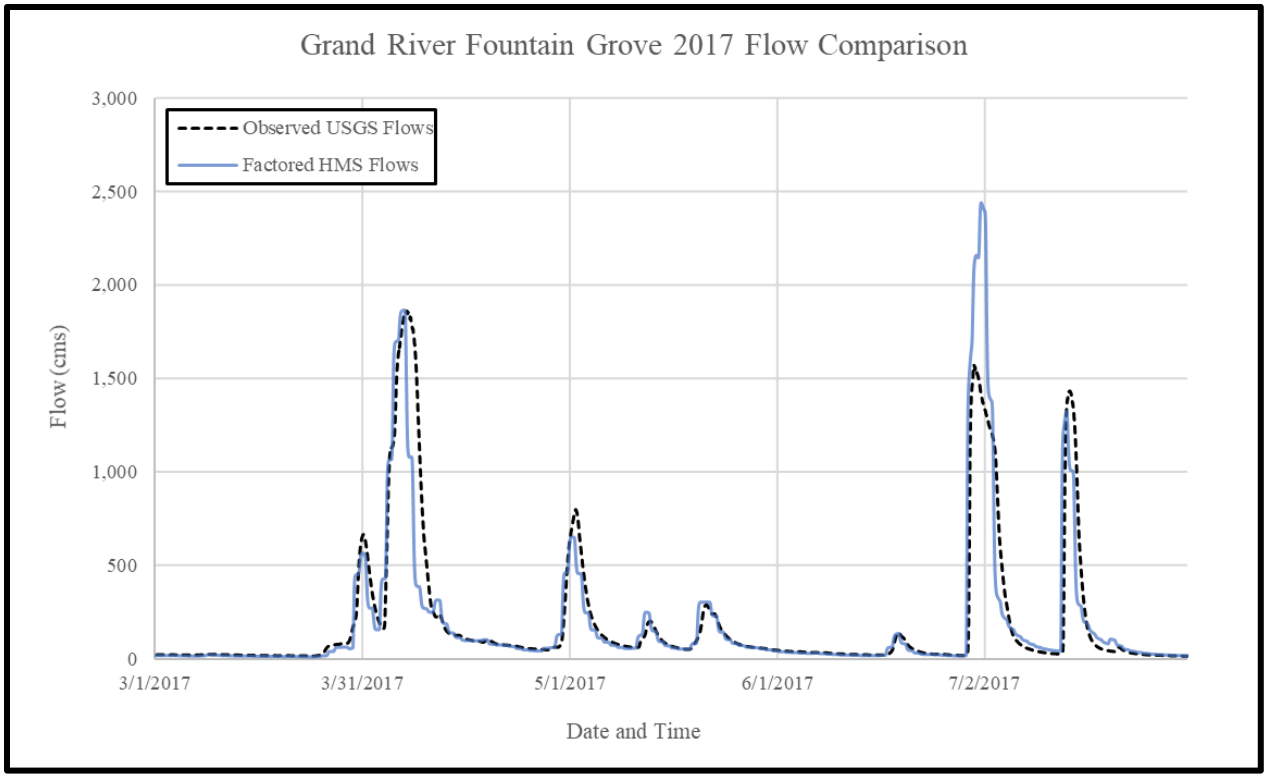

Figure A.3:
Fountain Grove Drainage Area Factored HEC-HMS Flows (blue) Compared to Observed Instantaneous Flows (black, dashed)

If the missing data represented the peak of the hydrograph, the entire event was supplemented with the USACE HEC-HMS data as shown in Figure A.4. If only the missing data was supplemented rather than the entire event, sudden increases or decreases in hourly flow would occur and result in model instability at the boundary conditions. To ensure smooth transitions between USGS instantaneous data and HEC-HMS flows, the entire event from the start of the rising limb to the end of the falling limb of the hydrograph was supplemented. Additionally, six hours before and after all supplemented data were interpolated between instantaneous and HEC-HMS flows to ensure a smooth transition.

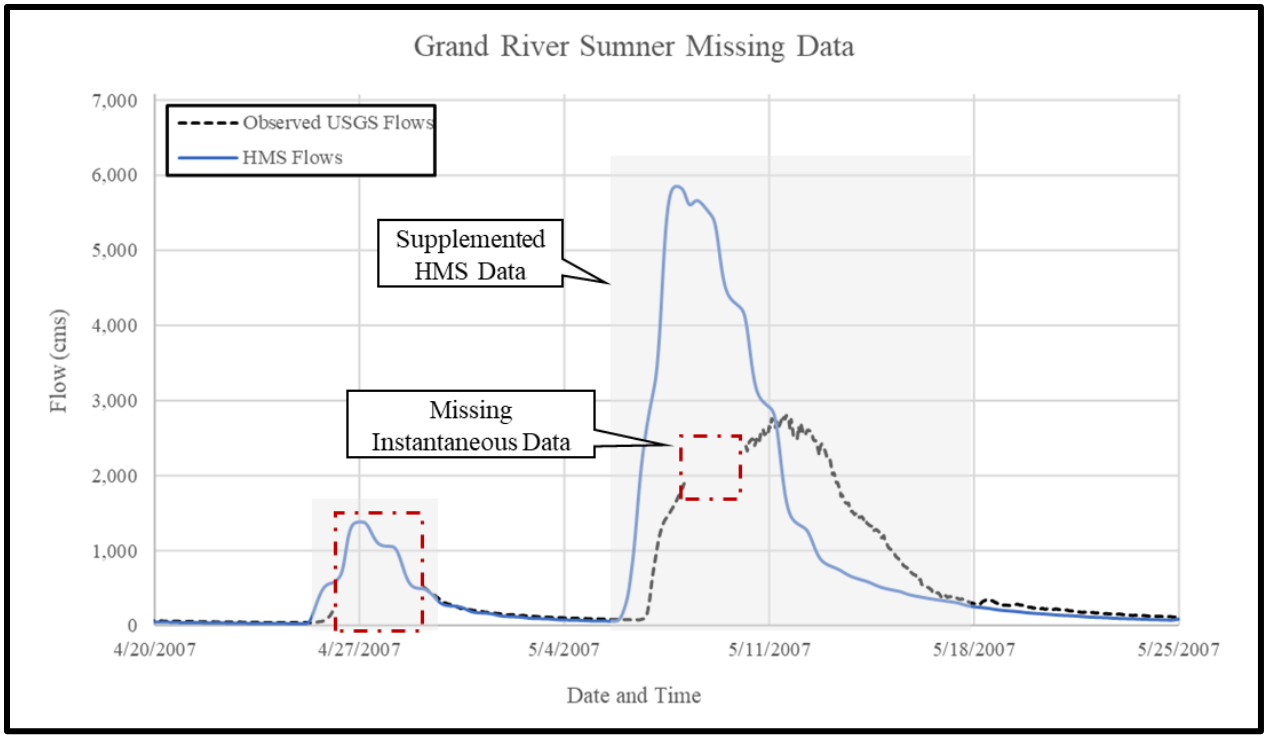

Figure A.4:
Example of Missing Instantaneous Peak Flows Supplemented with HEC-HMS Data

As documented in the Grand River Feasibility Study (U.S. Army Corps of Engineers, 2020), the HEC-HMS model utilized daily averaged flows to generate a continuous period of record at various nodes throughout the Grand River watershed, including the Grand River at Chillicothe, MO; Grand River near Sumner, MO; and Locust Creek near Linneus, MO. The influence of daily averaged flows is visible in Figure A.5 where the HEC-HMS flows are plotted against USGS instantaneous flows for Locust Creek near Linneus, MO. As a result, the supplemented peak flows for an event may not represent the instantaneous flows. Upon comparison of the HEC-HMS and instantaneous flows, the HEC-HMS data appeared to overestimate the flows for large events. This may result in additional water volume entering the floodplain, producing larger inundation depths and inundation durations on wetland vegetation than what occurred.

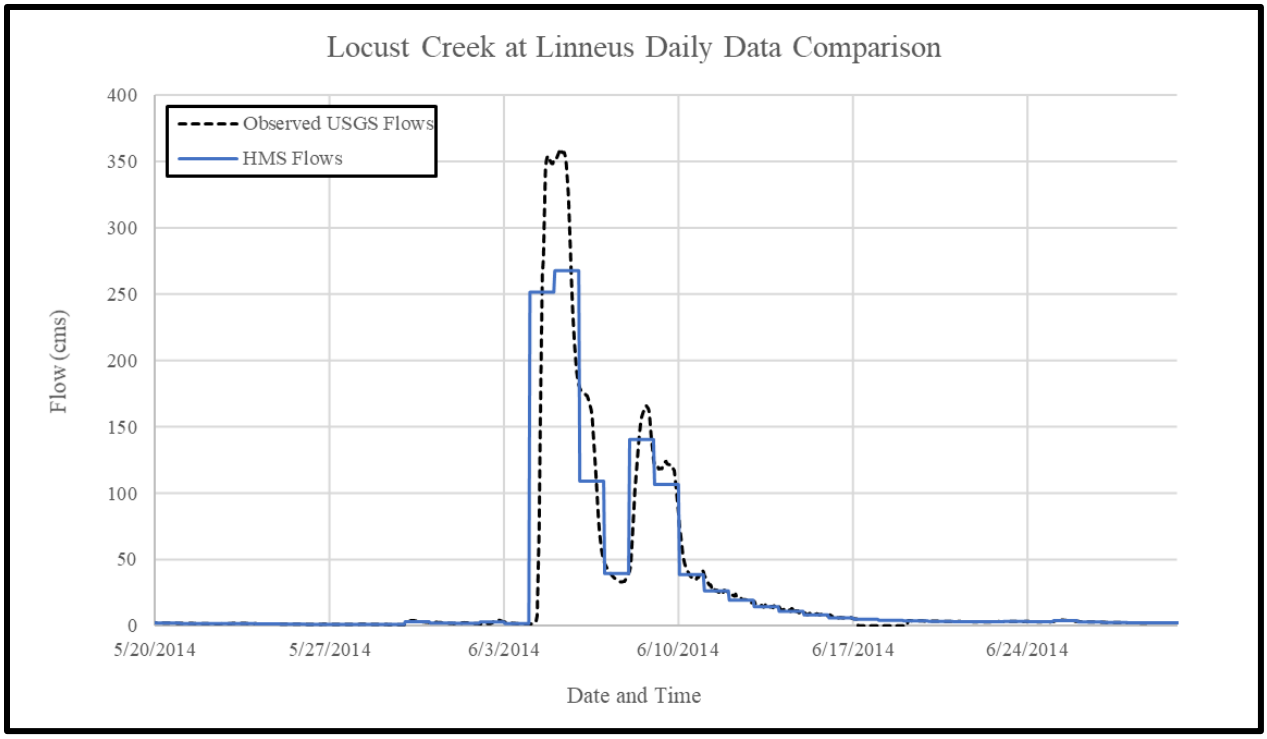

Figure A.5:
Locust Creek near Linneus, MO HEC-HMS (blue) and Instantaneous Flows (black dashed)

Since HEC-HMS flows were only available through October 2018, missing values for the remaining months of 2018 was interpolated. This only occurred at the Locust Creek near Linneus, MO gage from 09 December 2018 18:00 to 13 December 2018 03:00. Further adjustments were not made to the missing values in 2019. The streamflows in 2019 were only intended for calibration of the model and were not used for the annual wetland community change evaluation. As a result, a continuous period of record for the entire year of 2019 was not needed. Only 3.5 days of missing data from 10 March 2019 23:00 to 14 March 2019 10:00 occurred in 2019 for the Grand River gage near Fountain Grove. All other USGS gages had data gaps less than or equal to 24 hours such that the data could be interpolated using the criteria previously discussed. Figure A.6 and Figure A.7 display the developed time series for the inflow locations compared to USGS observed values.

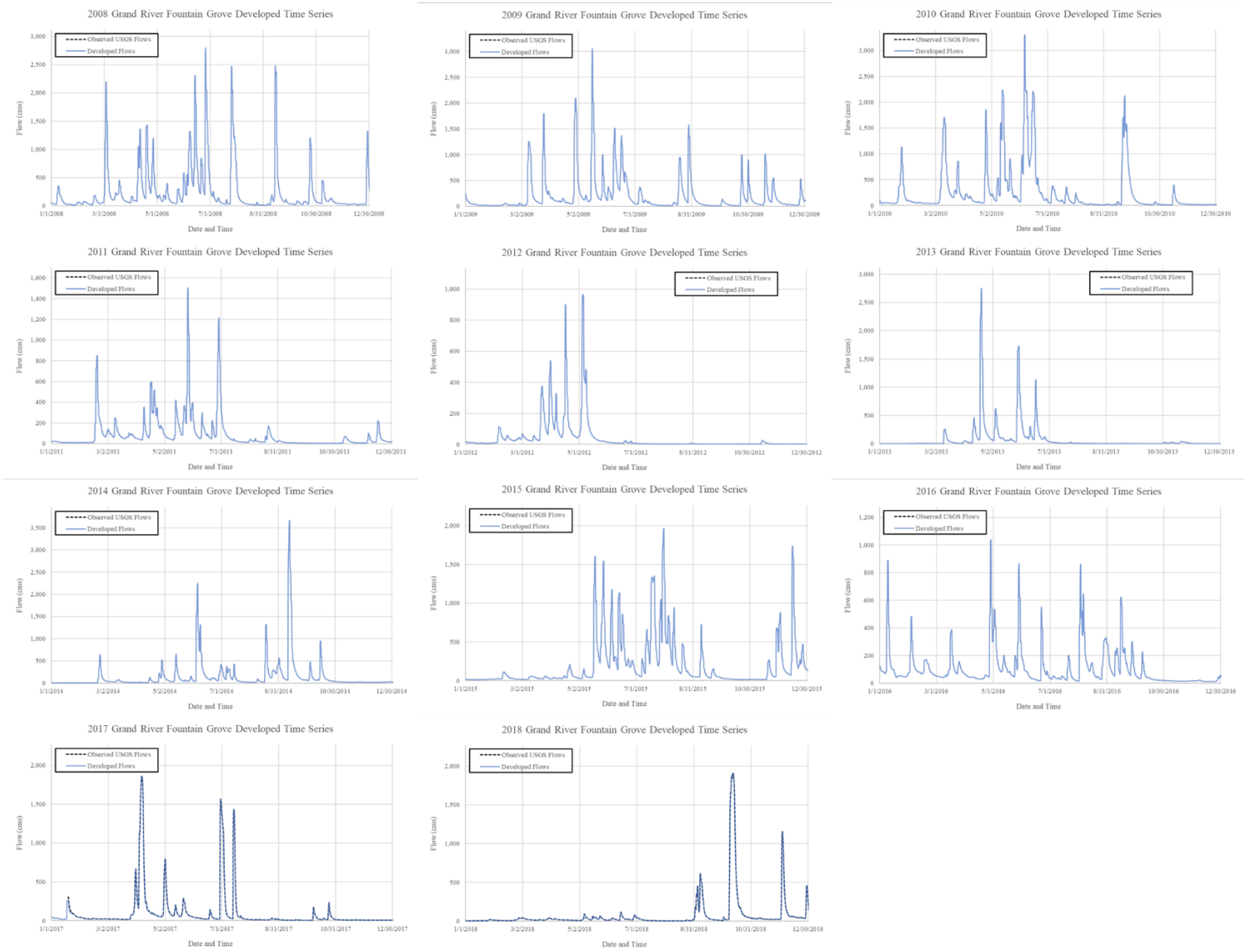

Figure A.6:
Developed Fountain Grove Grand River Flow Records Compared to USGS Observed Flows

Figure A.7:
Developed Locust Creek Flow Records Compared to USGS Observed Flows

Ungaged Inflows

Two inflow locations for the model were located on the ungaged streams Hickory Branch and Muddy Creek (Figure A.8). The ungaged inflows were located at an HEC-HMS node and thus had HEC-HMS flows available through October 2018. However, HEC-HMS flows were nonexistent after October 2018. In order to complete a continuous record for all of 2018 and have flows representative of 2019 for calibration, the missing data was supplemented using the drainage-area ratio method using Equation A.1 (Emerson et al., 2005).

Equation A.1: $$Y = (\frac{DA_y}{DA_x}) \times X$$

Where,

Y = Estimated Streamflow for Basin of Interest, cubic meters per second

X = Streamflow at Gage Station, cubic meters per second

DA_y = Drainage Area of Basin of Interest, square kilometers

DA_x = Drainage Area of Gaged Stream at Gage Station, square kilometers

Streamflow records from nearby gages with similar basin characteristics were multiplied by a ratio of the two drainage areas.

USGS gages located within a 80.5 kilometer radius of each ungaged inflow node were identified and their drainage areas recorded. The drainage area ratio between the ungaged inflow node and the USGS gages was computed by dividing the drainage area of Hickory Branch or Muddy Creek by the drainage area of the USGS gage. Table A.3 displays the USGS gages, drainage areas, and drainage area ratios for Hickory Branch and Muddy Creek. The five gages with instantaneous data from October 2018 to December 2018, with zero impacts from upstream regulation, and with drainage area ratios closest to unity (1.0), were further analyzed for each

ungaged inflow location. Additionally, the selected basins had similar basin characteristics including land use and streamflow direction.

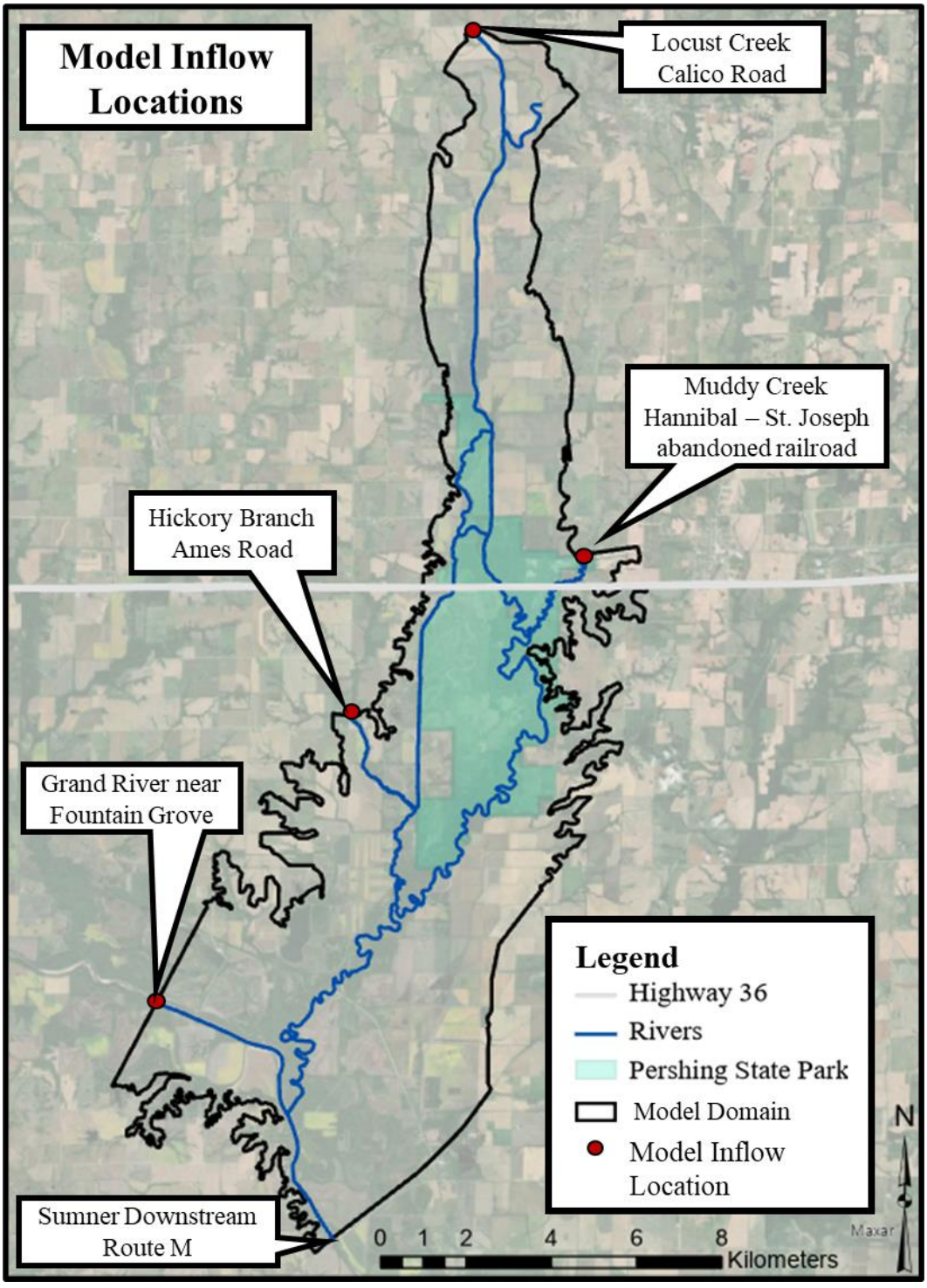

Figure A.8:
Inflow Locations Relative to Model Domain

Table A.3:
USGS Gages Within 80.5-km Radius of Hickory Branch and Muddy Creek

Hickory Branch				Muddy Creek			
River	Location	Drainage Area, km^2	DA Ratio	River	Location	Drainage Area, km^2	DA Ratio
Hickory Branch		20	1	*Muddy Creek*		60	1
Grand River	Gallatin, MO	5,830	0.00	Grand River	Gallatin, MO	5,830	0.01
Shoal Creek	Braymer, MO	1,010	0.02	Shoal Creek	Braymer, MO	1,010	0.06
Crooked River	Richmond, MO	412	0.05	Wakenda Creek	Carrollton, MO	663	0.09
Wakenda Creek	Carrollton, MO	663	0.03	Thompson River	Trenton, MO	4,460	0.01
Thompson River	Trenton, MO	4,460	0.00	Medicine Creek	Laredo, MO	919	0.07
Locust Creek	Linneus, MO	1,420	0.01	Grand River	Chillicothe, MO	12,670	0.00
Medicine Creek	Laredo, MO	919	0.02	Locust Creek	Linneus, MO	1,420	0.04
Grand River	Chillicothe, MO	12,670	0.00	Grand River	Fountain Grove	16,160	0.00
Grand River	Fountain Grove	16,160	0.00	Grand River	Sumner, MO	17,820	0.00
Medicine Creek	Lucerne, MO	306	0.07	Grand River	Sumner, MO (auxillary gage)	17,820	0.00
East Locust Creek	Boynton, MO	88	0.23	Missouri River[1]	Waverly, MO	1,258,500	0.00
Grand River	Sumner, MO	17,820	0.00	Missouri River[1]	Glasgow, MO	1,292,100	0.00
Grand River	Sumner, MO (auxillary gage)	17,820	0.00	Medicine Creek	Lucerne, MO	306	0.20
Missouri River[1]	Waverly, MO	1,258,500	0.00	East Locust Creek	Boynton, MO	88	0.68
Mussel Fork	Musselfork, MO	692	0.03	Spring Creek	Stahl, MO	187	0.32
Chariton River	Prairie Hill, MO	4,840	0.00	Chariton River	Novinger, MO	3,550	0.02
East Fork Little Chariton River[1]	Macon, MO	290	0.07	Long Branch	Atlanta, MO	60	1.00
Long Branch Creek	Atlanta, MO	60	0.34	East Fork Little Chariton River[1]	Macon, MO	290	0.21
Chariton River	Novinger, MO	3,550	0.01				
Spring Creek	Stahl, MO	187	0.11				

[1] Gage influenced by upstream regulation

Instantaneous data in UTC was downloaded using the HEC-DSSVue data import function for the gages identified in the previous process. Each USGS dataset was multiplied by their corresponding drainage area factor using the HEC-DSSVue multiply math function. The HEC-HMS generated flows for Hickory Branch and Muddy Creek were subtracted from the factored datasets using the DSSVue subtract math function to determine the difference in flows at each time step. Differences were not computed for a time step with missing data in one of the two time series. Then, the DSSVue absolute value math function was applied to the differences and the time series were clipped to the same time frame of the smallest available dataset so that averages were

compared across the same time period (27Jan2017 00:00 to 21Oct2018 00:00). The gage with the smallest average of the absolute value differences was selected to complete the remaining months of data for the Hickory Branch and Muddy Creek inflow locations. Table A.4 and Table A.5 display the gages analyzed and the selected gage to supplement flows for Hickory Branch and Muddy Creek, respectively.

Table A.4:
Basin Characteristics and Average Absolute Differences Compared to Hickory Branch

Hickory Branch	Stream	Location	Drainage Area, km^2	Drainage Area Factor (HB:XX)	Predominate Flow Direction	Land Use	Average Absolute Difference, cms
	Hickory Branch		20.0	1	N-S	Rural	
	East Locust Creek	Boynton, MO	87.5	0.229	N-S	Rural	**0.1**
	Long Branch Creek	Atlanta, MO	59.6	0.336	N-S	Rural	0.119
	Crooked River	Richmond, MO	412	0.049	NW-SE	Rural	0.119
	Medicine Creek	Lucerne, MO	306	0.065	N-S	Rural	0.118
	Spring Creek	Stahl, MO	187	0.107	NW-SE	Rural	0.109

Table A.5:
Basin Characteristics and Average Absolute Differences Compared to Muddy Creek

Muddy Creek	Stream	Location	Drainage Area, km^2	Drainage Area Factor (MC:XX)	Predominate Flow Direction	Land Use	Average Absolute Difference, cms
	Muddy Creek		59.8	1	N-S	Rural	
	East Locust Creek	Boynton, MO	87.5	0.683	N-S	Rural	0.343
	Long Branch Creek	Atlanta, MO	59.6	1.004	N-S	Rural	0.374
	Wakenda Creek	Carrollton, MO	663	0.090	E-W	Rural	0.399
	Medicine Creek	Lucerne, MO	306	0.196	N-S	Rural	0.507
	Spring Creek	Stahl, MO	187	0.320	NW-SE	Rural	**0.334**

The selected gage time series with the applied drainage area factor was then converted to hourly flow and missing data interpolated using the same methodology described in Appendix A, Inflows at USGS Locations. The data was then used to supplement the Hickory Branch and Muddy Creek HEC-HMS generated flows using the merge time series function in HEC-DSSVue with the HEC-HMS flows receiving higher priority. Table A.6 displays the percentage of each data source

comprising the timeseries from 2007 to 2019. Table A.7 displays the percentage of each data source comprising the timeseries for each year from 2008 to 2018.

Table A.6:
Percentage of Data from Each Source

% Data from Each Source

Inflow/Outflow Location	USGS	HMS	Interpolated	USGS Geo-Scaling
Grand River near Fountain Grove	17.8%	77.7%	4.6%	0.0%
Locust Creek near Linneus, MO	75.1%	8.1%	16.8%	0.0%
Muddy Creek	0.0%	91.0%	0.26%	8.8%
Hickory Branch	0.0%	91.0%	0.13%	8.9%
Grand River near Sumner, MO	71.3%	11.9%	16.8%	0.0%

Note: Grand River near Fountain Grove HEC-HMS flows were derived by Geo-Scaling upstream HEC-HMS flows.

Most of these datasets, with the exception of the Grand River near Sumner, MO, were used to simulate model inflows. The data associated with the Grand River near Sumner, MO was used to calibrate the model at the most downstream location. Since the area of analysis was located within Pershing State Park, the area of interest primarily relied on Locust Creek, Muddy Creek, and Hickory Branch data.

Table A.7:
Percentage of Data from Each Source per Year of Analysis

% Data from Each Source per Year of Analysis

Inflow/ Outflow Location	Data Source	2008	2009	2010	2011	2012	2013	2014	2015	2016	2017	2018
Grand River near Fountain Grove	USGS	0%	0%	0%	0%	0%	0%	0%	0%	0%	76%	81%
	HMS	100%	100%	100%	100%	100%	100%	100%	100%	100%	9%	0%
	Interpolated	0%	0%	0%	0%	0%	0%	0%	0%	0%	16%	19%
	USGS Geo-Scaling	0%	0%	0%	0%	0%	0%	0%	0%	0%	0%	0%
Locust Creek near Linneus, MO	USGS	73%	73%	59%	78%	76%	71%	69%	79%	82%	82%	82%
	HMS	12%	10%	28%	4%	6%	12%	14%	4%	1%	1%	0%
	Interpolated	16%	16%	14%	17%	19%	17%	17%	17%	17%	17%	18%
	USGS Geo-Scaling	0%	0%	0%	0%	0%	0%	0%	0%	0%	0%	0%
Muddy Creek	USGS	0%	0%	0%	0%	0%	0%	0%	0%	0%	0%	0%
	HMS	100%	100%	100%	100%	100%	100%	100%	100%	100%	100%	82%
	Interpolated	0%	0%	0%	0%	0%	0%	0%	0%	0%	0%	2%
	USGS Geo-Scaling	0%	0%	0%	0%	0%	0%	0%	0%	0%	0%	16%
Hickory Branch	USGS	0%	0%	0%	0%	0%	0%	0%	0%	0%	0%	0%
	HMS	100%	100%	100%	100%	100%	100%	100%	100%	100%	100%	82%
	Interpolated	0%	0%	0%	0%	0%	0%	0%	0%	0%	0%	0%
	USGS Geo-Scaling	0%	0%	0%	0%	0%	0%	0%	0%	0%	0%	17%
Grand River near Sumner, MO	USGS	42%	68%	64%	60%	81%	71%	81%	83%	77%	83%	81%
	HMS	46%	15%	20%	22%	1%	13%	2%	0%	5%	0%	0%
	Interpolated	12%	18%	16%	18%	18%	16%	17%	17%	17%	17%	19%
	USGS Geo-Scaling	0%	0%	0%	0%	0%	0%	0%	0%	0%	0%	0%

Note: Grand River near Fountain Grove HEC-HMS flows were derived by Geo-Scaling upstream HEC-HMS flows.

Appendix B: Hydraulic Model Calibration

The model was calibrated by adjusting Manning's roughness coefficients, the downstream boundary friction slope, and computation equation set. Two different events were calibrated: one without a log jam and one with a log jam present. Roughness coefficients, downstream boundary friction slope, and computation equation set were calibrated to observed data from the non-log jam calibration event. The resulting calibrated parameters were applied to the log jam calibration event. The log jam calibration event was performed to calibrate a roughness coefficient associated with log jams. Log jam characteristics such as time of occurrence, length, and width were available from MoDNR, USGS SIR 2017-5120 (Heimann & Survey, 2017), Google Earth, and project staff (Woodward, 2020). The following sections discuss the calibration processes for the two separate scenarios.

Calibration: No Log Jams

Calibration Event

The model was calibrated to an individual event that occurred between March 25th and April 8th of 2017. The 2017 event was selected for calibration because the event resulted in floodplain inundation and had calibration data availability throughout the floodplain in Pershing State Park. The April 2017 event involved a series of small precipitation amounts resulting in 10.2 to 15.2 cm of rainfall across the Grand River Basin with a storm center of 18.5 cm located near Redding and Bedford, Iowa. For this event, the peak discharge on the Grand River at Sumner, MO occurred April 7th, 2017.

The timeseries for the April event from March 23rd 2017 through April 20th 2017 was comprised of 83% USGS data and approximately 17% of interpolated values for both the Fountain Grove and Locust Creek inflow locations. This indicates majority of the inflows were based off

instantaneous and observed data when possible and that overestimation and underestimation at Locust Creek and Fountain Grove were not a result of the hydrologic model errors.

Calibration Data

Several sources of data existed for model calibration including highwater marks (HWMs), USGS streamflow, and USGS instantaneous measurements. The 2017 event was selected for calibration because of data availability throughout the floodplain in Pershing State Park via HWMs. HWMs include, but are not limited to, water lines on trees and debris lines. HWMs are impacted by wind wave action, super elevation, and debris which may push the water surface elevation to higher elevations in isolated locations. Additionally, due to the frequency of Locust Creek flood events, high water marks may represent different hydraulic events. As a result, HWMs can introduce error into the model. However, the HWMs provided a measurement of the floodplain hydraulics within Pershing State Park. USACE surveyed high water marks (HWMs) on April 11th, 2017 and elevations reported in meters-NAVD88 are provided in Figure B.1.

Additionally, USGS Grand River discharges at Sumner, MO, developed from the USGS rating curve, were used to compare flows at the downstream model domain. However, the stage discharge relationship captured in the rating curve was subject to error due to altered channel geometry caused by scour and sedimentation during a flood event (McMillan et al., 2012; Rojas et al., 2020). As a result, the error in extrapolation from the rating curve can compound in hydraulic models that use the data for calibration and lead to incorrect results (Westerberg et al., 2016; Wilby et al., 2017). Despite this shortcoming, the USGS gage site was located at the downstream boundary of the model and provided the best available flow estimate to gage model performance.

The USGS also documented instantaneous velocity and flow measurements during the April 2017 event on April 6th, 2017 at 11:24 CDT, equivalent to April 6th, 2017 at 16:24 UTC. The

measurements were collected using acoustic Doppler current profilers (ADCP). ADCP uses the Doppler effect to measure velocity by reflecting sound off of material in the water and recording the change in frequency between the waves initially sent out and the waves received after bouncing off the material (Mueller, 2009). During the time of measurement, moderate debris was documented at the site. Overall, the instantaneous measurements received a "poor" quality rating which may be a result of debris, measurement error, or post-processing issues. The instantaneous measurements also documented the Stanley Lake split flow discharge and velocity. According to USGS, when the Grand River reached a stage of 10.1 meters at the Sumner gage, the Stanley Lake split flow was activated (U.S. Army Corps of Engineers, 2020). Stanley Lake is a small lake located east of the Grand River channel along the BNSF railroad bridge that only receives water during Grand River flood events. When activated, a split flow formed at the USGS gage location with flows passing under the BNSF bridge at the main Grand River channel and Stanley Lake.

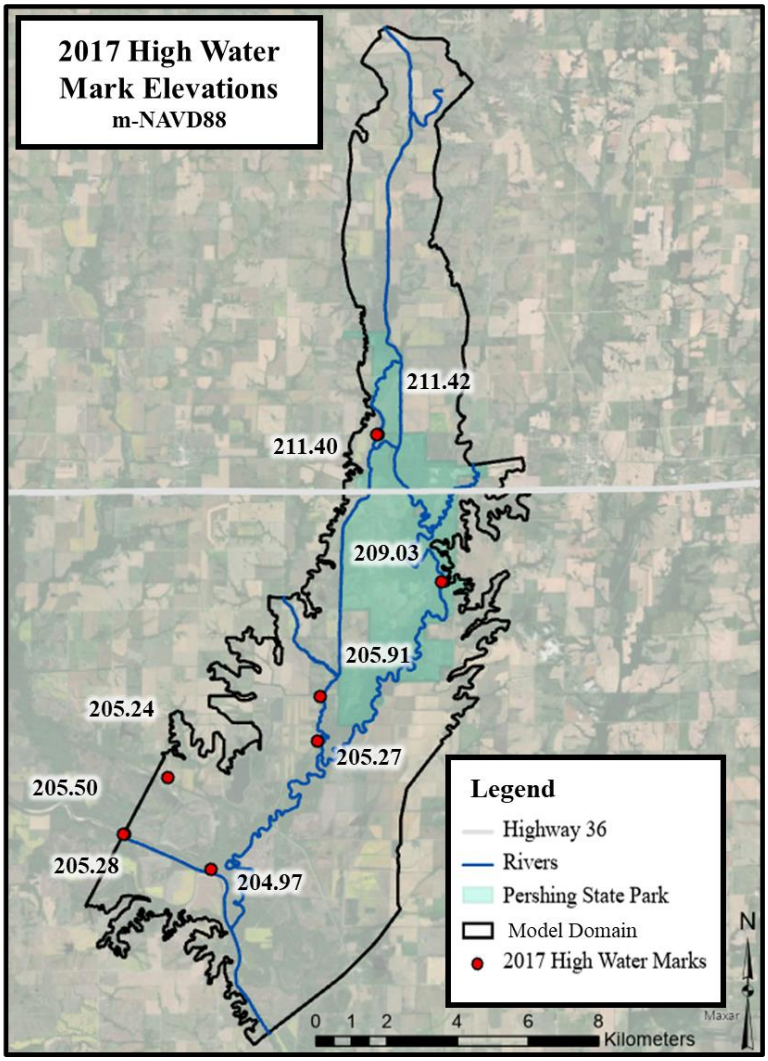

Figure B.1:
April 2017 Surveyed High Water Mark Locations Labeled with Elevations in meter-NAVD88

Calibration Methodology

The calibration event used a simulation time period from 23 March 2017 00:00 to 20 April 2017 24:00 in order to model all components of an individual hydrograph: initial baseflow, rising limb, peak, falling limb, and return to baseflow. A computation interval of one minute and an initial conditions warmup period of 252 hours was used to ensure computational stability. Diffusion wave methodology and a water surface elevation and volume tolerance of 0.008 meters

were initially selected to improve model run time efficiency and stability. All other computation options and tolerances used the default parameters.

Several parameters were adjusted for calibration through an iterative process. These parameters included roughness coefficients, friction slope at the normal depth downstream boundary, and computation equation set. Roughness coefficients were applied to each individual cell. If the spatial roughness delineation produced multiple roughness coefficients within a cell, the averaged area roughness coefficient was computed and applied to that cell. The friction slope was applied across the downstream boundary condition extent spanning approximately 2,530 meters. The spatial distribution of the roughness coefficients established in the 2020 Grand River Feasibility Study were used for the Manning's n polygons in this analysis and are displayed in Figure B.2. The initial roughness coefficients selected were also adopted from the final calibrated roughness coefficients (2019ExistingConditions) documented in the 2020 Grand River Feasibility Study. Roughness coefficients for varying landcovers were factored up or down (ManN01 – ManN05) until the simulated water surface elevations were similar to gaged data and surveyed highwater marks. Geometry adjustments were not made to the model for calibration purposes; however, copies of the same geometry were created and the Manning's n polygons were associated with the different geometries in RAS Mapper. Aerial imagery and MoDNR project documentation did not indicate the presence of a log jam in Pershing State Park throughout all of 2017. As a result, the calibration event did not include increased channel roughness to simulate the presence of a log jam. Other simulations adjusted the energy grade line slope at the downstream boundary condition in the flow file or the computation method from diffusion wave to full momentum in the plan file.

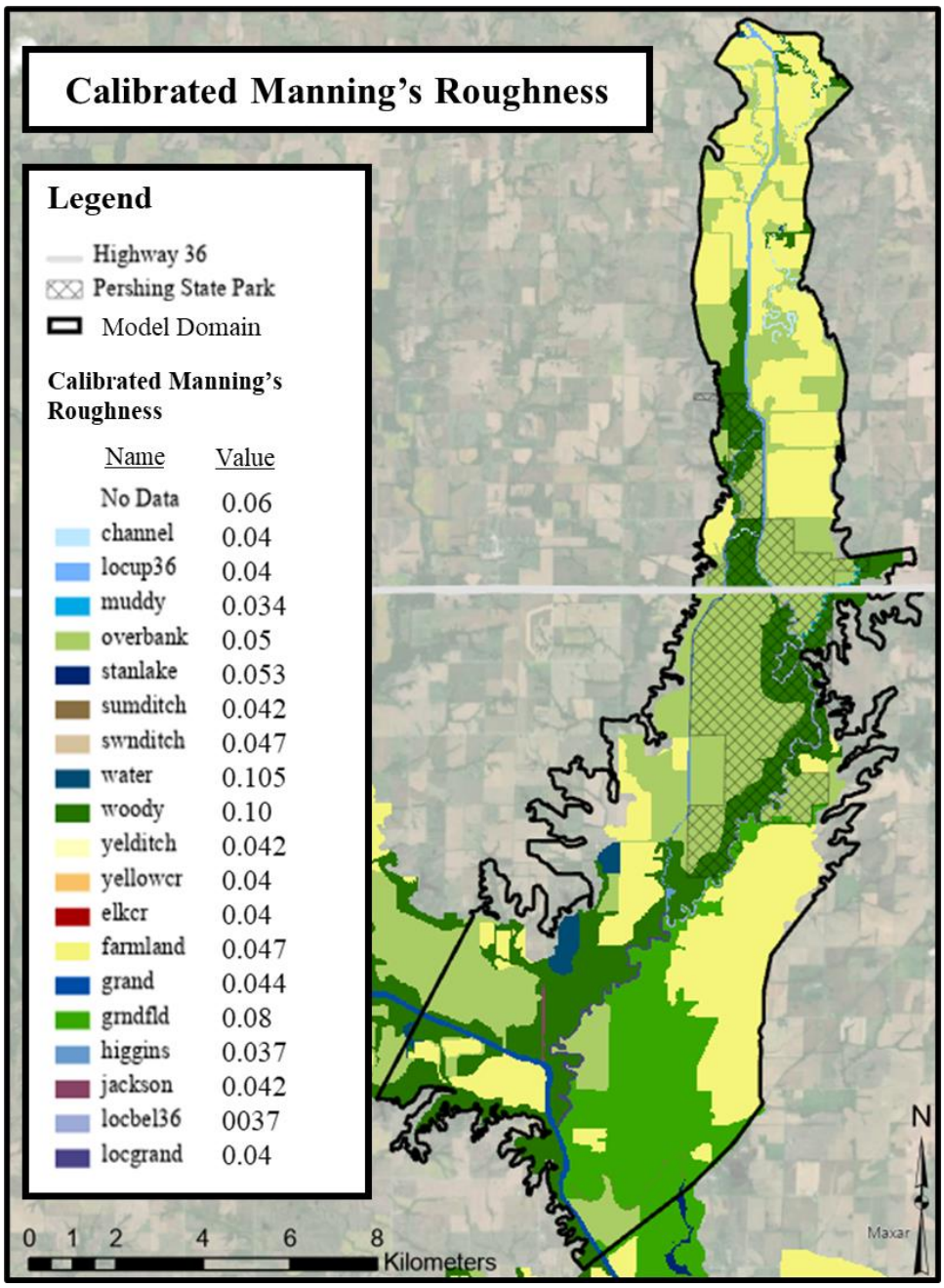

Figure B.2:
Manning's n Polygon Spatial Distribution and Calibrated Roughness Coefficients (ManN05)

Both the 30.5 meter (100 feet) (Model-100) and 7.62 meter (25 feet) (Model-25) computational grids were used in calibration. Initially, Model-100 was used to preliminarily screen the calibration simulations due to significantly decreased run times (approximately 3 hours)

compared to Model-25 (approximately 18 hours). The screening process first compared hydraulic impacts due to widespread roughness coefficient increases. Then, impacts resulting from downstream boundary condition adjustments and computation methodology, respectively, were analyzed. Finally, individual roughness coefficients or Manning's n values were adjusted and the hydraulic results were compared.

Calibration priority was given to areas in the intended area of analysis, specifically Pershing State Park. In other words, parameter adjustments producing hydraulic results that most closely represented observed data within Pershing State Park received higher priority over parameters producing better results at Sumner, MO. Based on this methodology, different simulations were screened and the remaining, unscreened calibration simulations were run through Model-25 for final comparison and selection of calibration parameters. Table B.1 and Table B.2 summarize the calibration simulations run through Model-100 and Model-25, respectively. Table B.3 describes the various Landcovers and roughness coefficients associated with the different landcover types.

Table B.1:
Model-100 Calibration Iterations and Descriptions

MODEL-100 CALIBRATION SIMULATIONS			
Plan Name	**Geometry**	**Flow File**	**Description**
Test01 or Test02	EC_LC_003_01	Test01	Geometry uses Model-100. Boundary conditions (BC) span across entire floodplain. Landcover uses 2019ExistingConditions from the 2020 Grand River Feasibility Study. Test01 and Test02 in the model are the exact same.
Test03	EC_LC_003_01_ManN01	Test01	Geometry is the same as Test01 but associated with a different Landcover. Landcover uses ManN01 (2019ExistingConditions increased by 5%).
Test04	EC_LC_003_01_ManN02	Test01	Geometry is the same as Test02 but associated with a different Landcover. Landcover uses ManN02 (2019ExistingConditions increased by 10%).

MODEL-100 CALIBRATION SIMULATIONS			
Plan Name	**Geometry**	**Flow File**	**Description**
Test05	EC_LC_003_01_ManN01	Test02	Geometry uses Model-100. BC span across entire floodplain. Downstream (DS) BC slope decreased by a factor of 10 (Flow File Test02). Landcover uses ManN01 (2019ExistingConditions increased by 5%).
Test06	EC_LC_003_01_ManN01	Test03	Geometry uses Model-100. BC span across entire floodplain. DS BC Slope increased by a factor of 10 (Flow File Test03). Landcover uses ManN01 (2019ExistingConditions increased by 5%).
Test07	EC_LC_003_01_ManN01	Test01	Plan is the same as Test03 except computation methodology changed from diffusion wave to full momentum.
Test08	EC_LC_003_01_ManN03	Test01	Geometry uses Model-100. Landcover uses ManN03 (2019ExistingConditions increased by 5% with "woody" increased to 0.1). BC span across entire floodplain. No adjustments made to DS BC (Flow File Test01).
Test09	EC_LC_003_01_ManN04	Test01	Geometry uses Model-100. Landcover uses ManN04 (2019ExistingConditions increased by 5% with "woody" increased to 0.12 and "grndfld" increased to 0.8). BC span across entire floodplain. No adjustment to DS BC (Flow File Test01).
Test10	EC_LC_003_01_ManN01	Test01	Geometry uses Model-100. Landcover uses ManN01 (2019ExistingConditions increased by 5%). Run time extended for the entire year of 2017.
Test11	EC_LC_003_01_ManN05	Test01	Geometry uses Model-100. Landcover uses ManN05 (2019ExistingConditions increased by 5% with "woody" increased to 0.10 and "grndfld" increased to 0.8). BC span across entire floodplain. No adjustment to DS BC (Flow File Test01)

Table B.2:
Model-25 Calibration Simulations and Descriptions

MODEL-25 CALIBRATION SIMULATIONS			
Plan Name	**Geometry**	**Flow File**	**Description**
25Test03	EC_LC_003_01_ManN01	Test01	Geometry uses Model-25. Landcover uses ManN01 (2019ExistingConditions increased by 5%).
25Test09	EC_LC_003_01_ManN04	Test01	Geometry uses Model-25. Landcover uses ManN04 (2019ExistingConditions increased by 5% with "woody" increased to 0.12 and "grndfld" increased to 0.8). BC span across entire floodplain. No adjustment to DS BC (Flow File Test01).
25Test11	EC_LC_003_01_ManN05	Test01	Geometry uses Model-25. Landcover uses ManN05 (2019ExistingConditions increased by 5% with "woody" increased to 0.10 and "grndfld" increased to 0.8). BC span across entire floodplain. No adjustment to DS BC (Flow File Test01).

Table B.3:
Landcover Names, Descriptions, and Roughness Values

Land Cover Name	**2019 Existing Conditions (EC)**	**ManN01**	**ManN02**	**ManN03**	**ManN04**	**ManN05**
	Roughness coefficients calibrated in the 2020 Grand River Feasibility Study	All 2019 EC increased by 5%	All 2019 EC increased by 10%	All 2019 EC increased by 5% with woody adjusted	All 2019 EC increased by 5% with woody and grndfld adjusted	All 2019 EC increased by 5% with woody and grndfld adjusted
nodata	---	---	---	---	---	---
channel	0.038	0.040	0.042	0.040	0.040	0.040
elkcrk	0.038	0.040	0.042	0.040	0.040	0.040
farmland	0.045	0.047	0.050	0.047	0.047	0.047
grand	0.042	0.044	0.046	0.044	0.044	0.044
grndfld	0.045	0.047	0.050	0.047	0.080	0.080
higgins	0.035	0.037	0.039	0.037	0.037	0.037
jackson	0.04	0.042	0.044	0.042	0.042	0.042
locbel36	0.035	0.037	0.039	0.037	0.037	0.037
locgrand	0.038	0.040	0.042	0.040	0.040	0.040
locup36	0.038	0.040	0.042	0.040	0.040	0.040
muddy	0.032	0.034	0.035	0.034	0.034	0.034
overbank	0.048	0.050	0.053	0.050	0.050	0.050
stanlake	0.05	0.053	0.055	0.053	0.053	0.053
sumditch	0.04	0.042	0.044	0.042	0.042	0.042
swnditch	0.045	0.047	0.050	0.047	0.047	0.047
water	0.1	0.105	0.110	0.105	0.105	0.105
woody	0.058	0.061	0.064	0.100	0.120	0.100
yelditch	0.04	0.042	0.044	0.042	0.042	0.042

Land Cover Name	2019 Existing Conditions (EC)	ManN01	ManN02	ManN03	ManN04	ManN05
	Roughness coefficients calibrated in the 2020 Grand River Feasibility Study	All 2019 EC increased by 5%	All 2019 EC increased by 10%	All 2019 EC increased by 5% with woody adjusted	All 2019 EC increased by 5% with woody and grndfld adjusted	All 2019 EC increased by 5% with woody and grndfld adjusted
yellowcr	0.038	0.040	0.042	0.040	0.040	0.040

Calibration Results and Discussion

Once the simulations were complete, the Model-100 April 2017 event hydrographs and USGS measurements at Sumner were compared. The resulting hydrographs are displayed in Figure B.3 and comparisons to instantaneous USGS measurements are provided in Table B.4.

Table B.4:

Grand River at Sumner, MO Simulated Main Channel and Overflow Discharge and Average Channel Velocity Comparisons with USGS Measurements Recorded at 4/6/2017 16:24:48 UTC

Simulation	Discharge, cms		Average Channel Velocity, mps	
	Main Channel	*Overflow*	*Main Channel*	*Overflow*
USGS	1,543	382	1.71	0.56
Test01 and Test02	1,453	399	2.03	0.83
Test03	1,417	413	1.96	0.82
Test04	1,385	428	1.90	0.82
Test05	844	500	0.82	0.49
Test06	1,524	383	3.64	1.02
Test07	1,362	454	1.92	0.83
Test08	1,408	407	1.95	0.82
Test09	1,466	346	2.00	0.73
Test11	1,466	349	2.00	0.73
Test10	1,417	413	1.96	0.82

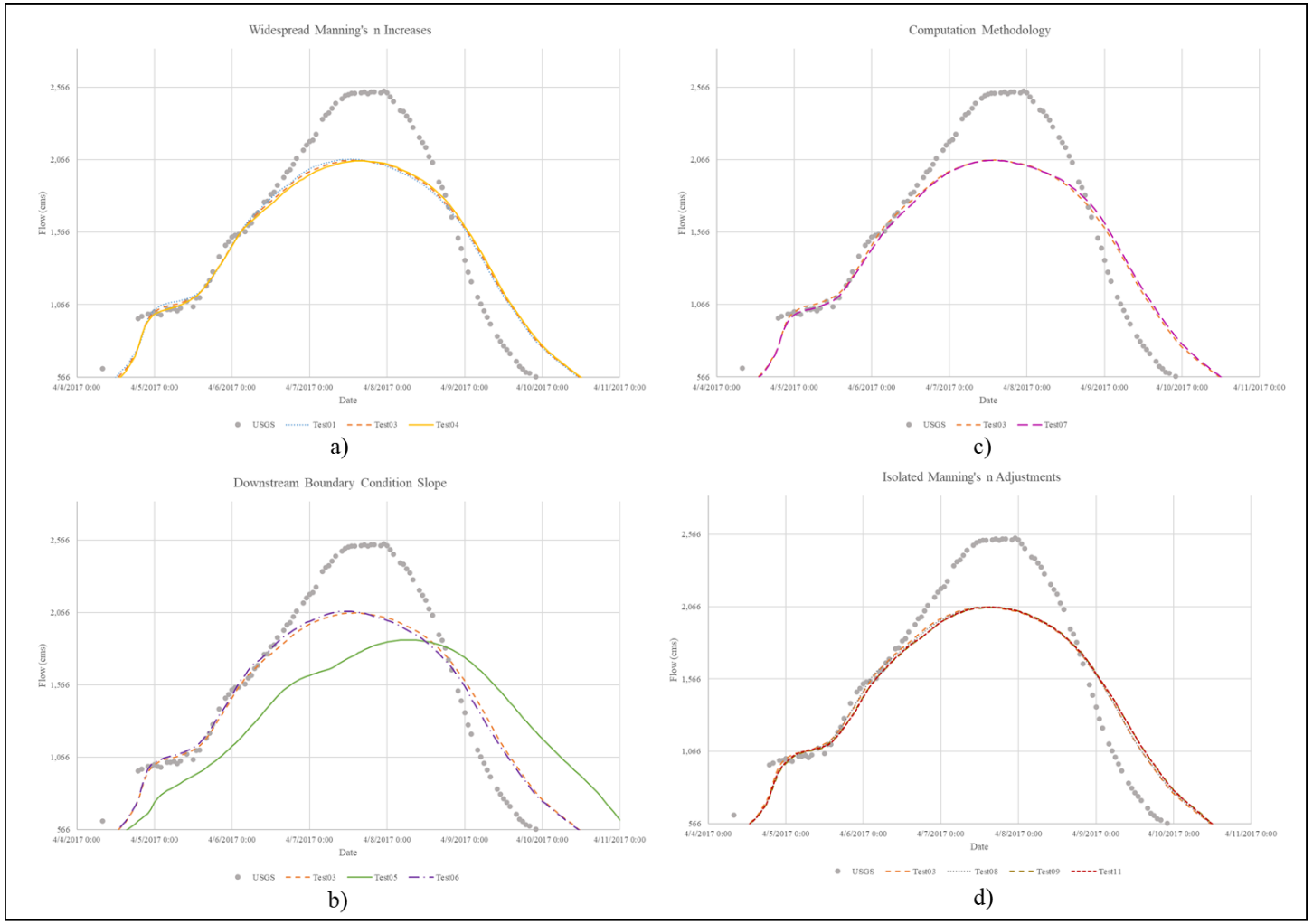

Figure B.3:
Grand River at Sumner, MO flow Sensitivity to Parameter Adjustments.
a) Resulting hydrographs from increasing all Manning's n by 5% (Test03) and 10% (Test04). b) Resulting hydrographs from decreasing and increasing the downstream boundary condition slope by a factor of 10 (Test05 and Test06, respectively). c) Resulting hydrographs from using Diffusion Wave (Test03) and Full Momentum (Test07) computation methodologies. d) Resulting hydrographs from increasing "woody" and "grndfld" land covers. See Table B.1 for specific simulation adjustments.

The simulated peak flow percent error from the April 2017 event was computed using the USGS peak flow. The percent errors are provided in Table B.5 and indicated that all simulations underestimated the peak Grand River discharge at Sumner by approximately 19% with the exception of Test 05. Test05 underestimated the peak discharge by approximately 26%. Underpredicting peak flows may underpredict inundation depths and duration of other stressed wetland community areas. Additionally, peak flow underestimation will likely have a greater impact on fringe wetland community areas where communities are currently deteriorating because the negative impacts will not be captured in the hydraulic analysis due to lower simulated water surface elevations.

Table B.5:
Grand River at Sumner April 2017 Event Peak Discharge Percent Error

Simulation	Peak Flow, cms	Percent Error
USGS	2,540	-
Test01 and Test02	2,070	-19%
Test03	2,064	-19%
Test04	2,059	-19%
Test05	1,877	-26%
Test06	2,076	-18%
Test07	2,061	-19%
Test08	2,064	-19%
Test09	2,061	-19%
Test10	2,064	-19%
Test11	2,061	-19%

Additionally, water surface elevations throughout the model were compared to the USACE surveyed HWMs and the differences between the two were computed. The water surface elevation differences are provided in Table B.6. Since the HWMs were the only data source located within the Pershing State Park Study Area, HWM calibration results received higher priority when eliminating simulations from further analysis.

Since several parameters were adjusted as part of the calibration, the discussions in this section of the thesis discuss the simulations with respect to the calibration parameter in question. The discussions are provided below.

Widespread Manning's n Roughness Adjustments (Test01, Test03 and Test04)

As part of this comparison, simulations Test03 and Test04 were compared to Test01/Test02, the base condition. Test03 and Test04 increased all roughness coefficients by 5% and 10%, respectively. As seen in Table B.4 and Figure B.3 a), Test01 best reflected the observed USGS discharges in both the main channel and overflow locations. This is largely because the simulation used the lowest roughness coefficients resulting in increased channel velocity and streamflow. However, Test01 most underestimated the surveyed HWM elevations. Since the study area is primarily within Pershing State Park, the HWM calibration received the highest priority and, as a result, Test01 was excluded from further testing.

When comparing Test03 and Test04 results, Test03 best simulated Grand River flows and velocities at Sumner, producing percent differences of approximately 8% for main channel and overflow discharges whereas Test04 produced percent differences of -10% and 12% for the main channel and overflow. However, Test 04 better simulated the main channel velocity.

The final consideration between Test03 and Test04 was how well each simulation reflected observed HWMs. Since Test04 used the highest roughness coefficients, the water surface elevations were higher than that of Test03 and better portrayed the surveyed elevations. However, the roughness coefficients used for Test04 were on the upper end of

accepted values. Table B.7 provides recommended roughness coefficients adapted from the HEC-RAS Reference Manual (U.S. Army Corps of Engineers Hydrologic Engineering Center, 2016a) which compiled a range of roughness coefficients from Chow's book "Open-Channel Hydraulics" (Chow, 1959). For example, the farmland roughness coefficient for Test04 was 0.05 which falls at the upper most range for mature field crops in Table B.7. Since the event occurred in April, the beginning of the growing season, it is unlikely that the roughness coefficient associated with the farmland landcover would be associated with mature crops. As a result, Test03 was carried forward for analysis.

Table B.6:
2017 Calibration Simulated Water Surface Elevations and Differences with USACE Surveyed HWMs

Simulation	Description	Simulated Water Surface Elevation in m-NAVD88 Water Surface Elevation Difference between Simulation Results and Observed in meters								
		Pershing State Park					*Grand River*			
USACE Surveyed HWMs	Observed Data	211.56	211.54	209.16	206.04	205.40	205.38	205.42	205.59	205.11
Test01 and Test02	Base condition for comparison	211.05	211.05	208.40	205.55	204.94	204.63	204.51	204.75	204.50
		-0.51	-0.49	-0.77	-0.50	-0.47	-0.75	-0.91	-0.85	-0.61
Test03[1]	Widespread roughness coefficient adjustments	211.09	211.09	208.41	205.55	204.96	204.67	204.63	204.78	204.53
		-0.47	-0.45	-0.75	-0.49	-0.44	-0.71	-0.79	-0.82	-0.58
Test04[1]		211.12	211.12	208.42	205.56	204.98	204.71	204.76	204.81	204.57
		-0.44	-0.42	-0.74	-0.48	-0.42	-0.67	-0.66	-0.78	-0.54
Test05	Boundary condition slope adjustments	211.09	211.09	208.41	205.77	205.70	205.77	205.92	205.85	205.74
		-0.47	-0.45	-0.75	-0.27	0.30	0.39	0.51	0.26	0.63
Test06		211.09	211.09	208.41	205.55	204.96	204.66	204.27	204.76	204.53
		-0.47	-0.45	0.75	-0.49	-0.45	0.72	-1.14	-0.84	-0.58
Test07	Computation methodology	211.25	211.25	283.61	205.66	205.02	204.73	204.97	204.83	204.59
		-0.31	-0.29	-0.55	-0.39	-0.38	-0.65	-0.45	-0.76	-0.52
Test08	Isolated roughness adjustments	211.07	211.07	208.52	205.65	205.00	204.79	204.62	204.84	204.68
		-0.49	-0.47	-0.65	-0.40	-0.40	-0.59	-0.80	-0.75	-0.43
Test09		211.06	211.06	208.54	205.70	205.12	204.89	204.78	204.92	204.77
		-0.51	-0.48	-0.62	-0.34	-0.28	0.48	-0.64	-0.68	-0.34
Test11		211.07	211.07	208.52	205.66	205.10	204.84	204.78	204.88	204.73
		-0.49	-0.47	-0.65	-0.38	-0.30	-0.54	-0.64	-0.72	0.38
Test10	Annual simulation	211.09	211.09	208.35	205.54	204.92	204.67	204.63	204.78	204.53
		-0.47	-0.45	-0.81	-0.50	-0.48	-0.71	-0.79	-0.82	0.58

[1] Simulations are compared to Test01 and Test02 for comparison. All other simulations are compared to Test03

Table B.7:

Part of Table 3-1 Excerpted from the HEC-RAS 5.0. Reference Manual (U.S. Army Corps of Engineers Hydrologic Engineering Center, 2016a)

Channel Type and Description	Minimum	Normal	Maximum
Main Channels			
Clean, straight, full, no rifts or deep pools	0.025	0.030	0.033
Clean, straight, full, no rifts or deep pools with more stones and weeds	0.030	0.035	0.040
Clean, winding, some pools and shoals	0.033	0.040	0.045
Clean, winding, some pools and shoals with more weeds and stones	0.035	0.045	0.050
Same as above, lower stages, more ineffective slopes and sections	0.040	0.048	0.055
Clean, winding, some pools and shoals with more weeds and more stones	0.045	0.050	0.060
Sluggish reaches, weedy, deep pools	0.050	0.070	0.080
Very weedy reaches, deep pools, or floodways with heavy stands of timber and brush	0.070	0.100	0.150
Flood Plains			
Pasture no brush			
Short grass	0.025	0.030	0.035
High grass	0.030	0.035	0.050
Cultivated Areas			
No crop	0.020	0.030	0.040
Mature row crops	0.025	0.035	0.045
Mature field crops	0.030	0.040	0.050
Brush			
Scatter brush, heavy weeds	0.035	0.050	0.070
Light brush and trees, in winter	0.035	0.050	0.060
Light brush and trees, in summer	0.040	0.060	0.080
Medium to dense brush, in winter	0.045	0.070	0.110
Medium to dense brush, in summer	0.070	0.100	0.160
Trees			
Cleared land with tree stumps, no sprouts	0.030	0.040	0.050
Cleared land with tree stumps, heavy sprouts	0.050	0.060	0.080
Heavy stand of timber, few down trees with little undergrowth, flow below branches	0.080	0.100	0.120
Heavy stand of timber, few down trees with little undergrowth, flow into branches	0.100	0.120	0.160
Dense willows, summer, straight	0.110	0.150	0.200

Downstream Boundary Condition Slope (Test03, Test05 and Test06)

As part of the calibration process, the downstream boundary condition slope was adjusted. Test05 decreased the downstream boundary condition slope by a factor of 10. As

seen in Figure B.3, decreasing the boundary condition caused the downstream hydrograph to attenuate, delaying the peak by approximately one day, decreasing flows and channel velocities (Table B.4) and increasing water surface elevations along Grand River and downstream portions of Pershing State Park (Table B.6). However, simulated water surface elevations within the upper portions of Pershing State Park showed no additional improvement than Test03. As a result, Test05 was eliminated from further analysis.

Test06 increased the boundary condition slope by a factor of 10 overestimating channel and overflow velocities at Sumner (Table B.4). Additionally, the increase in downstream slope allowed water to leave the model faster, contributing to decreased water surface elevations along the Grand River and downstream portions of Pershing State Parks resulting in larger magnitude underestimations of the HWMs (Table B.6). As a result, Test06 was eliminated from further analysis and the downstream boundary conditions slope specified in Test03 was used for all other simulations.

Computation Methodology (Test03, Test07)

Model sensitivity to computation methodology was also explored. Test07 used the full momentum equation set which accounted for acceleration whereas Test03 used diffusion wave. If a different computation methodology is ever used, the model should be recalibrated using the new equation sets. However, the model for Test07 was not recalibrated with the full momentum equation set and as a result, may not show the best possible results for the full momentum equations.

Water surface elevations resulting from Test07 produced water surface elevations closer to all HWMs when compared to Test03 results (Table B.6). Additionally, the full

momentum equations did not alter the downstream hydrograph shape (Figure B.3) although channel velocities were larger than observed and Test03 results (Table B.4).

Another important difference occurred when mapping the floodplain velocities. Figure B.4 displays the maximum velocities that occurred at any point in time during the simulations for both diffusion wave and full momentum computation methodologies. As seen in Figure B.4, full momentum produced isolated "pockets" of high velocities randomly throughout the entire model. These isolated pockets did not always occur around culverts (where high velocities might be expected) and were often present in areas where minimal velocities would be anticipated. However, it is likely these high velocity areas could be removed with additional calibration efforts.

Additionally, using full momentum increased computation time for the April 2017 event by 150%. Due to the significant increase in computation time, the intended application in annual simulations and more detailed models, and increased "pockets" of large velocities, full momentum was not recommended. As a result, Test07 was eliminated from future calibration efforts.

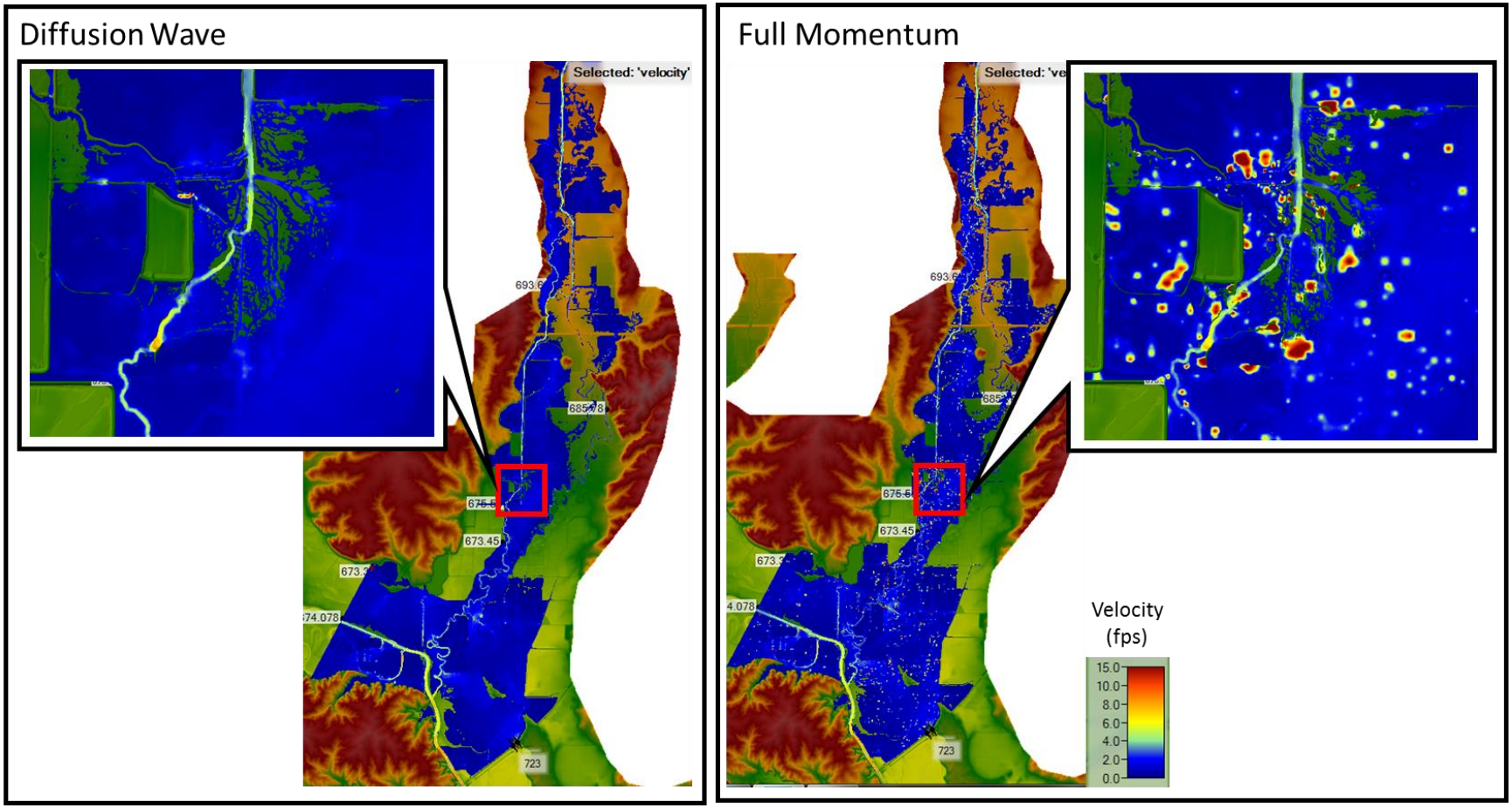

Figure B.4:
Simulated Maximum Velocities Resulting from Diffusion Wave and Full Momentum Computation Methodologies

Isolated Roughness Coefficients (Test03, Test08, Test09, Test11)

Further refinements were made to landcover roughness coefficients; however, roughness coefficient adjustments were applied to individual landcover categories rather than in a widespread manner. As seen in Table B.6, Test09 better estimated more HWMs than Test08 and Test11 and better reflected the main channel discharge. As a result, Test09 was carried forward for more detailed analysis. However, Test09 slightly attenuated the hydrograph (peak delayed by ~4 hours) and used a roughness coefficient at the upper most end of acceptable values specified in Table B.7. Without considering Test09, Test11 produced water surface elevation more closely reflecting HWMs than Test08 and Test03 and, thus, was also carried forward for analysis.

Annual Simulation (Test03, Test10)

Finally, the simulation time period was extended from the singular event to include the entire 2017 calendar year from January 1st to December 31st (Test10). This was done in order to determine if the model consistently underestimated peak discharges. Figure B.5 displays the simulated Grand River flows at Sumner with respect to the USGS observed flows. As seen in Figure B.5, the peak discharges were routinely underestimated for events ranging in magnitude. Again, underpredicting peak flows may underpredict inundation extents, depths, and durations, thus underpredicting wetland community degradation and other ecosystem impacts.

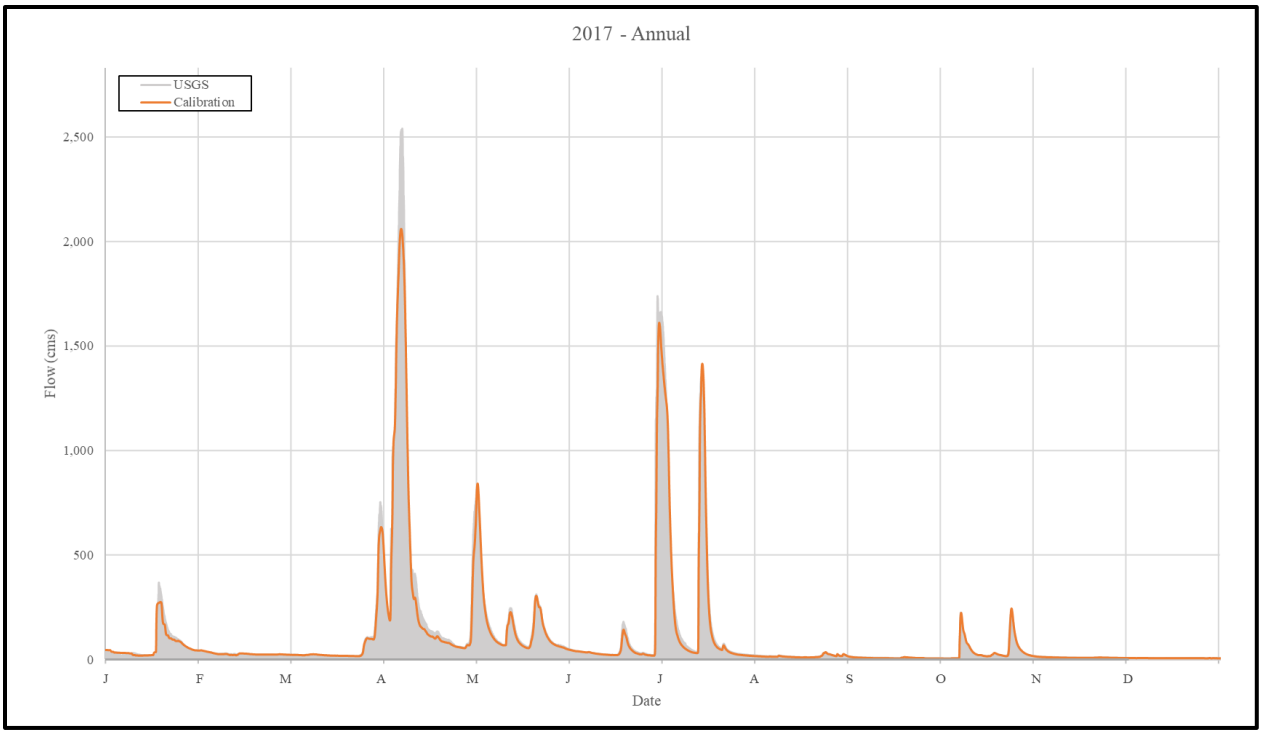

Figure B.5:
Simulated Flows at Sumner for the 2017 Annual Simulation compared to USGS Observed Flows

Although peak flows were underpredicted, Test10 HWM results in Table B.6 appeared to produce the same elevations as Test03, indicating that increasing the simulation time period did not alter the peak water surface elevations simulated for individual events.

Based on the previous discussions, three simulations were carried forward for additional analysis using Model-25 geometries: Test03, Test09, and Test11. The simulations within Model-25 were referenced with "25" proceeding the original simulation name. For example, Test03 in Model-25 was referred to as 25Test03.

Table B.8 compares the simulated peak flow for the April 2017 event to the USGS peak flow and provides the percent error. All Model-25 simulations produced percent errors of -19%

indicating that all simulations underestimated the peak flows. Underpredicting peak flows may underpredict inundation depths and duration of stressed wetland communities. Additionally, peak flow underestimation will likely have a greater impact on deteriorating fringe communities where negative impacts will not be captured in the hydraulic analysis due to lower simulated water surface elevations.

Table B.8:
Model-25 Grand River at Sumner April 2017 Event Peak Discharge Percent Error

Simulation	Peak Flow, cms	Percent Error
USGS	2,540	-
25Test03	2,059	-19%
25Test09	2,064	-19%
25Test11	2,061	-19%

Figure B.6 displays the Grand River hydrographs at Sumner for the individual April 2017 event and Table B.9 compares simulated discharges and velocities to instantaneous USGS measurements at Sumner. Overall, the hydrograph shapes for all three simulations were very similar; however, 25Test11 best portrayed the instantaneous USGS flow measurement in the main channel when compared to 25Test09. 25Test03 best represented the overflow discharge and main channel velocity compared to the other two simulations.

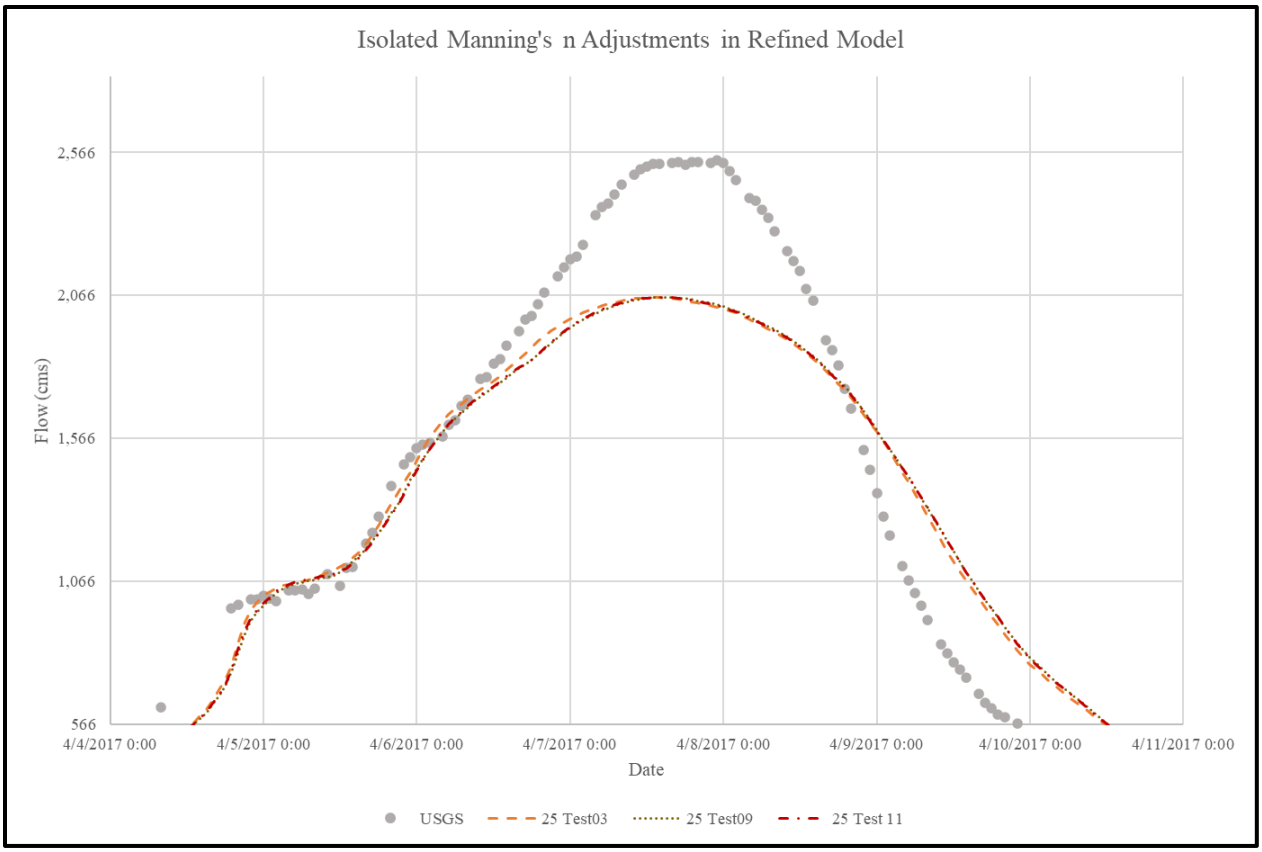

Figure B.6:

Isolated Manning's n Model-25 Adjustments Simulated Grand River Flows at Sumner Compared to USGS Flows

Table B.9:

Model-25 Grand River at Sumner, MO Simulated Main Channel and Overflow Discharge and Average Channel Velocity Comparisons with USGS Measurements Recorded at 4/6/2017 16:24:48 UTC

Simulation	**Discharge, cms**		**Average Channel Velocity, mps**	
	Main Channel	*Overflow*	*Main Channel*	*Overflow*
USGS	1,543	382	1.71	0.56
25 Test03	1,463	405	1.96	0.83
25 Test09	1,463	338	2.00	0.76
25 Test11	1,463	340	2.00	0.76

Additionally, the Nash-Sutcliffe model efficiency (NSE), was used to compute how well the Grand River flows at Sumner predicted the USGS observed flows. NSE for each simulation

was computed using Equation B.1 where y_i is the observed USGS flow at a given time step, $y_{i,sim}$ is the simulated flow at a given time step, and $\bar{y}$ is the average observed USGS flow for the simulation period.

Equation B.1: $$NSE = 1 - \frac{\sum(y_i - y_{i,sim})^2}{\sum(y_i - \bar{y})^2}$$

In a perfect model, the NSE would equal 1.0. Table B.10 provides both the NSE and correlation for the Model-25 simulations. As seen in the table, both the NSE and correlation were close to 1.0 indicating a good calibration. However, both the NSE and correlation were biased in this calculation as the calculation used every time step within the April 2017 event simulation. By accounting for all time steps, more datapoints reflective of baseflow conditions were incorporated into the calculations which reduced the overall impact of the underestimated peaks in the NSE and correlation calculations.

Table B.10:
Model-25 Simulations Computed NSEs and Correlations

Simulation	NSE	R^2
25Test03	0.960	0.967
25Test09	0.958	0.966
25Test11	0.958	0.966

Although the NSE was similar for all three Model-25 April 2017 event simulations, the HWM results varied. Table B.11 displays the Model-25 simulated water surface elevations and differences with respect to USACE surveyed HWMs. All simulations largely underestimated the HWMs by 0.5 to 0.8 meters, further indicating that the model underpredicted peak flows and stages. Based on those water surface elevation differences, 25Test09 best simulated the most HWMs within Pershing State Park in addition to areas along the Grand River. However, 25Test09 used a roughness coefficient at the upper most end of acceptable values specified in Table B.7 for wooded land covers. The April 2017 event likely occurred primarily during a "leaf-off" period

where vegetation is sparse or just starting to spring out of winter hibernation. Thus, the large roughness coefficient that added friction, reduced velocities, increased stage, and thus contributed to higher water surface elevations was not representative. As a result, the calibration parameters associated with 25Test09 were not used in the final model.

Table B.11:
Model-25 Simulated Water Surface Elevations and Differences with USACE Surveyed HWMs

Simulation	**Description**	**Simulated Elevation in m-NAVD88** Water Surface Elevation Difference between Simulation Results and Observed in meters Pershing State Park					Grand River			
USACE Surveyed HWM	Observed Data	211.56	211.54	209.16	206.04	205.40	205.38	205.42	205.59	205.11
25 Test03	Isolated roughness adjustments in the refined model	211.01	211.02	208.42	205.59	204.87	204.68	204.62	204.78	204.54
		-0.55	-0.52	-0.74	-0.46	-0.54	-0.70	-0.80	-0.81	-0.57
25 Test09		210.98	210.98	208.55	205.73	205.05	204.81	204.78	204.93	204.78
		-0.59	-0.56	-0.61	-0.31	-0.35	-0.47	-0.64	-0.67	-0.33
25 Test11		210.99	211.00	208.52	205.70	205.03	204.85	204.78	204.89	204.73
		-0.57	-0.55	-0.64	-0.35	-0.37	-0.52	-0.64	-0.71	-0.38

With 25Test09 removed from HWM considerations, 25Test11 produced water surface elevations closer to the HWM elevations for more points in Pershing State Park and along the Grand River than 25Test03. As a result, 25Test11 calibration parameters were carried forward for log jam calibration and model simulations.

Log Jam Calibration

Due to the complexities and impact LWD had on riparian wetland communities in Locust Creek and Pershing State Park, LWD was accounted for in the modeling process. Records of log jam formation and removal obtained from MoDNR, USGS SIR 2017-5120 (Heimann & Survey, 2017), and Google Earth were used to estimate changes to channel capacity and split flows. If a log jam year was not specified in the MoDNR accounts or USGS SIR 2017-5120, Google Earth historic imagery was examined to determine if the year could be identified. If the year was not

identified, the log jam was not included in the analysis. The historic imagery from Google Earth was also reviewed and log jams identified in the streams were traced. Figure B.7 displays the location, length, and year of formation for each documented log jam. Final log jam lengths may differ than what is recorded in the figure since the log jams identified in Google Earth were based off of a single snapshot in time.

Log jams have been represented in hydraulic models using several methods. Numerical models often adjusted the Manning's roughness coefficient (Manning's n) to reflect the increased roughness caused by LWD (Addy & Wilkinson, 2019). Log jams in a 1D steady HEC-RAS model were represented by adjusting the geometry of two cross-sections to reflect the height, width, and length of a solid log jam (Abbe, 2006; Valverde, 2013). In a 2D unsteady HEC-RAS model, weirs with orifices were used to simulate log jams and were calibrated to stages at upstream cross section (Keys et al., 2018). Additionally, manual adjustments to the 2D mesh elements were used to simulate a log jam (Rasche et al., 2019). In a literature review conducted by Rasche, et al. in 2019, the various methods used to model LWD were compared. The review concluded that modeling LWD with roughness adjustments is widely used and acceptable for "representing the effects of single or multiple log jams at the site or reach scale" (Rasche et al., 2019). However, roughness coefficients change with variable flows (Hydrologic Engineering Center, 2020) and HEC-RAS 5.0.7 2D did not have the capability to include variable flow roughness coefficients. Additionally, the comparison indicated geometry adjustments (HEC-RAS terrain or mesh adjustments) may overexaggerate hydraulics and prevent sufficient modeling of porous LWD (Rasche et al., 2019). When log jams were modeled as solid features, damming and dispersal impacts from the LWD were simulated (Addy & Wilkinson, 2019). For this study, log jams were modeled using increased

roughness coefficients in order to simulate both the hydraulic impacts and permeability of large woody debris.

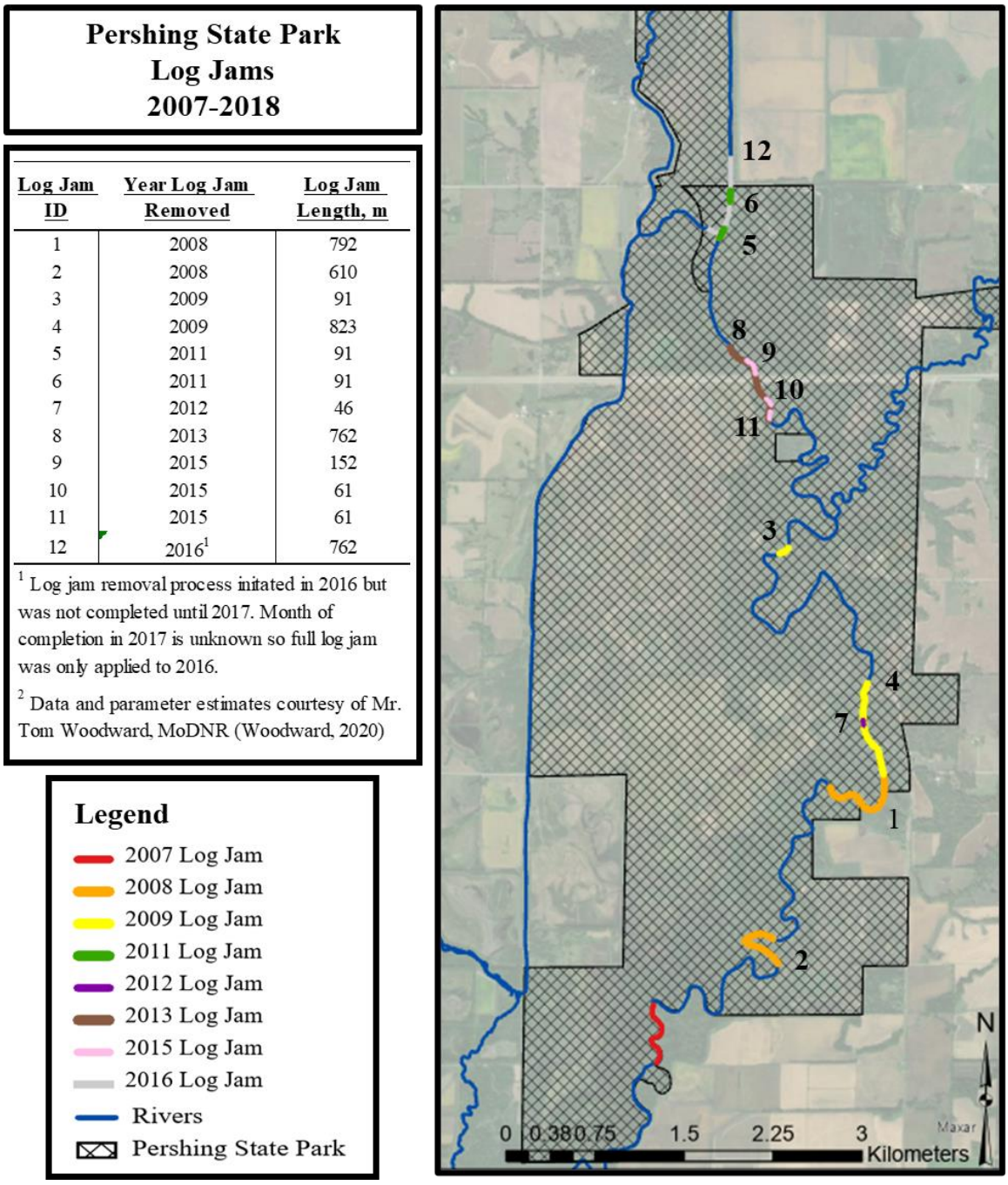

Figure B.7:
Log Jams Identified by MoDNR and Google Earth from 2007 to 2018

Calibration Event

Log jam characteristic were calibrated to an individual event that occurred between March 8th and March 13th of 2009 on Locust Creek. The March 2009 event was selected for calibration because the event resulted in floodplain inundation and had calibration data available throughout the floodplain in Pershing State Park. This event was characterized by a multipeak hydrograph on Locust Creek. For this event, the initial peak discharge on Locust Creek near Linneus, MO occurred March 9th, 2009 with a peak discharge of 402 cms. The second peak occurred March 10th, 2009 with a peak discharge of 396 cms. Additionally, the developed flow record at Muddy Creek produced a peak discharge of 32 cms on March 8th, 2009. A smaller peak also occurred on the Muddy Creek hydrograph on March 10th, 2009 with a peak discharge of 9.3 cms.

The timeseries for the March 2009 event from March 8th 2009 through April 9th 2009 was comprised of 83% USGS data and approximately 17% of interpolated values for Locust Creek inflows. However, Grand River inflows at Fountain Grove for this simulation were completely based on HEC-HMS developed flows. This indicates that Grand River results at Sumner may be influenced by hydrologic model errors within the HEC-HMS generated time series.

Calibration Data

HWMs, discharge, and velocity measurements directly upstream and downstream of log jams were not collected within Pershing State Park. Thus, limited information was available for log jam calibration. The March 2009 event was largely selected for log jam calibration because documentation of the log jam existed and Landsat aerial imagery of floodplain inundation extents was available for reference within Pershing State Park. Inundation extents and duration from aerial imagery were previously used to quantify wetland change in other studies (Martínez-Espinosa et al., 2021). Additional datasets including soil moisture and other sources of aerial imagery were

also used to quantify wetland change (Martínez-Espinosa et al., 2021); however, available datasets were too coarse to be applied to Pershing State Park. As a result, the USGS Landsat 7 aerial imagery was used to calibrate the model for log jams. USGS Landsat 7 aerial imagery, available from the USGS LandLook web tool (U.S. Geological Survey, 2018), displayed inundation extents on March 14th, 2009 as a result of flooding from the March 2009 event. However, a timestep was not included. As a result, it was assumed that the image, collected during daylight hours, was collected at 1200 hours. The inundation aerial imagery extents are provided in Figure B.8 with respect to the model domain and important stream alignments. Specifically, the available inundation extents included sections of the floodplain upstream and downstream of the 2009 log jam.

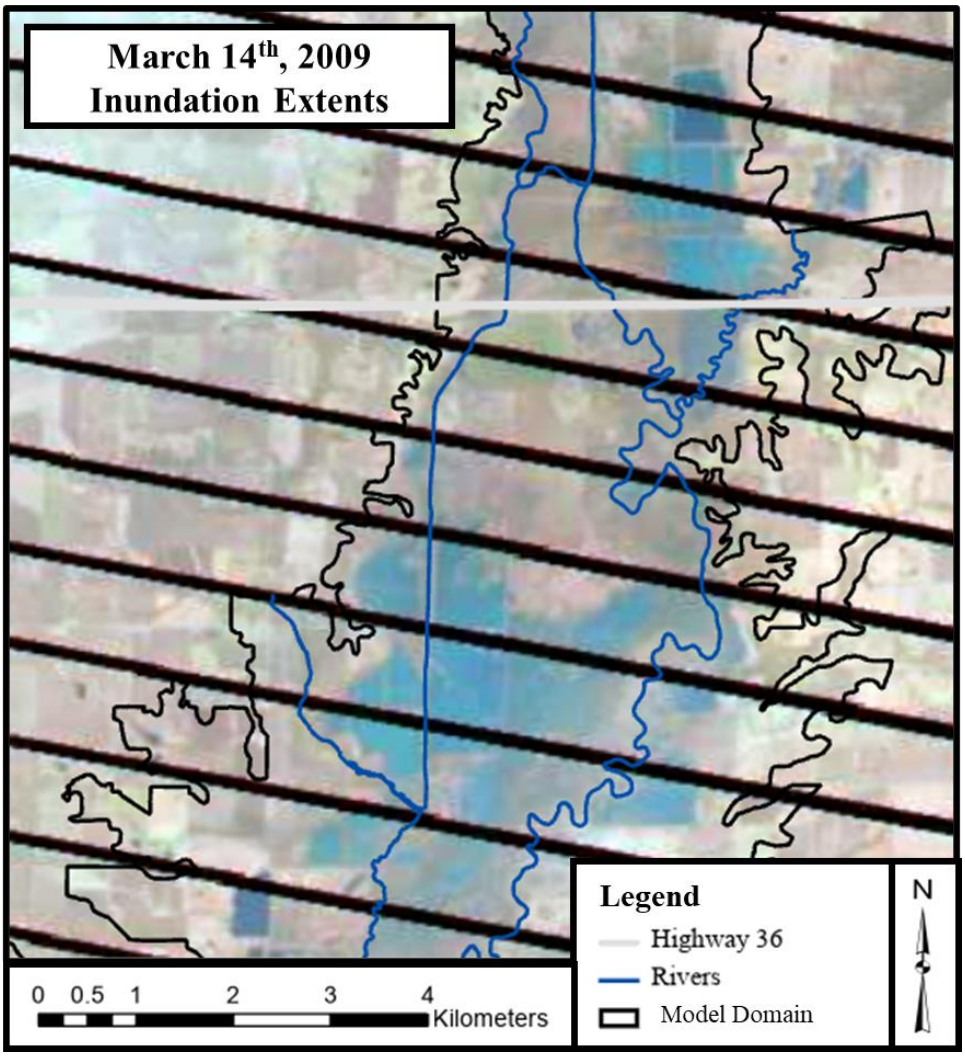

Figure B.8:
USGS Landsat 7 Floodplain Inundation Extents on March 14th, 2009

Calibration Methodology

The calibration event used a simulation time period from 08 March 2009 00:00 to 09 April 2009 00:00 in order to model all components of an individual hydrograph: initial baseflow, rising limb, peak, falling limb, and return to baseflow. A computation interval of one minute and an initial conditions warmup period of 252 hours (10.5 days) were used to ensure computational stability. All other calibrated parameters associated with Plan 25Test11, discussed under the No

Log Jam Calibration Results and Discussion section were used in the simulations. This included the use of diffusion wave computation methodology, water surface elevation and volume tolerance of 0.008 meters, and the ManN05 Landcover layer.

For this study, log jams were modeled using increased roughness coefficients in order to simulate both the hydraulic impacts and permeability of large woody debris. For the calibration event selected, a new Landcover was created in RAS Mapper by importing a shapefile that included a polygon representing the documented length of the 2009 log jam in Figure B.7. The width of the log jam was assumed to span the entire channel width. Once imported, the polygon representing the log jam was assigned a roughness coefficient. Every time the log jam roughness was adjusted, a new Landcover layer in RAS Mapper was created. All other roughness coefficients associated with the Landcover layer used the calibrated ManN05 roughness coefficients in Table B.3. For easier organization, a new geometry was created for every Landcover layer so the Landcover layer could be associated with an individual geometry for each plan in RAS Mapper. All geometries were based off of the EC_LC_003_01_ManN05 geometry used in the "No Log Jam" calibration. No changes were made to the geometries themselves other than the naming convention. All changes to roughness coefficients were reflected in the Landcover files. Initially, the Model-100 geometry was used to preliminarily screen the calibration simulations due to significantly decreased run times. The remaining, unscreened calibration simulations were then run through Model-25 for final comparison and selection of calibration parameters. Table B.12 provides a summary of the plan names, corresponding geometry names, and log jam roughness coefficients. All plans were run in HEC-RAS and the resulting inundation extents were compared to the Landsat imagery to identify the best calibration.

Table B.12:
Log jam Calibration Plans, Geometries, Flow Files, and Log Jam Roughness Coefficient

Plan Name	Geometry	Flow File	Log Jam Roughness Coefficient
LJ_ManN_2009_0.10	EC_LC_003_01_LJManN_2009_0.10_100ft	Test01	0.10
LJ_ManN_2009_0.15	EC_LC_003_01_LJManN_2009_0.15_100ft	Test01	0.15
LJ_ManN_2009_0.20	EC_LC_003_01_LJManN_2009_0.20_100ft	Test01	0.20
LJ_ManN_2009_1.0	EC_LC_003_01_LJManN_2009_1.0_100ft	Test01	1.00
LJ_ManN_2009_1.5	EC_LC_003_01_LJManN_2009_1.5_100ft	Test01	1.50
LJ_ManN_2009_2.0	EC_LC_003_01_LJManN_2009_2.0_100ft	Test01	2.00

Calibration Results and Discussion

The inundation extents are displayed in Figure B.9. As seen in the figure, log jams represented with roughness coefficients equal to 0.10, 0.15, and 0.20 largely underestimated the inundation extents, especially on the eastern side of the floodplain where wet prairie exists. Thus, those roughness coefficients were not selected to represent LWD in the model. Increasing the log jam roughness coefficient to 1.0 largely increased the inundation extents compared to the smaller roughness coefficients. Underestimation of the inundation extents may result in fewer hydraulic impacts (shallower depths and smaller inundation durations) to key wetland communities, resulting in underestimation of wetland community changes. However, the underestimation of the simulated inundation extents may be a result of changes in topography due to floodplain sedimentation that occurred between 2009 and 2018. Additionally, a roughness coefficient of 1.0 fell within the acceptable range of roughness coefficients used in past studies to represent LWD (Addy & Wilkinson, 2019). Further increasing the roughness coefficient to 1.5 and 2.0 did not significantly expand the inundation extents. Additionally, roughness coefficients of 1.5 and 2.0 fell on the upper end of roughness coefficients used to represent log jams in past studies (Addy & Wilkinson, 2019) as seen in Table B.13. As a result, the roughness coefficient of 1.0 produced the

most representative inundation extents, fell within the acceptable range of roughness coefficients, and thus, was used for all log jam roughness coefficients in the annual simulations.

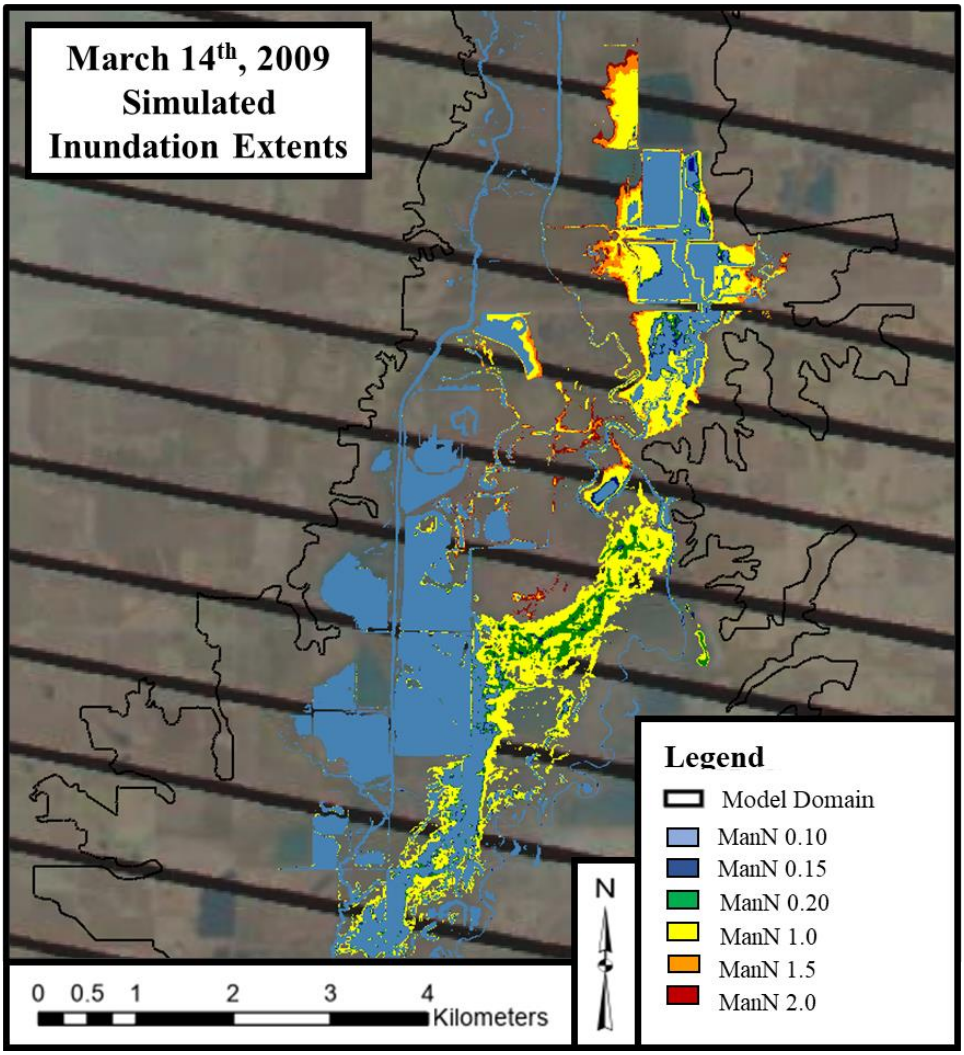

Figure B.9:
Log Jam Roughness Coefficient Calibration March 2009 Inundation Extents

Table B.13:
*Manning's n Values of LWD from Dif*ferent Studies *Adapted from (Addy & Wilkinson, 2019)*

Study	Location	Reach Slope, m/m	Drainage Area, km^2	Channel Type	Mean Manning's n (min-max)	Flow Conditions	% Blockage	Calibration Description
Curran and Wohl 2003	Washington State, USA	0.06 - 0.18	9.6 – 0.13	Step-pool gravel/cobble bed	0.6 (0.2-1.5)	Low flows less than bankfull		
Shields Jr and Gippel 1995	Tennessee	0.0005 - 0.0008 [1]	927	Straight, sand bed	0.058 (0.0435-0.0807)	Range of flows		
	SW Australia	0.001 - 0.0015 [1]	-	Sinuous, gravel/sand bed	0.075 (0.0652-0.0875)	Less than bankfull		
Dixon 2013	New Forest, S. England	0.004 [1]	< 15	Meandering, coarse gravel bed	0.24 (0.137-0.362)	High (above 0.80 cms)		
		0.012 - 0.013			0.083 (0.027-0.199)			
Kitts 2010	New Forest, S. England	0.0057 [1]	11.1	Meandering, coarse gravel bed	1.4 (0.58-2.22)	Less than 0.2 cms (low)	100%	Calibration was achieved with predicted inundation extents that visually matched observed inundation extents
					0.27 (0.142-0.398)			Validation: Simulated flow extent was 1,659 m^2 compared to observed extent of 1,619 m^2. Velocity was over predicted but the average difference was 0.05 cms
					0.32 (0.173-0.467)			
Linstead and Gurnell 1998	New Forest, S. England				0.677	Low flows less than bankfull		
					0.348			
Gregory, Gurnell, and Hill			< 15		0.224			

[1] The log jam spans across the entire channel and induced a step in the water surface profile at all flows

Appendix C: Hydraulic Model Validation

A validation process was applied to the hydraulic model to ensure that the calibrated model produced predictive results outside of the calibration datasets.

Similar to calibration, the model was validated for two different events: one without a log jam and one with a log jam present. The first validation event did not include a log jam and was used to validate overall model characteristics such as roughness coefficients, downstream boundary friction slope, and computation equation set. The second validation event occurred during a year where a log jam was documented within Pershing State Park and was only used to validate the roughness coefficient associated with log jams. Once the two events were examined, the entire analysis period between 2008 and 2018 was simulated and the peak flows from each annual simulation were analyzed to ensure the simulated results were valid. The following sections discuss the validation processes for the three different scenarios.

Validation: No Log Jams

Once the model was calibrated to the 2017 event, an additional event was run through the model to test performance and validate the results without the influence of log jams.

Validation Event

After calibration, a separate event was run through the model to validate model performance without a log jam present. The model was validated against an individual event that occurred between October 7th and 15th of 2018. The 2018 event was selected for validation because the event resulted in floodplain inundation and had validation data available throughout the floodplain in Pershing State Park. The October 2018 event involved a series of rainfall events resulting in 15.2 to 20.3 cm of rainfall across the Grand River Basin with a storm center of 29.0

cm located near Kingston, Missouri. The peak discharge on the Grand River at Sumner, MO occurred October 11th, 2018 with a peak discharge of 2,220 cms.

The timeseries of the October 2018 event from 05 October 2018 00:00 through 25 October 2018 00:00 was comprised of 80% USGS data and approximately 20% of interpolated values for Fountain Grove. The Locust Creek inflow timeseries for the same timeframe was comprised of 82% USGS data and 18% of interpolated values. This indicates that majority of the inflows were based off instantaneous and observed data when possible and that overestimation and underestimation at Locust Creek and Fountain Grove were not a result of the hydrologic model errors.

Validation Data

Several sources of data existed for model calibration including highwater marks (HWMs), USGS streamflow, and USGS instantaneous measurements. The 2018 event was selected for calibration because of data availability throughout the floodplain in Pershing State Park via HWMs. HWMs include, but are not limited to, water lines on trees and debris lines. HWMs are impacted by wind wave action, super elevation, and debris which may push the water surface elevation to higher elevations in isolated locations. Additionally, due to the frequency of Locust Creek flood events, high water marks may be representative of different hydraulic events. As a result, HWMs can introduce error into the model. However, the HWMs provided a measurement of the floodplain hydraulics within Pershing State Park. USACE surveyed high water marks (HWMs) on October 11th, 2018 and elevations reported in meter-NAVD88 are provided in Figure C.1.

Additionally, USGS Grand River discharges at Sumner, MO, developed from the USGS rating curve, were used to compare flows at the downstream model domain. The stage discharge

relationship captured in the rating curve was subject to error due to altered channel geometry caused by scour and sedimentation during a flood event (McMillan et al., 2012; Rojas et al., 2020). As a result, the error in extrapolation from the rating curve could compound in hydraulic models that used the data for calibration and lead to incorrect results (Westerberg et al., 2016; Wilby et al., 2017). However, the USGS flows were located at the downstream boundary of the model and provided the best estimates to gage model performance. Instantaneous USGS measurements were not available on the Grand River at Sumner, MO. However, According to USGS, when the Grand River reaches a stage of 10.1 meters at the Sumner gage, the Stanley Lake split flow was activated (U.S. Army Corps of Engineers, 2020). Stanley Lake is a small lake located east of the Grand River channel along the BNSF railroad bridge that only receives water during Grand River flood events. When activated, a split flow formed at the USGS gage location with flows passing under the BNSF bridge at the main Grand River channel and Stanley Lake

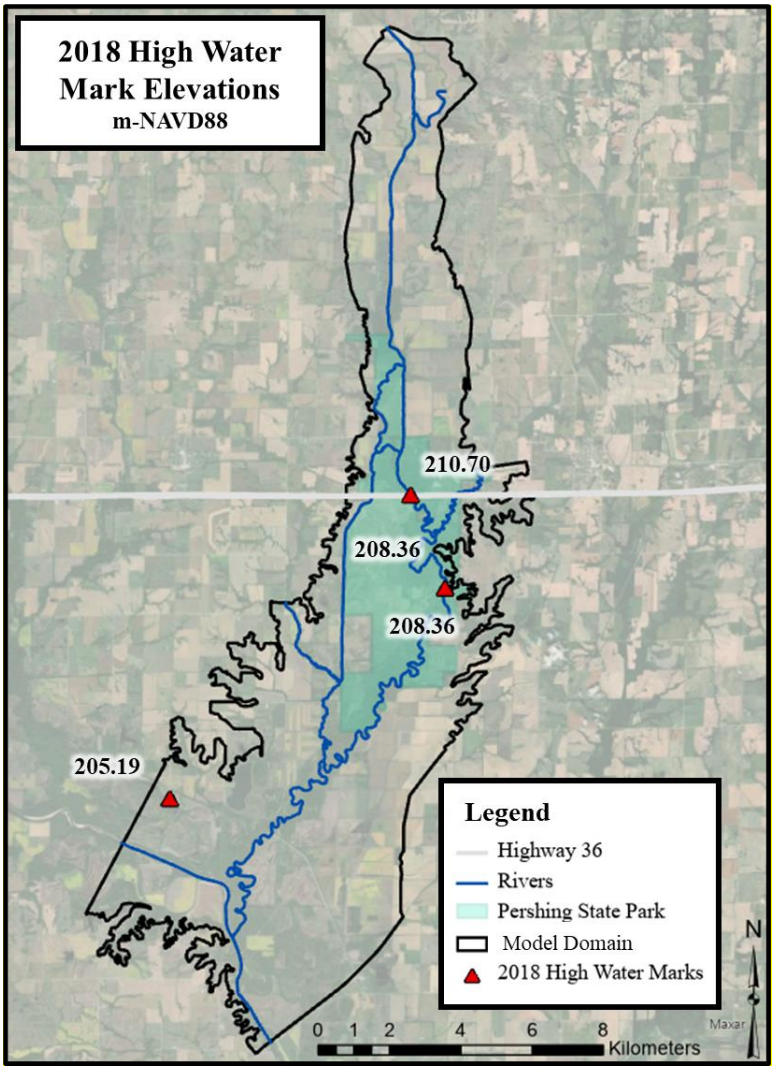

Figure C.1:
October 2018 Surveyed High Water Mark Locations Labeled with Elevations in meters-NAVD88

USGS Landsat 7 aerial imagery, available from the USGS LandLook web tool (U.S. Geological Survey, 2018), displayed inundation extents on October 24th, 2018 as a result of flooding from the October 2018 event. However, a timestep was not included. As a result, it was assumed that the image, collected during daylight hours, was collected at 1200 hours. The inundation aerial imagery extents are provided in Figure C.2 with respect to the model domain and important stream alignments. Within the model domain, Landsat inundation imagery was only available along the Grand River near the Locust Creek confluence.

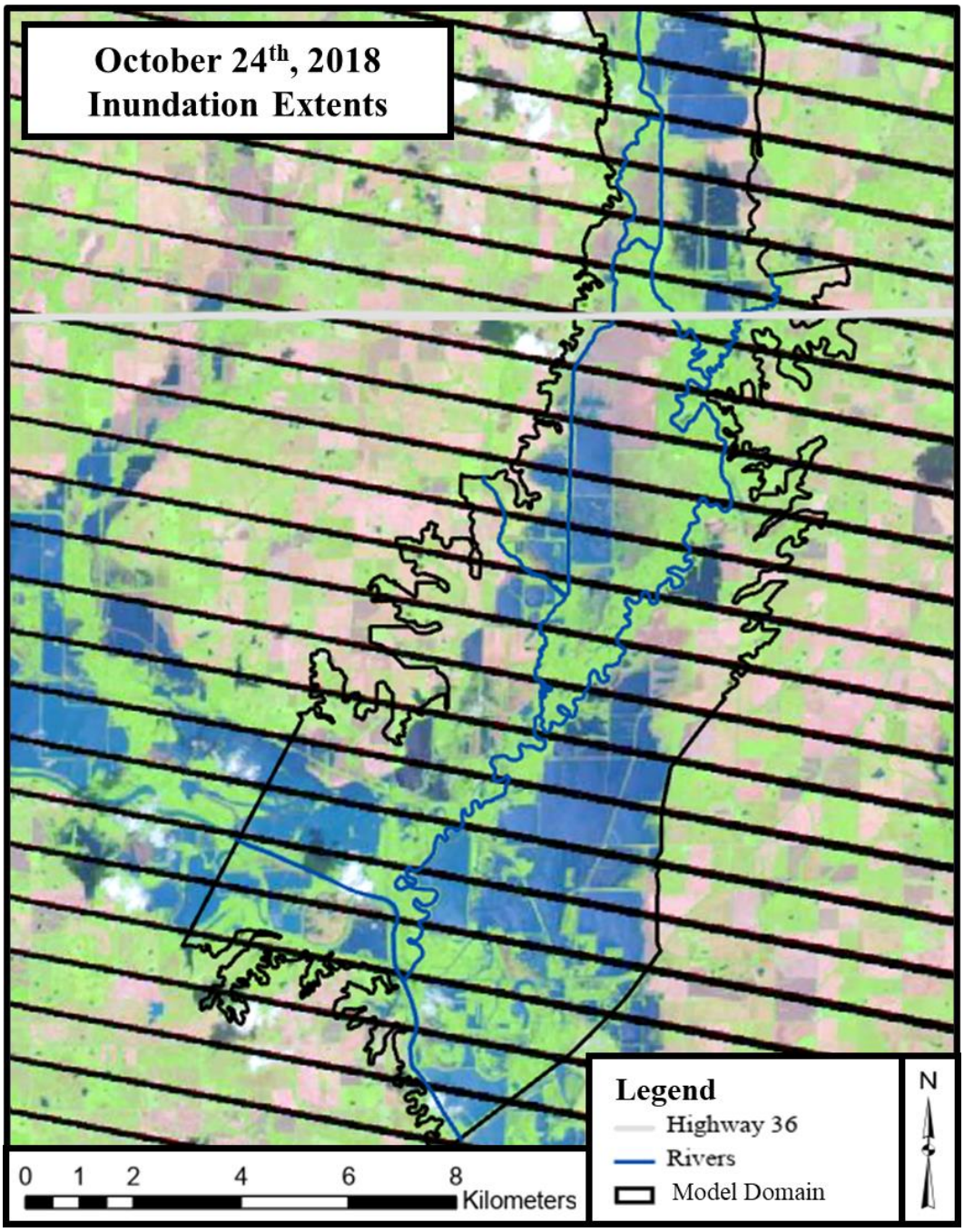

Figure C.2:
USGS Landsat 7 Floodplain Inundation Extents on October 24th, 2018

Validation Methodology

The validation event used a simulation time period from 05 October 2018 00:00 to 25 October 2018 00:00 in order to model all components of an individual hydrograph: initial baseflow, rising limb, peak, falling limb, and return to baseflow. Additionally, a simulation for the full 2018 calendar year was performed with a simulation time period from 01 January 2018 00:00 to 31 December 2018 24:00. A computation interval of one minute and an initial conditions warmup period of 252 hours (10.5 days) were used to ensure computational stability. Diffusion wave methodology and a water surface elevation and volume tolerance of 0.008 meters were initially selected to improve model run time efficiency and stability. All other computation options and tolerances used the default parameters. All other parameter adjustments made in 25Test11 (discussed in Appendix B) were included in the validation simulations. Only 7.62 meter (25 feet) computational grids (Model-25) were used in the validation.

The validation runs were simulated and the results were compared to available validation data. No additional parameter adjustments were made to the model. NSE for the individual event was computed using Equation C.1 where y_i was the observed USGS flow at a given time step, $y_{i,sim}$ was the simulated flow at a given time step, and $\bar{y}$ was the average observed USGS flow for the simulation period. In a perfect model, the NSE would equal 1.0.

Equation C.1: $$NSE = 1 - \frac{\sum(y_i - y_{i,sim})^2}{\sum(y_i - \bar{y})^2}$$

Validation Results and Discussion

Once the simulations were complete, the Model-25 October 2018 event hydrographs and USGS measurements at Sumner were compared. The resulting hydrographs are displayed in Figure C.3 and Figure C.4. As seen in Figure C.3, the timing of the rising limb and the falling limb appeared to match observed USGS data. However, the peak discharge was underestimated by

approximately 7.4%. Additionally, the hydrograph volume appeared to be underestimated on the falling limb possibly due to increased floodplain attenuation in the Grand River floodplain. The annual simulation indicated that peak discharges were routinely underestimated for events ranging in magnitude of peak flows. Again, underpredicting peak flows may underpredict inundation extents, depths, and durations, thus underpredicting wetland community degradation and other ecosystem impacts.

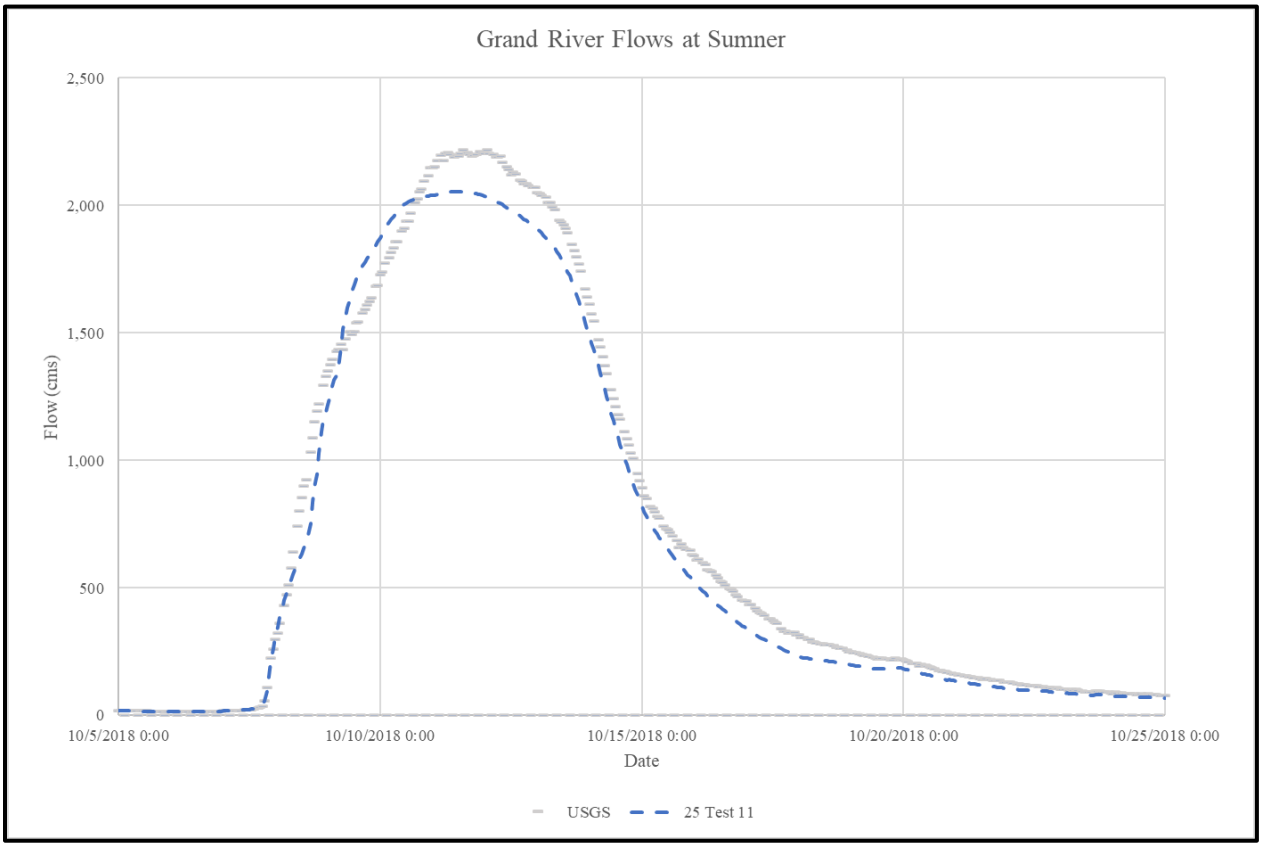

Figure C.3:
Simulated Flows at Sumner for the 2018 October Event Compared to USGS Observed Flows

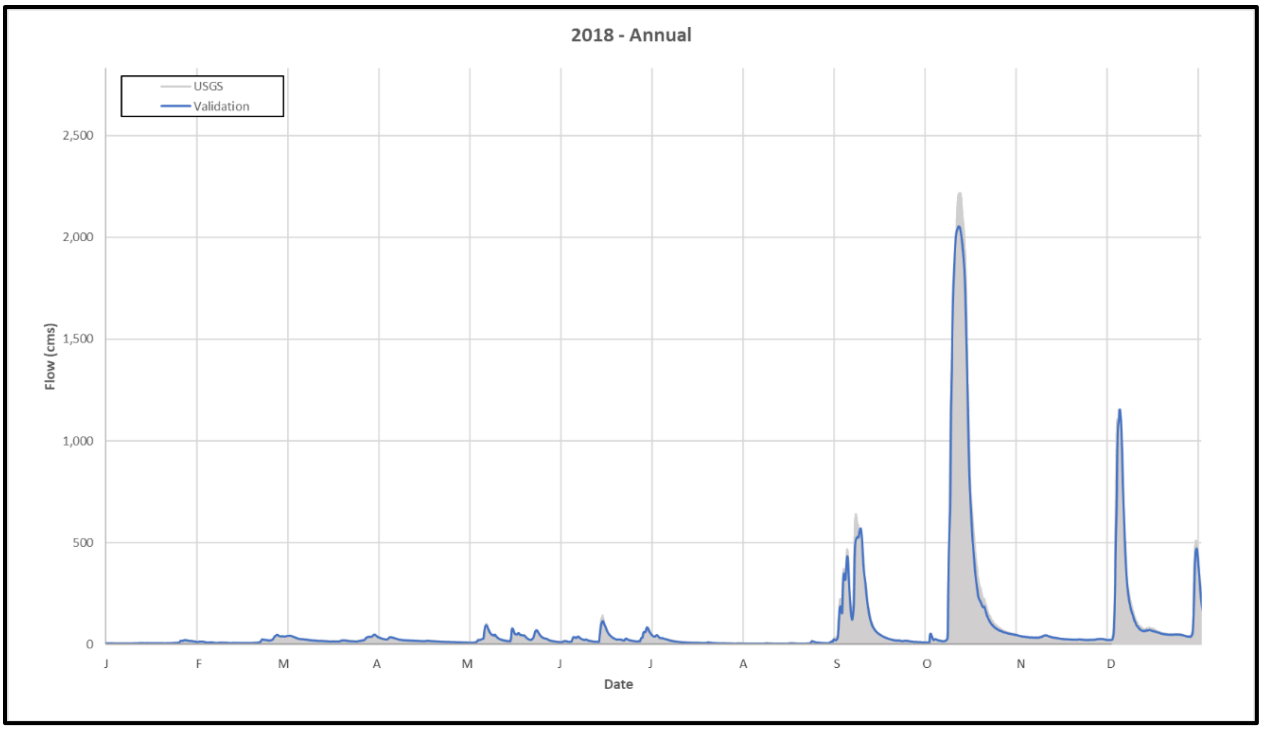

Figure C.4:
Simulated Flows at Sumner for the 2018 Annual Simulation Compared to USGS Observed Flows

Table C.1 provides both the NSE and correlation for the validation simulation. In a perfect model, the NSE would equal 1.0. As seen in the table, both the NSE and correlation were close to 1.0 indicating a good validation. However, both the NSE and correlation were biased in this calculation as the calculation used every time step within the October 2018 event simulation. By accounting for all time steps, more datapoints reflective of baseflow conditions were incorporated into the calculations which reduced the overall impact of the underestimated peaks in the NSE and correlation calculations.

Table C.1:
Model-25 Simulations Computed NSEs and Correlations for the October 2018 Event

Simulation	NSE	R^2
25Test11	0.986	0.991

After examining Grand River flows at Sumner, the HWMs were evaluated. Two highwater marks were eliminated from the analysis because the elevations were significantly lower than other nearby highwater marks indicating an error in measurement. Locations at other highwater marks showed no simulated water surface at those locations. As a result, a water surface elevation could not be compared to the surveyed HWMs. Table C.2 displays the 2018 simulated water surface elevations and the differences between the simulated water surface elevations and remaining surveyed HWMs. Upon comparing the remaining HWMs, the water surface elevation at Locust Creek along Highway 36 was about 0.45 meters higher than the surveyed WSE. Simulated water surface elevations along the old Locust Creek channel downstream of the Muddy Creek confluence were less than or equal to 0.07 meters higher than the surveyed HWMs. Overestimation of the water surfaces may over predict inundation durations and impacts to wetland communities. Only one HWM remained in Fountain Grove for comparison against simulated water surface elevations as all other locations remained dry in the simulation. The simulated water surface elevations were approximately 0.53 meters lower than the surveyed HWM. This may indicate that lower than observed peak volumes were simulated at Grand River at Fountain Grove due to methodologies used to develop a continuous flow record.

Table C.2:
2018 Validation Simulated Water Surface Elevations Comparison to USACE Surveyed HWMs

Dataset	**Simulated Water Surface Elevation in m-NAVD88** Water Surface Elevation Difference between Simulation Results and Observed in meters Pershing State Park			Grand River
USACE Surveyed HWM	210.84	208.50	208.50	205.31
25 Test11	211.29 0.45	208.57 0.07	208.56 0.06	204.79 -0.53

A comparison of the inundation extents is provided in Figure C.5. As seen in Figure C.5, the simulated inundation extents surrounding the Grand River near Fountain Grove overestimated the inundation extents on October 24th, 2018. The overestimation of the inundation was likely attributed to the placement of the Grand River Fountain Grove boundary condition. The boundary condition was placed such that it extended across the entire floodplain to allow for flow distribution across the entire floodplain during larger flows. As part of that methodology, the boundary condition extended through a levee system which likely reduced the amount of flow entering the leveed overbank areas in real world scenarios. Additionally, the areas circled in red appeared to drain slowly, contributing to increased inundation duration and extents. This may be a result of inaccurate culvert data used in the model. However, the areas along Locust Creek are the primary areas of interest and appeared to reflect the inundation extents observed in the satellite imagery.

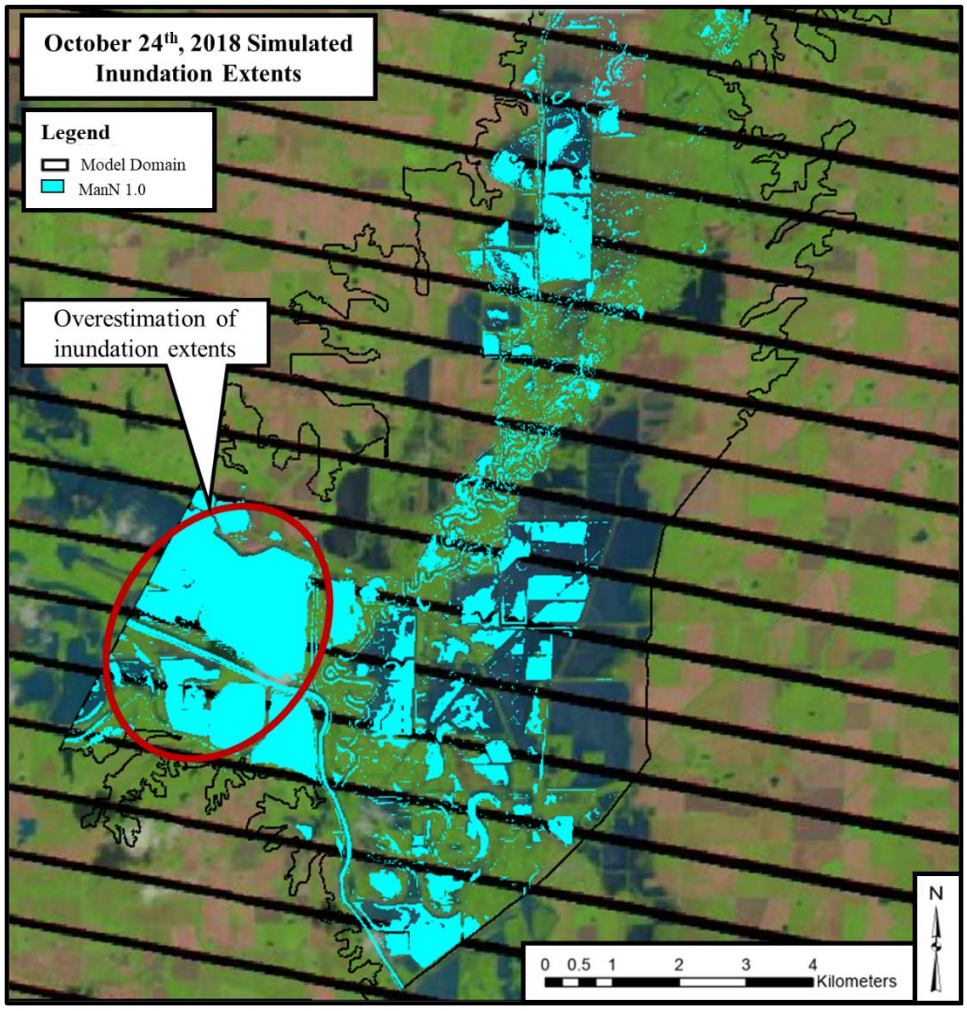

Figure C.5:
2018 Event Inundation Extent Validation

Log Jam Validation

Validation Event

Log jam characteristics were validated to an individual event that occurred between March 24th and April 2nd of 2009 on Locust Creek, hereafter referred to as the April 2009 event. The April 2009 event was selected for validation because the event resulted in floodplain inundation and had validation data available throughout the floodplain in Pershing State Park. The event was characterized by one large event followed by a smaller multipeak hydrograph on Locust Creek.

For this event, the initial peak discharge on Locust Creek near Linneus, MO occurred March 25th, 2009 with a peak discharge of 323 cms. The second peak occurred March 30th, 2009 with a peak discharge of 46.4 cms. Additionally, the developed flow record at Muddy Creek produced a peak discharge of 32.3 cms on March 24th, 2009. A smaller peak occurred on the Muddy Creek hydrograph on March 30th, 2009 with a peak discharge of 9.48 cms.

The timeseries for the March 2009 event from March 8th 2009 through April 9th 2009 was comprised of 83% USGS data and approximately 17% of interpolated values for Locust Creek inflows. However, Grand River inflows at Fountain Grove for this simulation were completely based on HEC-HMS developed flows. This indicates that Grand River results at Sumner may be influenced by hydrologic model errors within the HEC-HMS generated time series.

Validation Data

The April 2009 event was largely selected for log jam validation because documentation of the log jam existed and Landsat aerial imagery of floodplain inundation extents was available for reference within Pershing State Park. Inundation extents and duration from aerial imagery were previously used to quantify wetland change in other studies (Martínez-Espinosa et al., 2021). The USGS Landsat 7 aerial imagery was used to calibrate the model for log jams. USGS Landsat 7 aerial imagery, available from the USGS LandLook web tool (U.S. Geological Survey, 2018), displayed inundation extents on April 7th, 2009 as a result of flooding from the April 2009 event. However, a timestep was not included. As a result, it was assumed that the image, collected during daylight hours, was collected at 1200 hours. The inundation aerial imagery extents are provided in Figure C.6 with respect to the model extents and important stream alignments. Specifically, the available inundation extents included sections of the floodplain upstream and downstream of the 2009 log jam.

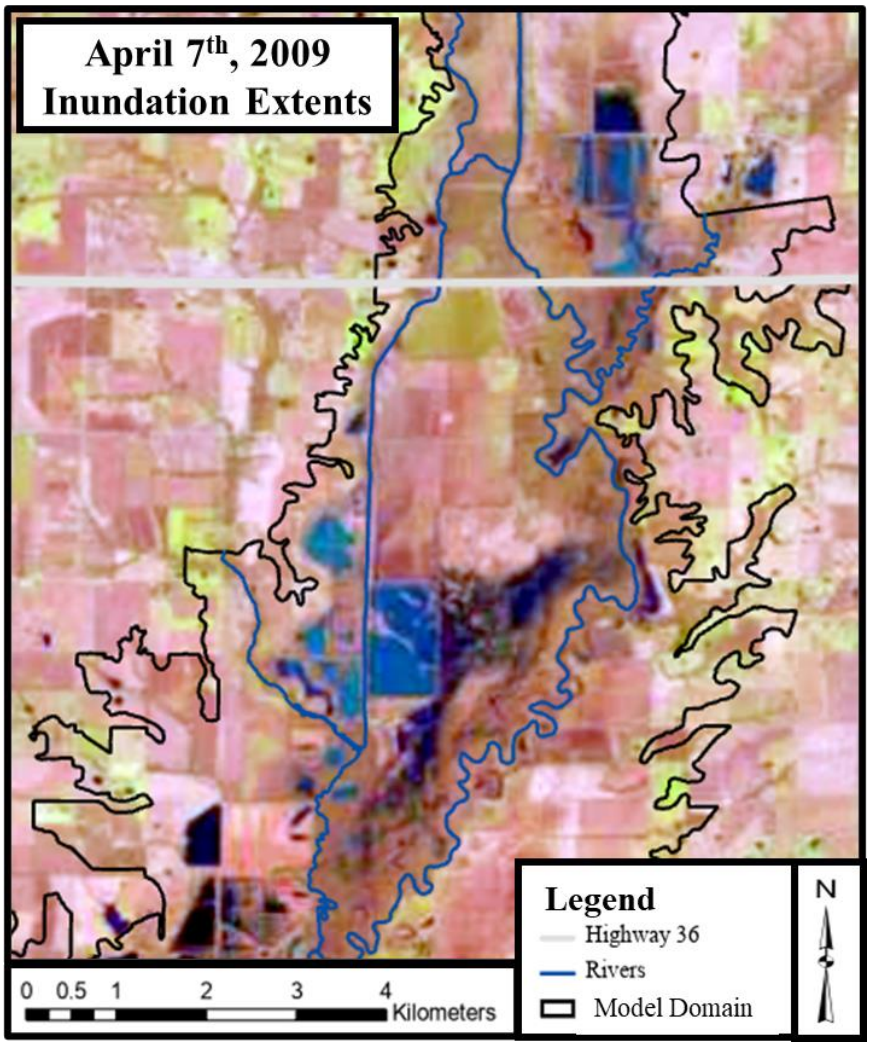

Figure C.6:
USGS Landsat 7 Floodplain Inundation Extents on April 7th, 2009

Validation Methodology

The validation event used the same simulation time period as the calibration time period (from 08 March 2009 00:00 to 09 April 2009 00:00) in order to model all components of an individual hydrograph: initial baseflow, rising limb, peak, falling limb, and return to baseflow. A computation interval of one minute and an initial conditions warmup period of 252 hours (10.5 days) were used to ensure computational stability. All other calibrated parameters associated with Plan 25Test11, discussed in Appendix B, were used in the simulations. This included the use of

diffusion wave computation methodology, water surface elevation and volume tolerance of 0.008 meters. However, the Landcover layer from the log jam calibration was used which included a log jam roughness coefficient of 1.0. The resulting water surface inundation April 7th, 2009 at 1200 was compared to the Landsat aerial imagery.

Validation Results and Discussion

The inundation extents are displayed in Figure C.7. As seen in the figure, log jams represented with roughness coefficients equal to 1.0 underestimated the inundation extents in the areas of existing wet prairie. Underestimation of the inundation extents may result in fewer hydraulic impacts (shallower depths and smaller inundation durations) to key wetland communities, resulting in underestimation of wetland community changes. However, the underestimation of the simulated inundation extents may be a result of changes in topography due to floodplain sedimentation that occurred between 2009 and 2018.

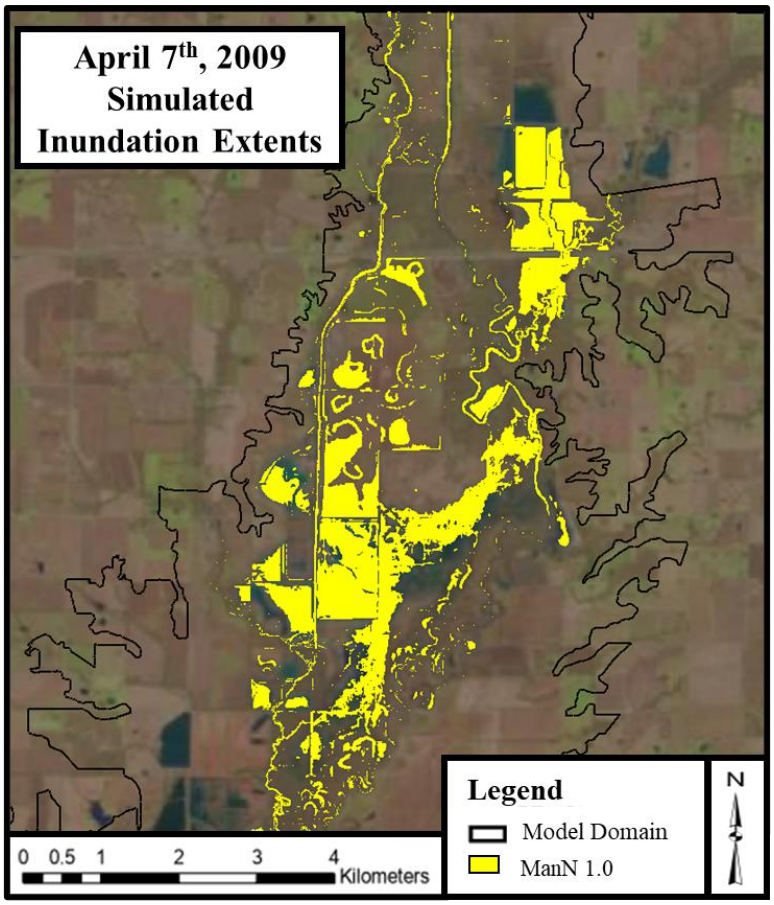

Figure C.7:
Log Jam Roughness Coefficient Validation April 2009 Inundation Extents

Annual Peak Discharge

Annual simulations were analyzed in order to understand how the simulated results differed from observed. This information was used to inform discussions pertaining to the validity of the simulated hydraulic results and their impacts to the habitat analysis.

Simulations

Simulations developed for each year used a start time of January 1st 00:00 and end time of December 31st 24:00. The four base computational grids described in Chapter 2 of the main thesis were copied and renamed using the format LC_**25**ft_**Year** to reflect the cell size used and the year

of simulation the geometry represented. An individual Land Cover layer was developed for each year of simulation. These annual Land Cover layers included spatial refinements to represent log jam extents for any given year between 2008 and 2018 (Figure C.8). Each yearly Land Cover layer was then assigned to the respective yearly geometry in RAS Mapper. When a log jam occurred in the Locust Creek modeling domain for a given year, the roughness coefficient was adjusted at the log jam location to reflect the length and width of the log jam for the entire annual duration. Log jams were assumed to fill the entire channel width along the documented log jam length. Once the simulation year was complete, the log jams for that year were removed and the log jams identified in the next year were included in the landcover map layer. This process was repeated for every year simulated resulting in a total of eight landcover layers.

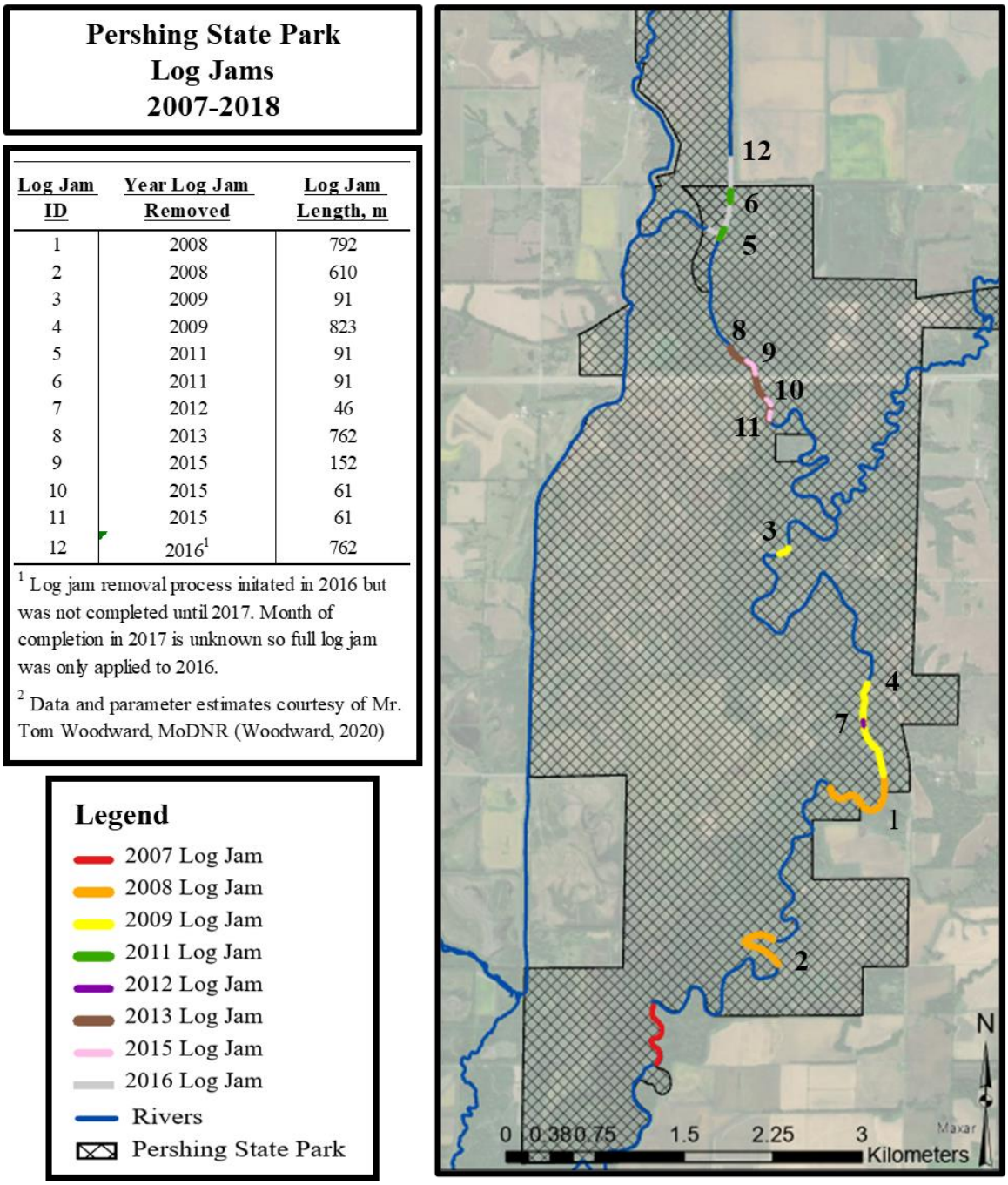

Figure C.8:
Log Jams Identified by MoDNR and Google Earth from 2007 to 2018

Each annual simulation used a warm-up period of 252 hours to establish initial conditions. The simulation unsteady flow file used the developed time series discussed in Chapter 2 of the main thesis and Appendix A. The calibrated parameters were used in both the HEC-RAS unsteady

flow file and geometries. A separate plan was created for each annual simulation and the corresponding geometry and the unsteady flow file were used. These plans were used as the starting point for all additional simulation analyses.

Analysis

The simulated Grand River timeseries was compared to observed USGS peak event flows. For each year, the three highest peak Grand River hydrograph flows with corresponding observed USGS flows were extracted from the model at Sumner, MO and used to compute the Nash-Sutcliffe model efficiency (NSE). Three maximum peak event flows from each annual simulation were used to ensure data from each annual simulation was included in the peak flow analysis. If, for instance, a bankfull threshold was used to filter peak flows instead of the three maximum peak event flows, data would not be included from 2012 and 2013 because those years simulated dry conditions. The NSE quantified how well the Grand River flows at Sumner predicted the USGS observed flows. NSE for each simulation was computed using Equation C.1. Only peak flows were analyzed so that the NSE was representative of how well the model simulated peak flows. In a perfect model, the NSE would equal 1.0.

Results and Discussion

The three largest simulated Grand River event discharges at Sumner, MO for each year of analysis were used to compute the NSE for peak event flows. Simulated discharges ranged from 515 to 3,990 cms. The estimated bankfull flow for the Grand River at Sumner was 8,230 cms (USACE, 2020), indicating that 91% of the analyzed simulated flows exceeded bankfull discharges. The resulting peak flow NSE was 0.30. The computed NSE of 0.30 was low and indicated that the hydraulic model did not accurately simulate Grand River peak discharges at the Sumner, MO gage location. In a perfect model, the NSE would equal 1.0. Only peak flows were

included in the NSE computation and, as a result, the NSE was representative of how well the model simulated peak flows.

When comparing the thirty-three simulated peak flows to USGS instantaneous peak flows, the simulated flows routinely overestimated Grand River streamflows near Sumner, producing an average overestimation of 166 cms and maximum overestimation of 18,800 cms in 2014. Annual simulations including 2008, 2009, 2010, and 2014 were primarily responsible for the overestimations of peak event streamflows. Inflows for these years used larger percentages of HEC-HMS flows to develop the Locust Creek inflow time series (Appendix A). Additionally, these years completely used HEC-HMS generated flows for Grand River inflows. As discussed in Appendix A, the HEC-HMS generated flows tended overestimate flows when compared to observed USGS flows. Overestimated flows may contribute to increased simulated inundation depths and duration, overestimating negative impacts to both wet prairie and bottomland hardwood forests.